Studies on constricted hollow anode plasma source for negative ion production

Mubarak A. Mujawar

March 2013

Studies on constricted hollow anode plasma source for negative ion production

A thesis for the degree of

PHILOSOPHIAE DOCTOR

Presented to

DUBLIN CITY UNIVERSITY

by

Mr. Mubarak A. Mujawar

School of Physical Sciences

Dublin City University

Supervisors:

Dr. Shantanu Kumar Karkari,

Prof. Miles M. Turner

External Examiner: Prof. James Bradley

Internal Examiner: Dr. Paul Swift

March 2013

<u>Declaration</u>

I hereby certify that this material which I now submit for assessment on the programme of study leading to transfer to the degree of Philosophiae Doctor is entirely my own work, that I have exercised reasonable care to ensure that the work is original, and does not to the best of my knowledge breach any law of copyright, and has not been taken from the work of others save and to the extent that such work has been cited and acknowledged within the text of this work.

Signed: Candidate ID No.: 57125244

        Mubarak A. Mujawar,   March 2013

Dedicated to

my loving parents

Abstract

Electronegative plasmas have a wide ranging applications following its primary role in the production of energetic neutral beams of hydrogen used for plasma heating in fusion devices. In technological plasma applications electronegative gases are used for plasma etching which readily form stable negative ions. Significant population of negative ions in a discharge can greatly influence the discharge properties by reducing electron density while modifying the sheath structures adjacent to the substrates.

Formation of negative ions is a complex process. They are primarily formed in the bulk phase by the dissociative attachment of low energy electron to an excited molecule. However intermediate excitation of the neutral molecules requires the presence of energetic electrons in the discharge. An efficient mechanism of negative ion production is via interaction with a low work function material such as Caesium coated surface as used in the negative ion source for neutral beam extraction. However, caesium migration between the acceleration grids can be a major concern for the failure of ion source during long pulse operation. Therefore suitably tailoring the plasma properties of the source can help in improving the efficiency of negative ion production in the bulk phase rather than surface production.

The thesis deals with the study of oxygen negative ion formation in the anodic glow plasma. The anodic glow is characterized by a double layer having a steep gradient in T_e and electron density. This region provides a natural favourable condition for the production of negative ions. The anodic glow is created via D.C discharge between a hollow tubular-anode in conjunction with parallel plate cathodes. The results show significant fraction of negative oxygen ions near the anodic glow. Theoretical estimates of negative ions at each spatial location are obtained by providing electron density and temperature measured using plasma diagnostic probes. The results show reasonable agreement with the experimental data suggesting that anodic glow can provide a suitable breeding ground for the production of negative ions. A qualitative model is presented for observing the oscillation in the discharge current due to ionization instability at the anode sheath.

Acknowledgement

It is great pleasure for me convey my sincere thanks to a number of people who gave suggestions, who encouraged me and who helped me with their valuable counsels and assistance during my PhD research.

First of all I am thankful to my supervisors Dr. Shantanu Karkari and Prof. Miles Turner for giving me an opportunity to undertake this research. Thanks to Association Euratom DCU- Fusion for funding my research. I express my deep sense of gratitude to my supervisor Dr. Shantanu Karkari for his constant support, encouragement, and valuable suggestions during the course of this work. The discussions with Shantanu have always encouraged me throughout my PhD research. The completion of this thesis is a result of his constant encouragement, guidance and constructive comments. I would like to thank Prof. Miles Turner for his invaluable guidance, feedback, motivation and encouraging remarks. I am thankful to him for taking my responsibility while Dr. Shantanu was away from DCU. I also thank Dr. Stephen Daniels for his support and encouragement throughout the process of my PhD.

It had been always a great experience to interact with academicians in DCU, especially with Dr. Paul Swift and Dr. Bert Ellingboe. My sincere thanks to Prof. Greg Hughes and Prof. John Castello, current and former head of Physics School. The experimental and

Table of Contents

Chapter 1 - Introduction

1.1   Background and motivation

In recent years, the world's energy needs have increased rapidly due to the increasing level of sophisticated living styles and the quicker growth of human population. To date , fossil fuels are one of the major energy sources which are set to be short supply in the near future. This shortage has necessitated the quest for the unconventional methods of producing energy on a large scale to fulfill the future energy demands [1, 2]. Alongside, there is also a need to develop viable technologies to produce energy efficient devices and applications.

During the last half century the advent of plasma science and technology has played a vital role in these areas. While plasma based fusion has emerged as a prospective and feasible energy source [2, 3], industrial plasmas are routinely used for manufacturing the lighting devices, large area solar cells, flat panel displays and electronic devices [4-6]. The modern day microelectronics industry is largely dependent on the plasma assisted processes such as cleaning, etching and deposition [7-9]. More recently, plasmas have also found important biomedical applications such as biocompatible coatings, biosensors, wound healing and sterilization [10-12].

The word 'plasma' is used to describe an ionized state of matter which is a collection of charged and neutral particles [13]. Taking into consideration the energy of the particles it constitutes, plasma is energetically the fourth state of matter in which electrons are separated from molecules and atoms [14]. The constituent plasma particles have random kinetic energy due to which they can move freely in random directions. Moreover, positive and negatively charged particles in plasma are constrained to move together under the influence of long range coulomb forces. This collective behaviour of the plasma particles is responsible to maintain the charge neutrality of the plasma ensemble [15, 16].

A typical plasma system comprises of equal number of positive ions and electrons in order to maintain the charge neutrality. While in some cases, plasma contains more positive ions than the electrons as a fraction of electrons become attached to the atoms or molecules and form 'negative ions'. Such plasmas, rich with negative ions are generally termed as 'electronegative' plasmas. These plasmas can occur naturally, for example, in the Earth's ionosphere and in the photosphere of the Sun [17, 18]. Electro-negative discharges used for cleaning, oxidising and etching of processing semiconductor substrates have significant negative ions. Their presence can influence the sheath structure and indirectly influence the ion flux and the energy of the positive ions impinging the substrate. In contrast to the positive ions, the interaction between negative ions and the substrate is an endothermic process. Therefore, plasma processing by negative ions minimizes the heat load on the polymeric substrates.

An important application of electronegative plasmas is for the generation of energetic (1-2 MeV) neutral hydrogen beam. The neutral beam sources are commonly used for plasma heating in various fusion devices (e.g. ITER, JET, JT-60). The energetic neutral beam is produced by the charge exchange collisions between the accelerated negative ions and the background neutrals. The negative ions are preferred over positive ions as the neutralization efficiency of positive ions falls drastically to zero, while for negative ions, it is about 60 % for 1MeV nucleon^{-1}. Therefore, negative ion source producing plasma densities in the range of 10^{18} m^3 at a low operating pressure 0.3 Pa is primarily the focus of attention, both in terms of fundamental understanding of the properties of negative ions and as the technological challenges in terms of optimizing the source parameters and extraction of the beam [19-21].

The existing negative ions sources for fusion applications are based on the surface production mechanism in which positive ions of hydrogen (H$^+$) interact with a low work function surface and capture two electrons to form a negative hydrogen ion. For this reaction, Cs gas is fed in the chamber along with the working hydrogen gas, where Cs deposits on the stainless steel chamber walls and provides the active low work function surface [20, 21]. However, Cs can migrate along with negative ions through the extraction grid. This has serious consequences as some negative ions are produced in between the accelerator grids and their energies are significantly lower than the major component of negative ions extracted from the plasma. This leads to poor optics of the beam and consequently causing the beam to diverge. These energetic beams striking the duct chamber walls can lead to the damage of the chamber walls besides polluting the beam by bringing

in the residual impurities into the chamber. Therefore making the volume production more efficient is a key to eliminate Cs injection inside the source.

The efficient production of negative ions in the bulk phase is the result of balance between the production and the loss rates. The production of negative ions in the bulk phase is a two-step process. In the primary step, an atom or a molecule is excited by energetic electrons in the distribution. These excited molecules then capture a low energy plasma electron to form a H- through the dissociative electron attachment process [19, 21]. The main cause for the destruction of negative ions is the fast electrons. Therefore, production of negative ions in the bulk phase is less efficient as compared to the surface process.

A systematic study of the kinetics behind the volume production requires controlling the electron temperature (T_e) distribution inside the plasma. Generally, the electron energy distribution can be manipulated by varying the collision frequency by changing the operating pressure. However, changing the external parameter such as the pressure also results in a change in the number density of electrons which is also responsible for the attachment process. Therefore, in an experiment, there is a limited scope for studying these mechanisms independently over a broad spectra of electron temperature.

One method of separating different electron temperature regions in a plasma is by applying magnetic filters in a plasma chamber which selectively screen the transport of electrons. These kind of sources are known as Tandem (two chamber) sources and have been implemented to study the negative ion production by volume process [21-24]. The distinct electron temperature can also be created in a pulsed plasma. In this case, electron

temperature in the ON phase of the pulse cycle is higher, which drops transiently in the OFF phase of the cycle [25, 26]. However in both these cases, the active control of electron temperature over a wide range is difficult to achieve.

In summary, understanding the kinetics behind the production and loss mechanisms of negative ions is vital for both industrial plasmas [8, 9, 27-29] as well as for the neutral beam heating source for fusion devices.

In view of the above discussions, we focus our objective on the properties of a D.C anodic glow plasma for the production of negative ions. The anodic glow region is characterized by the spatial gradient in the electron temperature ranging from 1eV to 5eV. The anodic glow, sometimes referred as 'fire ball' is a bright luminous glow formed in front of the positively biased electrode (anode) due to the intense secondary ionization. The glow is associated with the presence of space charge double layer structure which confines the energetic electrons near the anode. The electron temperature outside the anodic glow shows a typical spatial decrease in the electron temperature. Such a situation is ideal to study the effect of electron temperature on the kinetics of negative ion formation and destruction at a fixed gas flow rate.

The overall thesis can be broadly classified into two parts. The first part deals with the properties of the plasma source which comprise of a differentially pumped constricted hollow anode for the production of anodic glow, in conjunction with number of parallel plate cathodes. Systematic studies are carried out to understand the role of the electrode configurations in the enhancement of local plasma production near the constricted anode

and its impact on the overall plasma properties. The investigations also look at some basic issues such as plasma instabilities due to the anodic glow. The second part of the thesis deals with the systematic study of negative oxygen ions formation in the anodic region. The experimental observations are explained on the basis of the quantitative analysis of different rate constants. The investigations described in this thesis are schematically shown in figure 1.1.

Introduction
Background and motivation
Outline of thesis work → **Chapter 1**

Experimental set-up
Design and development of
plasma diagnostic tools → **Chapter 2**

Basic discharge properties
Formation of anodic glow
Properties of Anodic glow
Theoretical explanation of
anodic glow properties → **Chapter 3**

Ionization induced
plasma instabilities in anodic glow
> Mechanism governing the
plasma instabilities
> Correlation with the bulk plasma
properties → **Chapter 4**

Measurement of
negative ion fraction in anodic glow
> Kinetic model describing
negative ion formation and
loss mechanism → **Chapter 5**

Conclusion / Future work → **Chapter 6**

Figure 1.1: *Schematic of thesis structure*

The following section briefly reviews the well-known plasma parameters.

1.2 Important plasma parameters

1.2.1 Plasma Temperature

Plasma is a collection of many bodies with range of velocities in three dimensional phase-space. When the density of particles in a velocity space is plotted against the velocity ranging from − infinity to + infinity, we get a peak at the centre which falls away from the centre as described by a Maxwellian distribution. The full width at half maximum of the distribution determines the temperature of the species and is associated with the mean velocity of the particles. The Maxwellian distribution of electrons is given by

$$f(v) = n \left(\frac{m}{2\pi k T} \right)^{3/2} \exp\left(-\frac{mv^2}{2kT} \right)$$

In the above expression, m denotes mass of electron and T denotes the temperature of the electron. The distribution function $f(v)$ describes the number of particles (dn) in a given velocity interval, $dn=f(v)dv$. This can be expressed in terms of energy and the electron energy distribution function, $f(E)$ is obtained from the velocity distribution function as

$$f(E) = n \left(\frac{4E}{\pi} \right)^{1/2} (kT)^{-3/2} \exp\left(-\frac{E}{kT} \right)$$

The average particle velocity, $\overline{v}$, as obtained from the velocity distribution function is

$$\overline{v} = \left(\frac{8kT}{\pi m}\right)^{1/2}$$

The T_e, T_i, T_- are generally used to denote the temperature of electrons, positive ions, negative ions.

If plasma species fulfil the following condition

$$T_g = T_i = T_e = T_{ex} = T_d = T_r$$

(T_g= gas temperature, T_i= ion temperature, T_e= electron temperature, T_{ex}= excitation temperature, T_d= dissociation temperature, T_r= radiation temperature)

then the plasma is said to be in *thermal equilibrium*. Complete thermal equilibrium is very difficult to observe, however, under certain laboratory conditions *local thermal equilibrium* can be achieved. If the ion temperature and gas temperature is comparable with the electron temperature i.e. $T_g \approx T_i \approx T_e$ the plasma is said to be in local thermal equilibrium.

Typically for low pressure plasmas,

$$T_e \gg T_i \approx T_g$$

And therefore, the plasma is said to be in non-thermal equilibrium

1.2.2   Debye Sheath

If a local potential is imposed in the plasma, the opposite charged particles organize in order to confine the electric field from leaking in to the plasma. The potential created due to thermal fluctuation of highly mobile electrons, is shielded to a distance called the Debye length, λ_D, and the phenomenon is termed as Debye shielding. The Debye length in the plasma can be obtained by equating the kinetic energy of thermal electrons ½ kTe to the electrostatic potential created as follows:

$$\lambda_D = \left(\frac{\varepsilon_0 k T_e}{e^2 n_e} \right)^{1/2}$$

where ε_0 is the permittivity of the free space and e is the charge of electron. When the values of ε_0 and e is inserted in above equation we get

$$\lambda_D = 743 \left(\frac{T_e (eV)}{n_e (10^{10} cm^{-3})} \right)^{1/2} \text{ in cm}$$

where $T_e = kT_e/e$ is in eV. Debye length is inversely proportional to the number of charges available for shielding the local potential. The Debye length is proportional to the electron temperature. The physical dimension L of the plasma must satisfy the condition $\lambda_D << L$.

An object in contact with the plasma is charged by the random fluxes of electrons and therefore it builds up a negative potential with respect to the plasma. The negative potential accelerates positive ions towards the walls while repelling the electrons. In a steady state,

plasma continues to provide electrons to the surface in order to maintain the negative potential just enough to make the electron and ion fluxes equal such that the net current is zero on an average. The potential at which the net current is zero is known as the floating potential.

The potential developed between the surface and the plasma bulk is confined to a layer of thickness of several Debye lengths. This layer of positive space charge that exists around all surfaces in contact with the plasma is called the plasma sheath.

The potential developed across is called sheath potential. For the floating surface the sheath potential is given by

$$\Phi_w = -T_e \ln\left(\frac{M}{2\pi m}\right)^{1/2}$$

where M is mass of ion. The velocity with which the ions enter into the sheath is called Bohm velocity and is given by $u_B = \left(\frac{eT_e}{M}\right)^{1/2}$

If certain voltage is applied to the surface immersed in plasma, the surface starts collecting the current which is given as $j_0 = en_s u_B$

In terms of the applied voltage on the surface, the current collected is given by the Child's law of space charge limited current

$$j_0 = \frac{4}{9}\varepsilon_0\left(\frac{2e}{M}\right)^{1/2}\frac{V_0^{3/2}}{s^2}$$

where *s* is the thickness of the sheath and is obtained by

$$s = \frac{\sqrt{2}}{3} \lambda_{Ds} \left(\frac{2V_0}{T_e} \right)^{3/4}$$

where λ_{Ds} is the Debye length at the sheath edge.

1.2.3   Electron plasma frequency

In line with the above discussion of Debye length, the local perturbations from the quazineutrality develop an electric field to limit the charge accumulations. The response of charged particles to these local electric fields is via fundamental mode of oscillations. The frequency of these oscillations is termed as the plasma frequency. For electrons it is given as

$$\omega_{pe} = \left(\frac{e^2 n_e}{m \varepsilon_0} \right)^{1/2}$$

The above equation is simplified as

$$f_{pe} = \frac{\omega_{pe}}{2\pi} \approx 8980 \sqrt{n_e} \; \text{Hz} \qquad (n_e \; \text{in} \; cm^{-3})$$

In a typical glow discharge, the plasma frequency is in the microwave band (1-10 GHz).

Recalling the expression for the Debye length, the plasma frequency is written as

$$\omega_{pe} = \frac{\bar{v}_e}{\lambda_D}$$

where $\bar{v}_e$ is the average thermal velocity of the electrons in plasma.

The above equation shows that, during the one plasma oscillation, electrons move with velocity $\bar{v}_e$ over a distance of a Debye length so as to maintain the neutrality of the plasma. However, this electron shielding is inefficient for the plasma perturbations with greater frequency than ω_{pe}.

1.2.4   Ambipolar diffusion of charged particles

If the discharge has nonuniform distribution or density gradient of charged particles, the plasma particles tend to move by diffusion towards the region of lower density. The electrons have higher mobility and tendency for faster diffusion than ions which causes the formation of positive space charge over a region greater than λ_D. In order to maintain the quazineutrality an electric field sets-up which restrains the electrons and accelerates the positive charges such that the flux of both the charged particles is balanced i.e. $\Gamma_e = \Gamma_i = \Gamma = nv$. This phenomenon is called ambipolar diffusion.

The flux of ion and electron in the presence of diffusion gradient $\dfrac{dn}{dx}$ is composed of two terms, and is given by

$$\Gamma_e = -D_e \nabla n_e - \mu_e n_e E \qquad\qquad (1.1)$$

$$\Gamma_i = -D_i \nabla n_i + \mu_i n_i E \qquad\qquad (1.2)$$

In the above expressions, $D\nabla n$ is the diffusive flux of charged particles induced by concentration gradients and $\pm\mu n E$ is the flux associated with the drift of charged particles under the influence of ambipolar electric field E. The symbols D and μ denote diffusion coefficient and mobility of charged particles and are given by

$$D = \frac{kT}{m\nu_m}$$

$$\mu = \frac{|q|}{m\nu_m}$$

where ν_m is the momentum transfer collision cross section. Using the mean speed $\bar{v} = (8kT/\pi m)^{1/2}$ and a mean free path $\lambda = \bar{v}/\nu_m$, we write

$$D = \left[\frac{\pi\lambda^2 kT}{8m}\right]^{1/2} \tag{1.3}$$

$$\mu = |q|\cdot\left[\frac{\pi\lambda^2}{8kTm}\right]^{1/2} \tag{1.4}$$

For $\Gamma_e = \Gamma_i = \Gamma$, from eq 1-1 and 1-2 we can write

$$-D_e\nabla n_e \pm \mu_e n_e E = -D_i\nabla n_i \pm \mu_i n_i E$$

Assuming the quasineutrality condition $n_e = n_i = n$, we can find the value of electric space charge field (E) generated due to ambipolar diffusion to maintain the local flux balance.

$$E = \frac{D_i - D_e}{\mu_i + \mu_e}\frac{\nabla n}{n} \tag{1.5}$$

The value of $\Gamma_e = \Gamma_i = \Gamma$ is

$$\Gamma = -\frac{\mu_i D_e + \mu_e D_i}{\mu_i + \mu_e}\nabla n = D_a\nabla n \tag{1.6}$$

where D_a is the ambipolar diffusion coefficient.

1.3   DC Discharges

The most common form of plasma generation in the laboratory is by applying a DC or time varying potential between two electrodes in a rarefied gas. The stray electrons present between the electrodes accelerate and gain energy in the electric field developed due to the applied potential. The accelerated electrons lose their energy in ionizing collisions with atoms or molecules of the gas and produce an electron-ion pair. The newly created electrons undergo further ionizing collisions. This electron multiplication process is characterized by the *first Townsend coefficient* (α) which represents the mean number of

ion-electron pair formed by an electron along the unit length . α depends on the electric field (E) and the relation between α and E is given by

$$\frac{\alpha}{p} = A\exp\left(-\frac{Bp}{E}\right)$$
(1.7)

where A and B are constants and p is the gas pressure. For a low applied voltage, the current flowing through the gas is due to the collection of charged particles available between the electrodes. As the applied voltage increases, due to the electron multiplication process the current monotonically increases. However this current is very small and requires sophisticated instrumentation for its measurement. This flow of electric current through gas is termed as *Townsend discharge*. The ionization in the Townsend discharge is very small and gas emits no significant light.
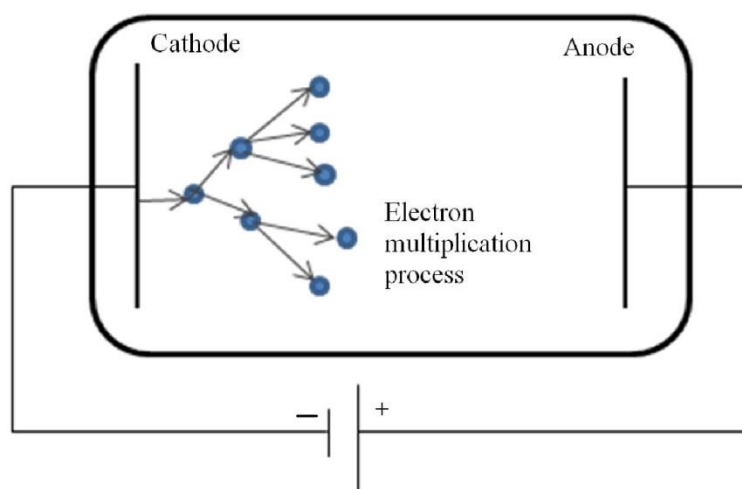
Figure 1.2: *Schematic of the DC discharge and electron multiplication process in Townsend discharge*

For a fixed distance, the electric field to neutral ratio increase by increasing the external applied voltage. If the applied voltage is further increased, at the critical value V_B, the current abruptly increases and the gas begins to glow and thus called glow discharge. The critical voltage at which gas begins to glow is called breakdown voltage (V_B) and it is given by

$$V_B = \frac{Bpd}{\ln Apd - \ln \left[\ln \left(1 + 1/\gamma_{se} \right) \right]} \tag{1.8}$$

In this relation d is the distance between the electrodes, γ_{se} is the secondary electron emission coefficient, which is the ratio of the number of emitted electrons at the cathode to the number of incident ions. From equation 1.5 and equation 1.6, it is clear that the breakdown voltage depends on the electric field (E), Townsend's coefficient (α) and system pressure (p).

Equation 1.6 is known as Paschen's law which correlates the breakdown voltage to the product pd. If the value of pd is large, very small number of ions reach at the cathode surface to produce the secondary electrons, thereby, increasing V_B. If the value of pd is small, number of ionizing collisions of electrons between the electrodes is greatly reduced and therefore V_B increases. The breakdown voltage has a minimum between the two extremes of pd. This behavior is described by Paschen's curve as shown in figure 1.3.
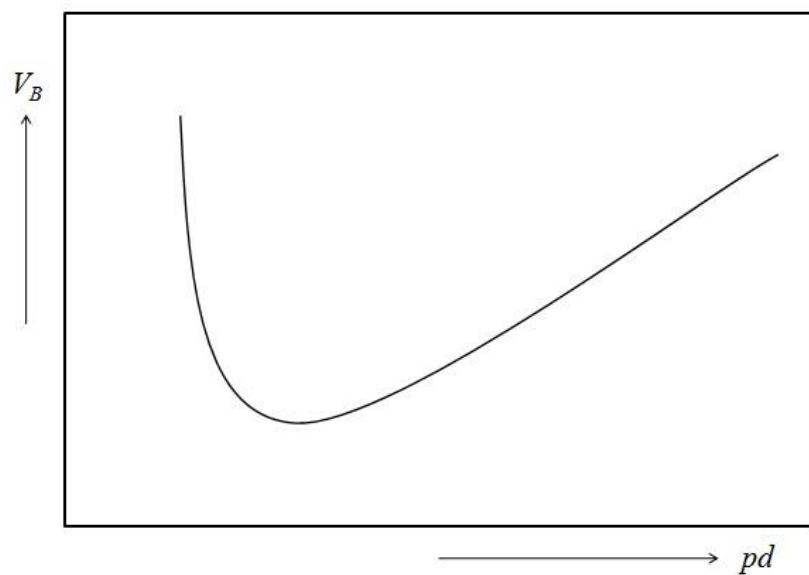
Figure 1.3: *Schematic Paschen curve for paralle plate DC discharge*
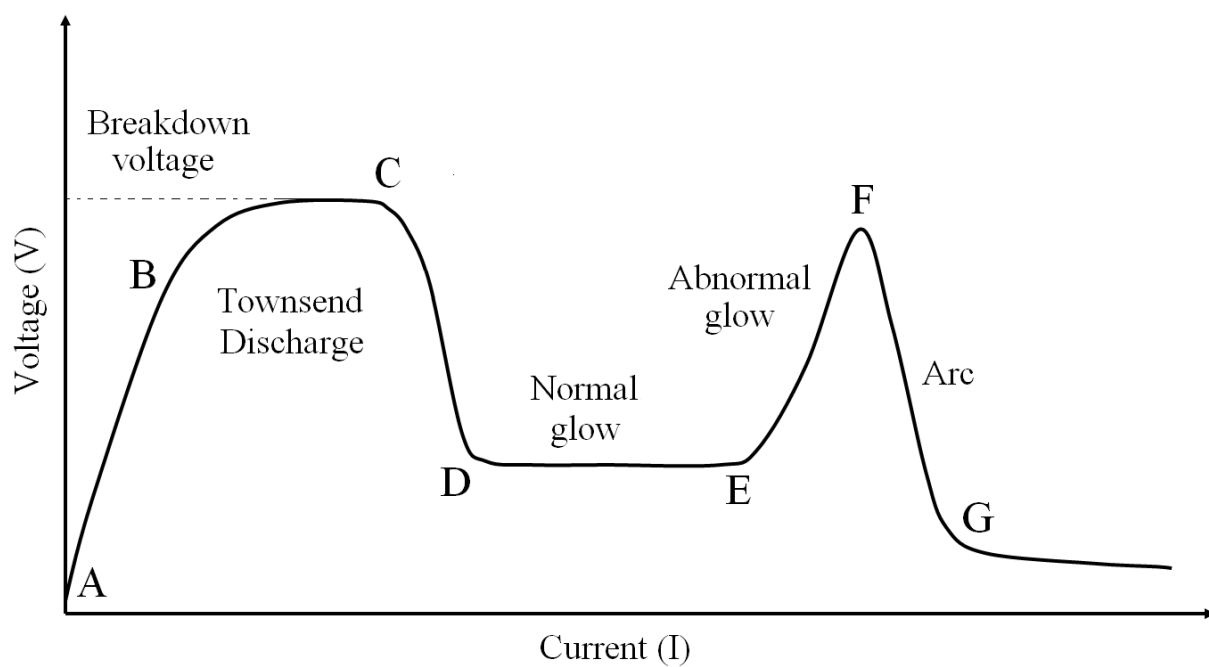
Figure 1.4: *I-V characteristics of DC discharge*

Figure 1.4 shows the I-V characteristics of the DC discharge. Region A-C corresponds to a dark discharge regime where the discharge current is very low. In region A-B, the current is mainly due to the migration of stray charges to the electrodes. In region B-C, the discharge current increases exponentially with a little increase in voltage. This region corresponds to the Townsend discharge. At point C, the electric breakdown occurs in Townsend regime with the addition of secondary electrons emitted from the cathode due to ion or photon impact exceeds the losses to form self-sustaining plasma and the current rises by a factor of 10^4–10^6. The discharge is characterized by a luminous glow because of excitation of neutrals by the electrons. This glow, called as the *normal glow*, which is visible close to the cathode, but does not cover the whole cathode surface. Further, increasing the current at a constant voltage leads to plasma covering the entire cathode surface (region D-E). Beyond this range, the voltage and current show a linear Ohm's relationship, and the discharge is called abnormal glow discharge (region E-F). In this region, the cathode gets heated by the increasing number of impinging ions, attracted by the negative potential. Abnormal glow region is of specific interest because the plasma density scales linearly with the applied power. The abnormal glow transfers in to an arc which is characterized by a sharp rise in the current while the discharge voltage drops. The arc regime is facilitated by strong a thermionic emission of electrons from cathode, local increase in sheath potential and enhance electric field close to the electrode.

1.3.1   DC Discharge Structure
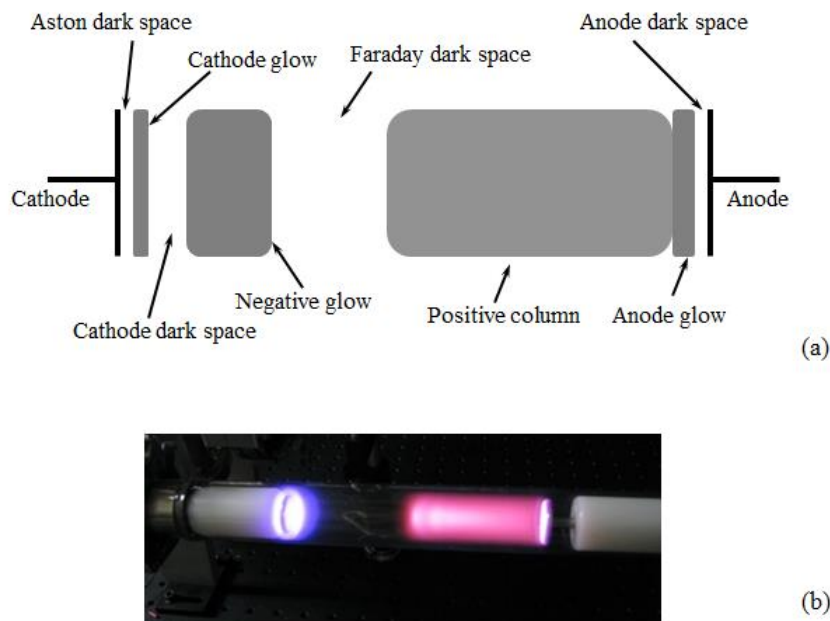
Figure 1.5: (a) Characteristic glow *structure of DC discharge (b) photograph of a*

DC discharge tube showing distinct luminous glow regions

The DC discharge is often shown as divided into distinct regions, as shown in Figure 1.5. Close to the cathode, a thin luminous layer is observed. This cathode glow is caused by atoms excited by electrons coming from the cathode, or ions accelerated from the plasma towards the cathode. The dark space between the cathode and the glow is called the Aston dark space. Here the electrons are too slow to cause excitation or ionization of the neutral gas. Moving towards the anode after the cathode glow, we see a dark region called the cathode (or Crookes or Hittorf) dark space. The largest potential drop occurs within the region cathode dark space. This region is often referred to as the cathode sheath or cathode fall. The major part of the cathode sheath has a net positive space charge due to the positive

ions attracted by the negative potential. The cathode dark space is directly adjacent to the negative glow, which is the lightest intensive part of the discharge. In this region, electrons gain enough energy to ionize and excite the neutral gas. After the negative glow, the Faraday dark space is observed followed by the positive column. The region adjacent to the anode is dark. This is because the electric field in the anode sheath is too weak to carry out any ionization and excitation. However, if the area of the anode is drastically reduced as compared to the area of the cathode, a bright luminescent glow appears in front of the anode. This glow is called as anodic glow.

1.3.2   Anodic glow and double layer

In a DC discharge, the polarity of the anode sheath is such that the plasma potential is always positive than the anode so as to repel the excess electron flux arriving at the anode due to their random thermal motion. However, if the anode is biased more positive compared to the plasma potential, electrons are attracted towards the anode. The electrons gain energy in this process and undergo ionizing and excitation collisions with the background neutrals in the anode region due to enhancement in the E/p ratio. This process leads to the formation of the intense glow around the anode. Similar intense discharge structures, sometimes called fireball, are also observed in plasma diagnostic probes when biased above the plasma potential[30-34].

The intense ionization in the fire ball is always described and associated with the formation of 'double layer' adjacent to the anode. A 'double layer' consists of two adjacent and opposite space charge regions. The opposite space charge layers create a strong electric

field and correspondingly sharp change in potential across the double layer. In case of anodic double layer, the electron sheath is attached to the anode and the adjacent positive space charge region is sandwiched between the electron sheath and the positive column [31, 35, 36].

The DC discharges based on the constricted hollow anode have also been subject of interest for last two decades because of their potential application as high density downstream plasma source for thin film synthesis and processing [37-39]. Miljevic, in 1984, described a DC discharge which consists of a concave cathode and a small disc with aperture at the center as anode[40]. The discharge is characterized by a bright plasma and maximum ion density in the small anode region. Miljevic discussed that this strong excitation and ionization of the gas in the anode region was due to the concave cathode which focused electrons towards the small anode located at the center of curvature of the cathode. However, later in 1995, Anders et al used a planar cathode and a small anode and showed that the dense discharge in the anode region is not the result of focusing of electrons by concave cathode but is essentially due to the secondary ionization in the anode region of constricted plasma source[41]. Since the area of anode in these plasma sources is sufficiently small as compared to the area of the cathode, they are called as constricted anode plasma source'. Anders further modified the constricted anode plasma source by addition of hollow cathode instead of plane cathode. The addition of hollow cathode increased the total discharged current which further enhanced the effect of anode constriction[42].

In this study, we present a constricted hollow anode plasma source in which an intense glow is created using a hollow tubular anode whose outer surface is shielded using a dielectric. The cathode consists of an array of equidistant parallel plates. This specific geometry of the cathode is useful to accommodate a large area cathode in the plasma source. Also, the distance between the parallel plate cathode is optimized in such a way to create a hollow cathode effect as described in the following section.

1.3.3 Hollow cathode effect

Instead of having a planar cathode in the DC discharge, the cathode can be made up of a cylinder or two parallel plates. If the distance between the parallel plates or the diameter of the cathode cylinder is such that the negative glow is confined inside the cathode cavity then it is called as hollow cathode discharge (HCD). A characteristic feature of hollow cathode configuration is the oscillation of fast electrons in the cathode cavity. The electrons which are emitted from the inner walls of cathode are accelerated in the cathode sheath region. These electrons meet the opposite cathode sheath where they are reflected. Therefore, the energetic electrons reside within the cathode cavity for a long period of time, instead of going into the positive column and then be lost to the anode. This has a direct effect on the increase of collision probability and higher ionization rate in the cathode region [9, 43-45].

HCD are characterized by a reduced breakdown voltage and higher current density. HCD are generally operated with DC however use of pulsed DC and RF bias allow more ionization efficiency and hence better performance of the source. One of the major

disadvantages of the HCD is that they operate at relatively higher pressure which limits their use where very low pressure operation is necessary.

1.4 Negative ions in a discharge

Negative ions are formed when an extra electron gets attached to the electron affinity level of an atom or molecule. The process of formation of negative ion can be (a) volume process in which the electrons in the bulk plasma get attached to the atom or molecule and (b) surface process in which positive ions impinge on the low work function metal surface and grab electrons from the metal surface to become negative ions.

1.4.1 Volume Production

Volume production of negative ions is a two-step process. In the first step, the vibrationally / rotationally excited molecules are created by direct impact of energetic electrons with the molecules. In the later step, these excited molecules either split into a negative ion and a neutral or they are stabilized by releasing the excess energy.

$$XY + e^- \rightarrow (XY^-)^* \rightarrow X^- + Y \qquad \text{Dissociative attachment}$$

$$XY + e^- \rightarrow (XY^-)^* \rightarrow XY^- + energy \qquad \text{Radiative stabilization}$$

Dissociative Attachment (DA) is the most common process for the formation of negative ions.

The formation of hydrogen negative ions by DA of slow electrons (with energy less than 1 eV) was first investigated by Bacal in 1977. Through this process hydrogen negative ions are effectively produced in the bulk of the plasma. However, fast electrons with energy more than 40 eV are required to produce excited molecules of H_2 or D_2 molecules.

$$H_2 + e_{fast}(40\,eV) \rightarrow H_2^* + e$$

$$H_2^* + e_{slow}(1\,eV) \rightarrow H^- + H + e$$
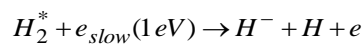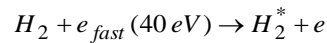
Since the electron energies for these two processes are different, the plasma in the ion source is divided in two regions by magnetic filters. In one region the high energy electrons excite the hydrogen molecule. These fast electrons are confined in that region by a magnetic field. Only heavier excited molecules selectively cross the magnetic field and go to the other region where the negative ions are produced by dissociative attachment of slow electrons.

1.4.2   Surface production

In the surface production of negative ions, an electron from the Fermi level of conduction band of a metal gets attached to the electron affinity level of a positive ion which moves away from the surface of the metal after reflection or sputtering.
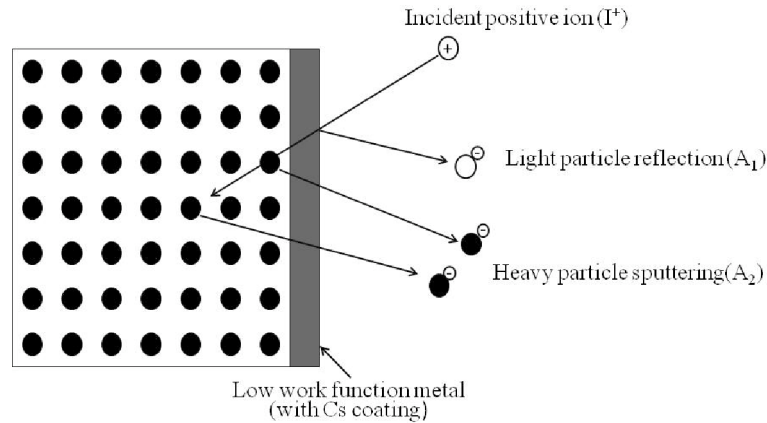
Figure 1.6: *Surface production of negative ions*

$$A^{+}+2e \rightarrow A^{-}$$
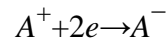
For lighter particles, reflection from the metal surface is a common process. The probability of formation of negative ions due to reflection ($P^{-}(v)$) has been theoretically given by Rasser et al [46].

$$P^{-}(v) = \frac{2}{\pi}\exp\left[\frac{-\pi(\varphi - E_a)}{2v\cos\Theta}\right]$$ (1.9)

where φ is the work function of a metal, E_a is the electron affinity, Θ is the angle of ejection and v is the velocity of the emitted particle. From the above equation, it is clear that probability of the formation of negative ions can be enhanced by using the low work function target metals.

The work function of a target metal surface can be lowered if the surface is coated by another low work function metal such as alkali or alkaline earth metal. The minimum value

of effective work function of the coated metal surface is lower than the work function of the deposited material. Ceasium has the lowest work function (1.81 eV) of all the elements, and therefore it is frequently used to obtain a low work function metal surface for the enhanced production of negative ions by surface process.

1.4.3 Negative ion destruction mechanism

The loss of a negative ion occurs due to the detachment of the single or double electron. The negative ion then becomes a neutral or positive ion. Most common negative ion destruction reactions are listed below.

$$X^- + e \rightarrow X + 2e$$ Electron detachment by fast electron

$$X^- + Y^+ \rightarrow X^* + Y^*$$ Mutual neutralization

$$X^- + Y \rightarrow X + Y + e$$ Collisional detachment
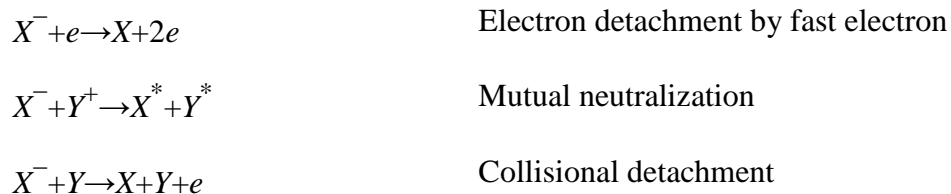
The value of electron detachment cross section increases with the pressure. For hydrogen negative ion, at the gas pressures of 10^{-2} Torr or above, no negative ion can survive. The negative ion survival percentage for 10^{-3} Torr and 10^{-4} Torr is 50% and 93% respectively.

Chapter 2 - Electric probes for negative ion diagnostic

2.1   Introduction

Information about the state of the plasma is obtained by means of a wide variety of plasma diagnostic tools. The most basic ones include measurements of voltage and current through the plasma, photography etc. Other, more sophisticated tools are electric probes, optical and mass spectrometry. Of these, measurement of plasma properties with electric probes is the oldest and most often used techniques. The advantages of probes over other diagnostics techniques are as follows.

1. The experimental arrangements are simple, require lesser space and can be easily fabricated in laboratories.

2. The physics of probe techniques is relatively simple and less complex. Therefore, the raw data obtained from the probe can be processed to determine the range of plasma parameters e.g. plasma density, plasma potential, electron temperature.

3. One of the most important features of probe technique is their ability to perform the time and space resolved measurements of the plasma parameters.

Here we are primarily interested in the local measurement of plasma parameters. Therefore the electrical probes were the obvious choice.

Although electric probes are popular for the reasons highlighted above, the negative ion density can only be obtained indirectly from the electron density and positive ion density measured by the probes. This chapter describes different probe techniques applied for the characterization of plasma parameters in Constricted Hollow Anode Plasma Source (CHAPS).

2.2   The Langmuir probe

The Langmuir probe is the most simple and commonly used method to measure almost all the important plasma parameters. Its construction is relatively simple comprising of a small conducting electrode inserted into the plasma. The electrode is either planar, cylindrical or spherical in shape and made up of high melting point metal such as tungsten or molybdenum. The potential on the electrode is varied by the external voltage source and current collected by the probe is measured as a function of applied bias. The current voltage (I-V) characteristic of the probe is thus obtained from which a number of important plasma parameters are obtained such as ion and electron densities, floating potential, plasma potential and electron temperature as well as electron and ion energy distribution functions.

There are three main sections of the current – voltage curve, namely ion saturation, transition and electron saturation regions. Section 2.2.1 describes the theory of the Langmuir probe to interpret the three regions of the IV curve and deduce the information

about the important plasma parameters. Before that we briefly discuss some of the important plasma parameters.

Plasma potential (V_p): It is defined as the potential at which all electrons arriving near the probe are collected and the probe current equals the electron current. If the probe is at the plasma potential, the perturbation it induces to the free ion and electron current is very small. The plasma potential is essentially the electric potential in the plasma in the absence of the probe.

Floating potential (V_f): If the probe is electrically isolated from the others parts of the plasma reactor i.e if the probe is floating, the probe gets negatively charged due to the higher flux of electrons as compared to positive ions. As the probe charges negatively with respect to plasma, the electron flux decreases and ion flux increases. The probe attains a potential at which the electron flux is repelled just enough to balance the ion flux. This potential (which is negative with respect to plasma) is floating potential.

In the current–voltage characteristics of the Langmuir probe, the plasma potential is at the boundary of electron saturation and transition region, while the floating potential is at the edge of ion saturation and transition region.

2.2.1   Theory of Langmuir probe

Langmuir and Mott-Smith first developed the basic theory to interpret the IV characteristics of the Langmuir probe[47]. Following are the basic assumptions of this theory.

1. The electrons follow Maxwell – Boltzmann velocity distribution

2. The probe does not perturb the plasma and that

3. Every particle which enters into the sheath is collected by the probe.

Let n_e is electron density in the undistributed plasma at potential V_P and n_0 is electron density in the immediate vicinity of the probe surface at potential $V_B < V_P$ then from the Boltzmann relation [9]

$$n_e = n_0 \exp\left(\frac{V_B - V_P}{T_e}\right) \tag{2.1}$$

The electron current (I_e) collected by the probe surface of area A in this region given by

$$I_e = \frac{1}{4} e n_0 \overline{v_e} A \exp\left(\frac{V_B - V_P}{T_e}\right) \tag{2.2}$$

The total current to the probe in the transition region is the difference between the electron current and the ion current.

$$I + I_i = I_e = \frac{1}{4} e n_0 \overline{v_e} A \exp\left(\frac{V_B - V_P}{T_e}\right) \tag{2.3}$$

At $V_B = V_P$, the exponential term in above equation vanishes. Also at V_P the ion current collected by the probe is zero. Therefore we get the electron saturation current given by

$$I_{se} = \frac{1}{4} e n_0 \overline{v_e} A \qquad (2.4)$$

By dividing and taking logarithm, we get

$$\ln\left(\frac{I_e}{I_{se}}\right) = \frac{V_B - V_P}{T_e} \qquad (2.5)$$

Thus the value of electron temperature is determined from the inverse slope of a plot of *ln I*

against applied probe bias (V_B)

$$T_e = \frac{V_B - V_P}{\ln\left(\dfrac{I_e}{I_{se}}\right)} \qquad (2.6)$$

2.2.2   Measurement of plasma density

Electron density (n_e) and ion density (n_i) are determined by knowing the I_{se} and I_{si} from IV

curve of the Langmuir probe. For the Maxwellian electrons, mean electron velocity is given

by $\overline{v_e} = (8e T_e / \pi m)^{1/2}$. Therefore,

$$n_e = \frac{I_{se}}{eA\left(\dfrac{8e T_e}{\pi m}\right)^{1/2}} \qquad (2.7)$$

For cold plasmas, $T_i \ll T_e$, the ion saturation current I_{si} is independent of the ion temperature and is given by

$$I_{si} = e n_i A u_B \qquad (2.8)$$

where u_B is Bohm velocity given by $u_B = (e T_e / M)^{1/2}$. Thus

$$n_i = \frac{I_{si}}{e A \left(\dfrac{e T_e}{M} \right)^{1/2}} \qquad (2.9)$$

The calculation of particles densities from the above equation assumes that the effective area of the probe through which the probe collects the particles is known. However, the particle collecting area may change significantly depending on the geometry of the probe. In case of cylindrical or spherical probe, due to the expansion of the sheath area, it is difficult to get the exact value of saturation currents and plasma potential which leads to the inaccurate measurements of particle densities.

In case of planar probes, the area of the probe is too large as compared to the sheath thickness such that effective area of the probe is independent of sheath thickness. This helps to the more accurate measurement of I_{se}. However, due to its large collection area, application of positive bias for determining I_{se} strongly perturbs the plasma. Thus the use of planar Langmuir probe is limited only to the measurement of ion density.

2.2.3 Current – Voltage Characteristics of the Langmuir probe

Consider a probe immersed in plasma which consists of only electrons and positive ions and no negative ions. If the potential on the probe is varied we get a current voltage characteristics as shown in figure 2.1. If the probe is floating i.e. no current is collected by the probe, a floating potential is developed on the probe surface which repels the excess flow of electrons and the current contributed by negative and positive charges at the probe becomes equal.
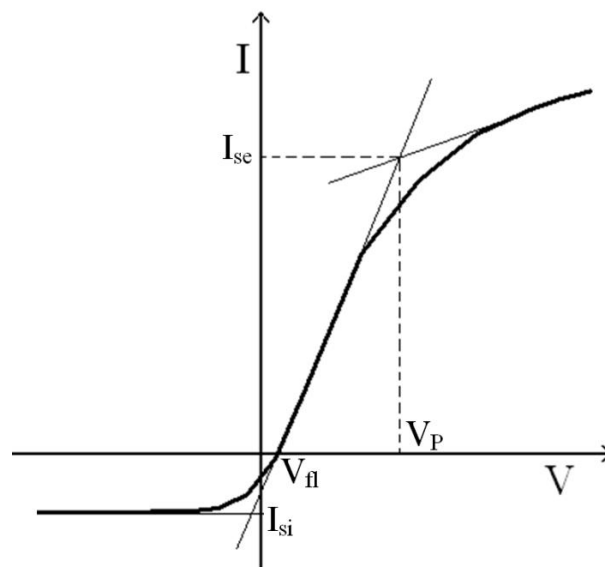

Figure 2.1: *I V characteristics of a Langmuir probe*

When the probe is biased with respect to the floating potential, but negative to the plasma potential, positive ions are repelled and electrons are attracted towards the probe surface.

The net current collected by the probe increases with the applied bias which is given by the Boltzmann distribution. For a perfect planar probe, where collection area is not a function of bias voltage, the ion current is essentially constant for $V_B < V_P$.

At $(V_P - \Delta V)=0$, there is no negative charge on the probe, and the probe attains the same potential as the plasma. In this case no sheath forms and the collection area equals to that of probe tip. Since there is no sheath, electrons and ions are neither attracted nor repelled, they simply collide randomly against the probe tip. Again, because of the higher thermal velocity of the electrons, the probe current is dominated by the electron current. As the bias is increased further, the probe becomes positive with respect to the plasma and electrons are attracted while ions are repelled. Equation 2.4 can be used to calculate the saturation electron current as a function of bias in this region.

The plasma potential lies on the edge of the transition region and the electron saturation region. This is usually seen as a 'knee' in the I-V curve. However in some cases, the knee cannot be defined distinctively. In this case V_P is determined by a linear extrapolation from the electron saturation region and an extrapolation from the transition region. The bias point at which the linear extrapolations cross is V_P. It can also be identified by the peak of the first derivative, or the zero crossing point of the second derivative of the I-V characteristic.

If the probe is biased sufficiently negative with respect to floating potential, ion current dominates as electrons do not have sufficient energy to cross the sheath and be collected on

the probe. Ion saturation occurs when a further increase in negative potential does not increase the collected current.

The ion current is independent of the probe bias and is determined by the product of density at the sheath edge and the Bohm's speed of ions entering the sheath. For obtaining the positive ion saturation the probe must be biased to strong negative potential to minimize the contribution of energetic electrons from the tail of the Maxwellian distribution.

In case of cylindrical probes, in the ion saturation region, collection area increases as a function of bias due to sheath expansion. Therefore as ion saturation approached, more current is collected, and so, incomplete saturation occurs.

For an ideal planar probe, whose sheath width expands with sheath voltage, but sheath area remains constant, the collection area of the probe does not change throughout the I-V characteristic.

For ideal planar probes, as the bias on the probe increases, the sheath expands but the sheath area remains constant. Therefore the accurate measurement of positive ion density is possible. In practice, the ion saturation is rarely seen due to edge effects and also hemispherical distortion of the sheath edge as a function of bias voltage. Guard rings are often used to reduce edge effects, thus allowing planar probes to produce I-V characteristics with more complete saturation regions.

2.3 Planar Langmuir probe (Ion flux probe)

As mentioned in section 2.2, measurement of ion density by planar Langmuir probe is one of the more accurate and simple techniques. Figure 2.2 shows the construction of the planar probe which is used to measure ion density in our experiments. A probe consists of metallic disk of diameter 1.75 mm. The disk is biased negatively by using an external stabilized power supply. The ion current collected by the disk is measured by measuring the voltage drop across the resistor (0.1-1 kΩ) connected between the battery and the ground.

The ion density (n_i) is calculated from the ion saturation current (I_{sat}) using the formula

$$n_i = I_{sat} / A\sqrt{eT_e/M} \tag{2.10}$$

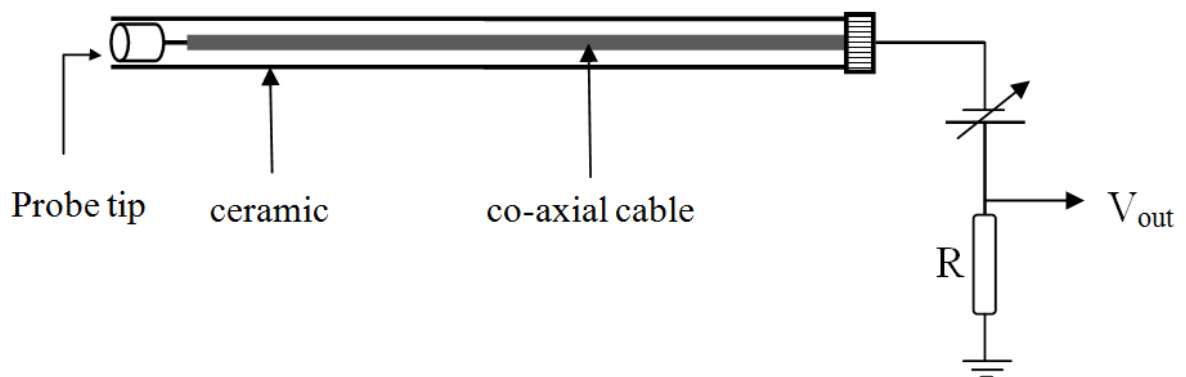where A is the area of the planar probe.

Figure 2.2: *Planar Ion flux probe*

For low temperature plasmas, the value of electron temperature lies in the range of 1-5eV, thus advantage of this technique is that it gives a reasonable estimate of ion density without knowing the exact value of T_e.

2.4 Plasma potential measurement by floating emissive probe

The measurement of plasma potential by Langmuir probe is carried out by finding the electron saturation current. As mentioned in section 2.2 which describes I-V characteristics of Langmuir probe, obtaining the accurate value of electron saturation current is practically difficult and therefore we have to find a 'knee point' on the current-voltage characteristics corresponding to the ion saturation current and the plasma potential. There are two major challenges in the measurement of plasma potential by Langmuir probe.

A highly positively biased Langmuir can disturb the plasma by drawing a large electron current.

It is difficult to find the exact 'knee point' corresponding to V_p due to some reasons such as fluctuations in the plasma potential or the existence of magnetic field.

The difficulties mentioned above can be overcome by using the 'emissive probe'.

2.4.1 Basic principles of emissive probe

The plasma potential is potential at which all the electron arriving near the probe are collected and therefore the potential difference between the probe and plasma is zero. This

can be achieved by biasing the probe or by simply making the probe emit electrons thermionically such that at an equilibrium value the random electrons received by the probe becomes equal to the electrons emitted thermionically from the probes surface [48, 49].

The emissive probe consists of a thin electrically floating wire. When the wire is placed inside the plasma it acquires the potential corresponding to the floating potential so as to balance the electron and ion flux to the probe. If the floating wire is sufficiently heated by passing the current through it then the wire starts emitting electrons. The energy of the emitted electrons is equal to $k_B T_W/e$ where T_W is the temperature of the wire. If the plasma potential is higher than the potential on the probe, then the electrons move to the plasma from the probe and thus the current flows towards the probe from the plasma. However, if the probe is floating (which means no current is flowing through the probe) the potential on the probe is developed which is equal to the plasma potential V_p. The uncertainty in the measurement of V_p by this method is of the order of $k_B T_W/e$ which nearly equal to 0.15 V.

2.4.2   Construction of the emissive probe and its circuit.
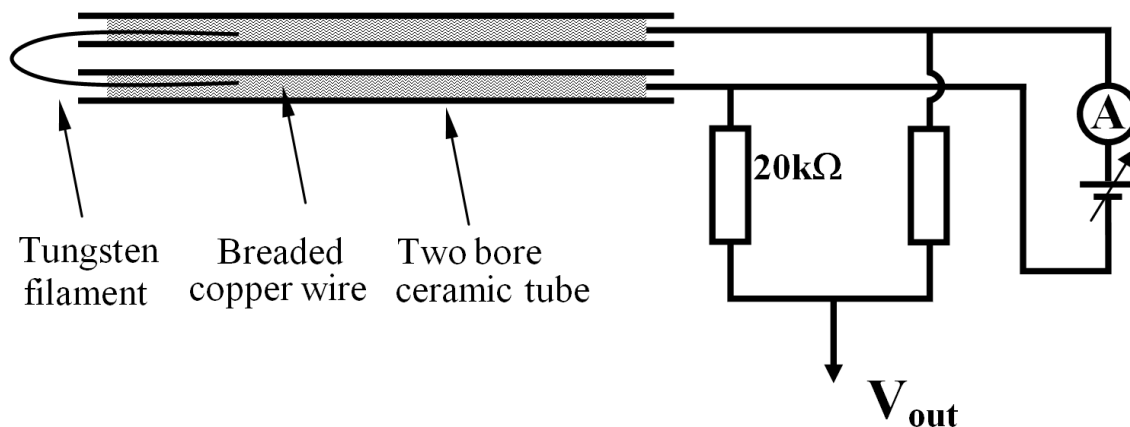
Figure 2.3: *Emissive probe*

The construction of the emissive probe is shown in figure 2.3. The probe consists of a fine

'V' shaped tungsten filament with radius 0.03 mm immersed the two bore ceramic tube.

The breaded copper wires inside the ceramic bores make good electrical contact with the

tungsten filament. The filament is heated by passing 2.0 A current through the regulated

constant current power supply. The potential (V_E) developed at the filament with respect to

ground is measured across the two 20 kΩ resistors connected to the two ends of the

filaments. When the filament is cold, V_E corresponds to the floating potential (V_{fl}) and for

hot filament, V_E corresponds to the plasma potential (V_p). The difference between the

floating potential and the plasma potential is the function of electron temperature (T_e) given

by

$$(V_p - V_{fl}) = T_e \ln\left(\sqrt{\frac{M}{2\pi m}}\right) \tag{2.11}$$

where M and m are ion and electron mass respectively.

2.5 Resonance hairpin probe for the measurement of electron density

A straightforward method of measuring electron density is by using a hairpin probe. This technique was investigated by Stenzel and Gould in mid 1970's and has attracted some renewed interest in recent years [50-52]. The principle is based on measuring cold plasma permittivity by imposing a time varying electric field in the plasma using a resonance wire in the shape of U. The U shape of the probe provides a most simple microwave resonator which consists of a parallel transmission line opened at one end and short-circuited on the other end. The resonance frequency depends on the length of the probe and the dielectric constant surrounding the probe tips. The resonating frequency (f_r) is given by

$$f_r = \frac{c}{4L\sqrt{\varepsilon}} \tag{2.12}$$

where c is the speed of light, L is the length of the transmission line and ε is the dielectric constant of a medium in which the transmission line is placed. With typical probe length of $L=3$ cm, the resonance frequency in vacuum f_o is found by taking ε is 1 to be 2.5 GHz falls in the microwave range.

In the case of unmagnetized plasma, the plasma dielectric constant is given based on cold plasma permittivity by

$$\varepsilon = \left(1 - \frac{\omega_p^2}{\omega^2} \right)$$

(2.13)

where ω_p is the electron plasma frequency.

The plasma permittivity in the case of unmagnetized plasma is always less than one. Therefore plasma permittivity increases with the electron density increases. Therefore according to eq. 2.12 the resonance frequency will shift to higher frequency. The difference between the f_r values in vacuum and in plasma is directly related to the electron density (n_e) of the plasma given by the relation

$$n_e = \frac{f_{r\_plasma}^2 - f_{r\_vacuum}^2}{0.81} \quad (10^{10} \ cm^{-3}).$$

(2.14)
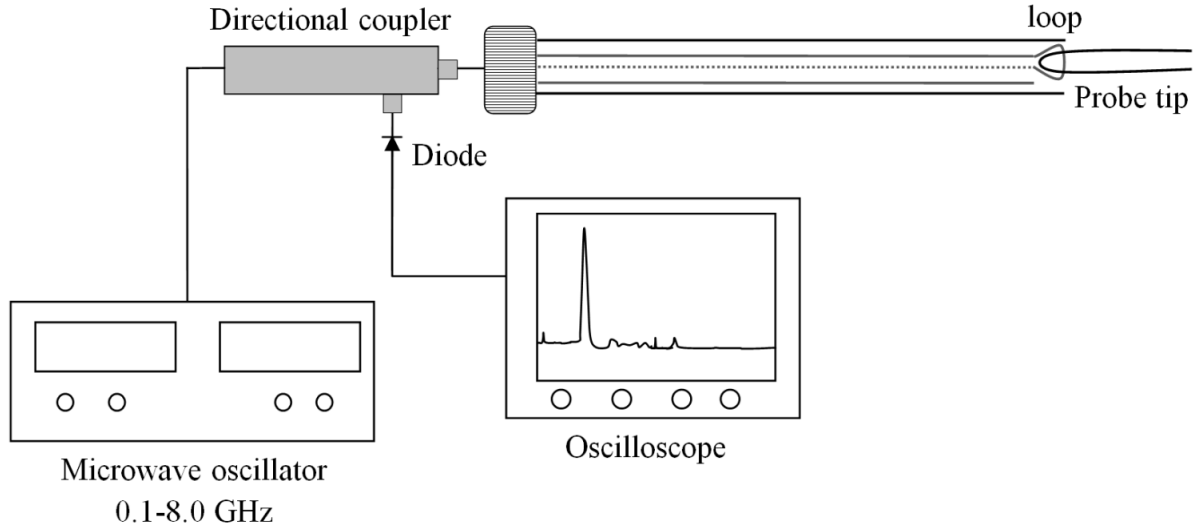
(a)

(b)

Figure 2.4: (a) *Microwave resonance hair-pin probe set-up for the measurement of electron density* (b) typical assembly of hairpin probe

A schematic of the hairpin probe setup and typical probe assembly is shown in figure 2.4. The hairpin probe system consists of a 50 Ω coaxial line with a tiny loop antenna at one end. The coaxial line and the loop are covered by ceramic tube. The hairpin probe tip, which is made up of either molybdenum or tungsten, is placed in the proximity of the loop as shown in the figure 2.4. The hardware consists of (a) scanning microwave source, (b)

directional coupler for measuring the reflected part in the coaxial line to which the loop is attached, (c) a diode for measuring the r.m.s value of the reflected power at each frequency and (d) an oscilloscope.

As the frequency is swept from typically 2-8 GHz, the reflected power is found to vary in amplitude and at the resonant frequency the amplitude drops significantly. In this way the resonance frequency can be identified. The electron density is then calculated by knowing the value of f_r in vacuum and in plasma using eq. 2.14.

L shaped hairpin resonance probe

The typical hairpin probe is 3.0 cm long and therefore spatial resolution of the hairpin probe is on the order of centimeters. However experiments planned in the thesis required a resolution on the order of a millimeter. Therefore a modified geometry of the hairpin probe is used. In this modified geometry, a loop is bend by 90° with respect to the co-axial line and a hairpin probe tip placed parallel to the loop and perpendicular to the coaxial line. This modified geometry is called as 'L shaped' hairpin probe which is shown in figure 2.5. Since the width of the hairpin wire is about 0.25 mm therefore we could achieve the probe resolution in the plane of the probe tip on the order of 0.1 mm. The typical error in the measurement of n_e by hairpin probe is less that 5%.
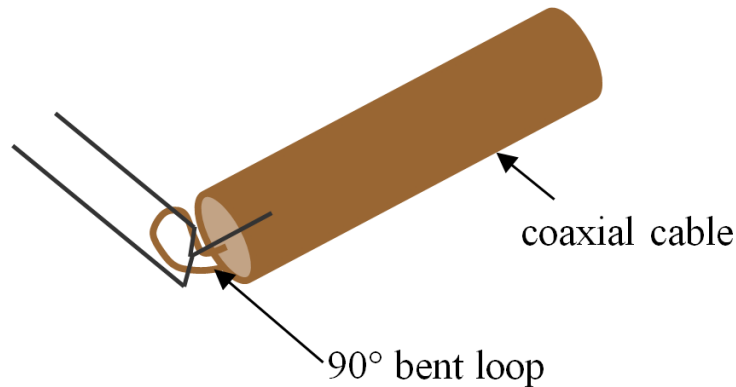
Figure 2.5: *Scematic of L shaped hairpin probe*

The hairpin probe is floating. Therefore sheath around the probe tips is on the order of 0.1 mm for electron density of 10^{10} cm^{-3} and Te ~ 1 eV . The width of the hairpin probe is 3.0 mm. In comparison that the sheathwidth around the tips can be neglected.

2.6   Measurement of negative ions using electrical probes

The Langmuir probe technique described in earlier section is directly used to diagnose the electropositive plasmas. Some of the most important features of Langmuir probe or in general, electrical probes are (a) the localized measurement of the plasma parameters, (b) easy instrumentation and (c) well developed plasma sheath theory which enables the accurate measurement of plasma parameters. However use of Langmuir probe in the electronegative plasmas is not straight forward. In this case, the negative ions contribute to the probe current as well as their presence in the discharge presence in the discharge influences the Bohm speed. This leads to inaccurate measurement of plasma parameters from the current-voltage characteristics of the Langmuir probe [53, 54]. The negative ions

diagnostics by mass spectroscopy technique requires the extraction of negative ions from the discharge. However in the presence of positive plasma potential, negative ions are confined in the plasma and therefore mass spectroscopy technique is limited to only pulsed plasmas[55].

One important method of extracting information of negative ion density and temperature is the pulsed laser photo-detachment technique and is widely used to characterise the electronegative plasmas. This technique is based on removal of electrons from the negative ions by irradiating laser beam and have been studied extensively [56-58]. In the probe assisted laser photo-detachment technique, negative ions are irradiated with the pulsed laser beam. The energy of the laser beam is greater than the electron affinity of the negative ion so that the electrons attached to negative ions are stripped off [59]. The negative ions density is then inferred from the time resolved measurement of excesses electrons by Langmuir probe. Recently hairpin probe has been successfully used in conjunction with laser photo-detachment to measure the negative ion density [60, 61].

Although probe assisted laser photo-detachment give quantitative measurement of negative ions; the technique demands expensive and complicated apparatus. Also, this technique can measure the line of sight integrated negative ion density [62] and therefore spatially resolved measurements are difficult. In the present study, the choice of negative ion diagnostic technique to characterise the electronegative discharges in the constricted plasma sources is very crucial. The focus of the study is to understand the formation and transport of negative ions in the constricted plasma source and which requires the measurement of

the localised plasma parameters. Therefore the choice of laser based technique is obviously excluded.

2.6.1   A two probe technique

In the quest of using the Langmuir probe for negative ion diagnostics, previous works by Boyd and Thomson[53], Braithwaite and Allen[54], Amemiya [63], and Chabert et.al[64] have provided a good a foundation to understand the sheath formation around the Langmuir probe in low pressure electronegative plasma. According to the theories described in the above literature, the saturation current above the plasma potential is given by

$$I(V_p) = Ae\left[n_e\left(\frac{kT_e}{2\pi m}\right)^{1/2} + n_-\left(\frac{kT_-}{2\pi M_-}\right)^{1/2} + n_+ v_{+th} \right]$$

Where A is the probe area, T_e, T_- are the electron and negative ion temperatures and v_{+th} is the ion thermal speed. The positive saturation current is given by

$$I_{sat}^+ = Ae\Gamma_+(\alpha, \gamma, n_e)$$

Where $\Gamma_+(\alpha, \gamma, n_e) = n_+ v_+$ is the modified Bohm flux to the probe of area A in the presence of negative ions which depends on the values of $\alpha = n_-/n_e$ and $\gamma = T_e/T_-$. Braithwaite and Allen, have proposed that if the values of saturation currents are known, then the negative ion fraction α can be determined from the saturation current ratio $R = I(V_p)/I_{sat}^+$ [54]. Although this technique is experimentally simple and gives relatively precise values of α [65], it requires accurate measurement of electron density and a good model for the positive

ion flux [66]. Chabert et.al have used two different probes to measure the value of α from R. In their studies, one of the probes was a cylindrical probe to collect the electron thermal current at the plasma potential. A planar probe was used to measure positive saturation current and a model was developed to measure the $\Gamma_+(\alpha,\gamma)=n_+v_+$ for the plane symmetric discharge. Curley et al further modified this two probe technique in which a hairpin probe is used for the measurement of electron density.

In our investigations, we have followed the two probe technique, in which the hairpin probe is used to measure n_e while a planar Langmuir probe, as described in section (3.3), is used to measure the positive ion flux. However, unlike Chabert and Curley's work where n_+ is determined from i_+ using the theoretical model, we have used a more straight-forward, experimentally feasible probe evaluation method [67]. In this method, hairpin probe and planar Langmuir probe are compared in the stable electropositive argon discharge as follows.

The ion saturation current for planar Langmuir probe is

$$I_{sat}^+ = eA_p n_+ \sqrt{\frac{kT_e}{M}} \cdot F \qquad (2.15)$$

Where A_p is the probe area and F is the factor which depends on set of parameters such as expanded sheath area, effect of fast electrons on ion saturation current etc. For electropositive plasma, $n_+=n_e$, hence the value of n_e measured by using hairpin probe is put in the above equation to determine F as

$$F = \frac{I_{sat}^{+}}{eA_p n_e \sqrt{\frac{kT_e}{M}}}$$

(2.16)

The value of electron temperature required in the above equation is inferred using emissive probe as described in section 2.4.

For the electronegative plasmas, it is assumed that the small value of $\alpha(< 2)$ and γ (~ 10 - 15) does not significantly affect the positive ion saturation current and therefore the same constant factor F is used to determine n_+.

$$n_+ = \frac{I_{sat}^{+}}{eA_p \sqrt{\frac{kT_e}{M}} \cdot F}$$

(2.17)

The value of n_- is determined by considering the quasi-neutrality condition $n_+ = n_e + n_-$ and electronegativity is calculated as $\alpha = (n_-/n_e) = (n_+/n_e) - 1$.

Calibration of planar Langmuir probe with Hairpin probe

The experiments to measure negative ion density by two probe technique described in this section are performed in an inductively coupled plasma source, BARIS (Basic Radio-frequency Ion Source) in Dublin City University. Argon and argon-oxygen gases are used to create electropositive and electronegative plasmas. The RF power is varied from 50 – 400 W at the constant pressure of 1.3 Pa. A hairpin probe and planar Langmuir probe are

simultaneously introduced in a discharge. The probe tips of both probes were at equal distance from the RF coil.

Figure 2.6 shows the graph of n_e measured by HP and $I_{sat\ t}^{+}$ measured by PP in the argon discharge. Both the electron density and ion density increase monotonically with power and pressure. The figure also shows the corresponding values of F power which are determined by using eq 2.16. From the figure, we see that F is almost constant with the applied RF power and lies between 0.71 to 0.77 with the average value of 0.74.
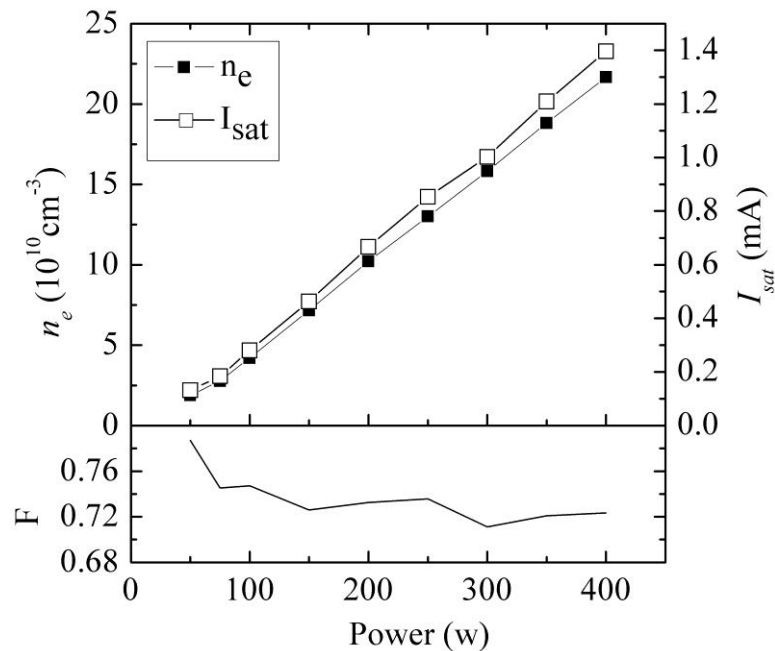

Figure 2.6: *Graph of n_e, I_{sat} and the factor F for the argon discharge operated at 1.3 Pa*

The graph in figure 2.7 shows the effect of applied power on electron and ion density for the Ar-O_2 (1:1) discharge. The positive ion density, n_+, plotted in the graph is calculated

from equation 2.15 and by putting $F = 0.74$. The negative ion density is computed by taking the difference in n_+ and n_e and is plotted in figure 2.8. As is seen from the figure, the negative ion density increases monotonically with the applied power and it is in the range of 10^{10} cm^{-3}. Figure 2.8 also shows the electronegativity (α) plotted as function of applied power which is as high as 1.4 for 50 W power and decreases to ~ 0.4 with increase in power up to 200 W. After 200 W, the value of α saturates to 0.35.
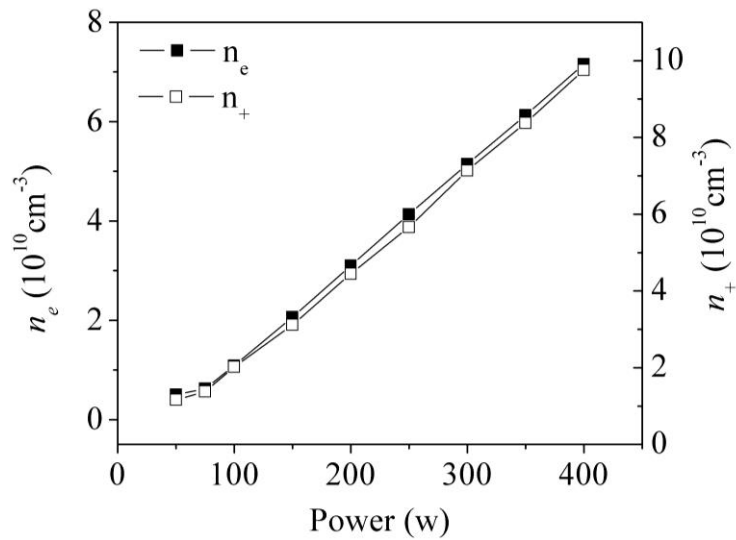

Figure 2.7: *Variation of n_e and n_+ with power for Argon – oxygen plasma operating at 1.3 Pa*
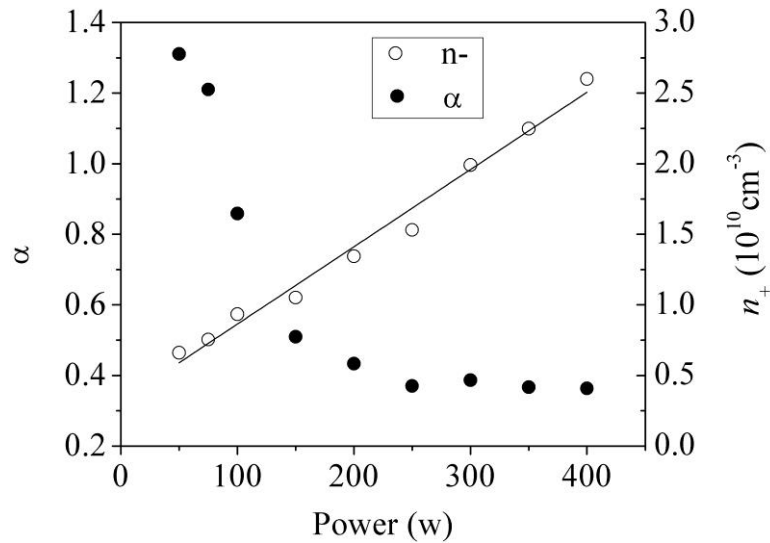
Figure 2.8: *Electronegativity (α) and negative ion density (n_-) versus power for argon – oxygen plasma operated at 1.3 Pa*

The measurements of n_- and α in the same experimental reactor (BARIS) have also been carried out by Conway et. al for the similar power conditions (5- 500 W) and at 4 Pa in the oxygen discharge[60]. Those experiments were performed using hairpin probe and laser photo-detachment technique and hence their data was more accurate as compared to our experiments. The typical behaviour and the values of negative ion density and the electronegativity of the Ar-O_2 discharge with power as obtained by the two probe technique resemble to the hairpin probe assisted laser photo-detachment technique. Therefore the two probe technique is later used for the investigations on the electronegative discharges which are described in details in chapter 5.

2.7   Summary

In this chapter, we presented the usefulness of electric probe techniques to measure the gross plasma parameters. A detailed description of Langmuir probe, emissive probe and hairpin probe has been given in order to simplify the understanding of the electric probes. A comparative study is carried to out to calibrate the planar Langmuir probe with the more accurate hairpin probe. A two probe technique comprising of these two probes is designed to estimate the negative ion density and the electronegativity of the oxygen discharge. This two probe technique is not only simple and accurate but it gives good information about the local plasma parameters.

Chapter 3   Anodic glow in constricted hollow anode plasma source

3.1   Introduction

The negative ion production and loss mechanism depends on the electron temperature. The operating pressure of the plasma governs the electron temperature. Therefore, the basic need in the present investigation is creating a broad spectrum of electron temperature in a discharge without varying the given plasma conditions e.g. operating pressure. It is well established that the double layer structures in plasma are characterised by distinct electron temperature regions. Such double layer structures have been observed in space plasmas [68] and also in laboratory plasma such as in RF plasmas expanding in a bigger chamber[69], in double plasma machines [70, 71], in a quenched discharge tube [31]. The presents study focuses on creating and investigating an anodic glow as a double layer structure.

Anodic glow is a term used for describing a luminous glow around the anode of a DC discharge. In ordinary parallel plate discharge the glow is confined in the cathode region due to energetic electrons releasing from the cathode surface. However, in special case, if

the area of the anode is restricted, then enhancement in the current density at the anode surface leads to localized ionization at the anode sheath which becomes accelerating for the electron. Anodic Glow is also observed in the case of a Langmuir probe when biased at higher potential than the plasma potential [13, 30, 33, 34].

This chapter describes a DC anodic glow created by reducing the effective area of the anode. It has been observed that if the area of the anode is reduced sufficiently, a bright luminescent glow appears in front of the anode. A systematic study is presented with different anode sizes and its impact on the global discharge properties. This chapter also describes the properties of the anodic glow and its influence on the overall DC plasma properties.

3.2   Experimental Set-up

The constricted hollow anode plasma source (CHAPS) is a plasma device which is designed and developed to generate the double layer structure in front of the anode. The source uses a series of parallel plate cathode in conjunction with a small cylindrical anode whose outer surface is insulated from the plasma. The basic concept behind CHAPS is inspired from the constricted anode plasma source which comprised of a large cylindrical grounded vacuum chamber as cathode while anode is a solid stainless steel rod insulated from the ground and vacuum chamber[72]. Since the cathode was grounded the typical plasma potential in that system was on the order of 1kV. Therefore measurement of plasma parameters required specially designed probes.
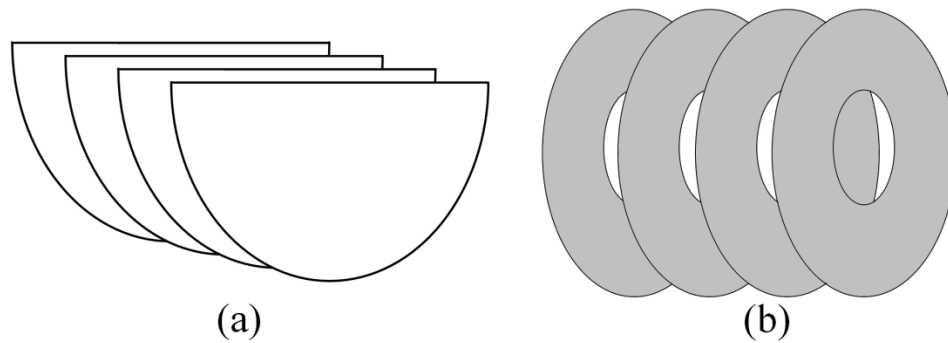
Figure 3.1*: Schematic of different cathodes. (a) Semicircular cathode plates (b) annular cathode plates*
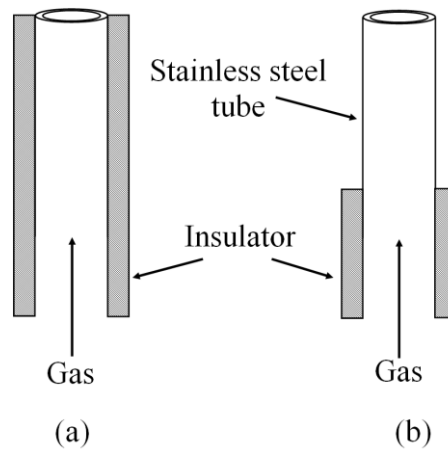
Figure 3.2: *Schematic of the constricted anodes, (a) small anode and (b) relatively large anode area achieved by shortening the length of the outer dielectric cylinder.*

In comparison, the CHAPS consists of the parallel plate cathodes geometry which is insulated from the grounded chamber. The cathode plates are either in the form of semicircular stainless steel plates or is an annular circular plate assembly as shown in figure 3.1(a) and (b) respectively having diameters 20 cm which are designed to fit inside a cylindrical vacuum chamber of inner diameter 22 cm which leaves a gap of approximately

1 cm from the grounded plasma chamber. The length of the vacuum chamber is 30 cm therefore typically four plates with the plate separation of about 5 cm are used as cathode. The motivation behind the use of multiple parallel plates is to achieve the plasma uniformity over the arbitrary area. The semi-circular cathode plates are designed to obtain the plasma uniformity above the cathode plates; while annular plates are used to achieve uniform plasma at the center of the cylindrical vacuum chamber. The anode in CHAPS is a differentially pumped cylindrical hollow anode, made up of stainless steel tube having inside diameter of 4 mm and 10 mm outer diameter. The anode is inserted in the plasma chamber from one of the ports equipped with a vacuum feed through which has several kV's insulation to ground. The outer surface of the anode is insulated using a ceramic macor tube as shown in figure-3.2(a). The length of the ceramic tube can be adjusted to increase the effective surface area exposed to the plasma as shown in figure 3.2(b).

The cylindrical 304 stainless steel vacuum chamber is fitted to rotary and turbo molecular pumping. A base pressure of 10^{-6} mbar (10^{-4}Pa) is achieved before either one of the working gases He, Ar, N_2 were gradually introduced through the anode via a mass flow controller. The operating pressure inside the chamber is kept in the range of 0.5 to 10 Pa. This can be achieved by reducing the pumping speed by a manually operated gate valve at the mouth of the pumps, and also by regulating the flow rate.. In some cases the gas is also fed directly into the vacuum chamber via one of the ports equipped with gas feedthrough Figure-3.3 shows the schematic of the setup and the respective positions of the electrical probes that are introduced inside the plasma chamber for characterizing the plasma properties. The position of the anode is independent with respect to the cathode plates. The
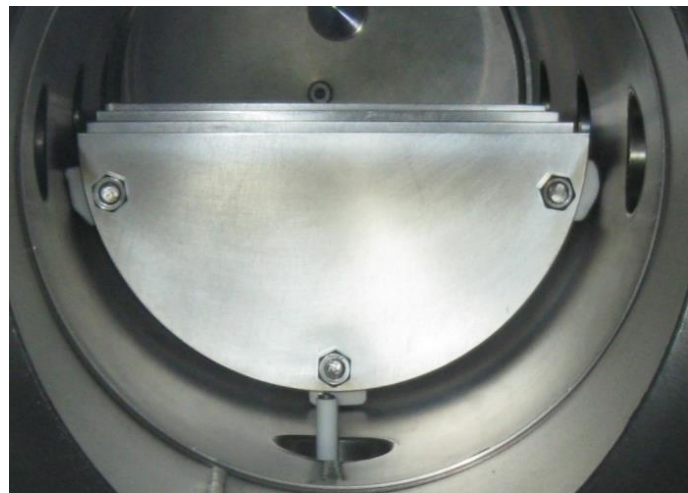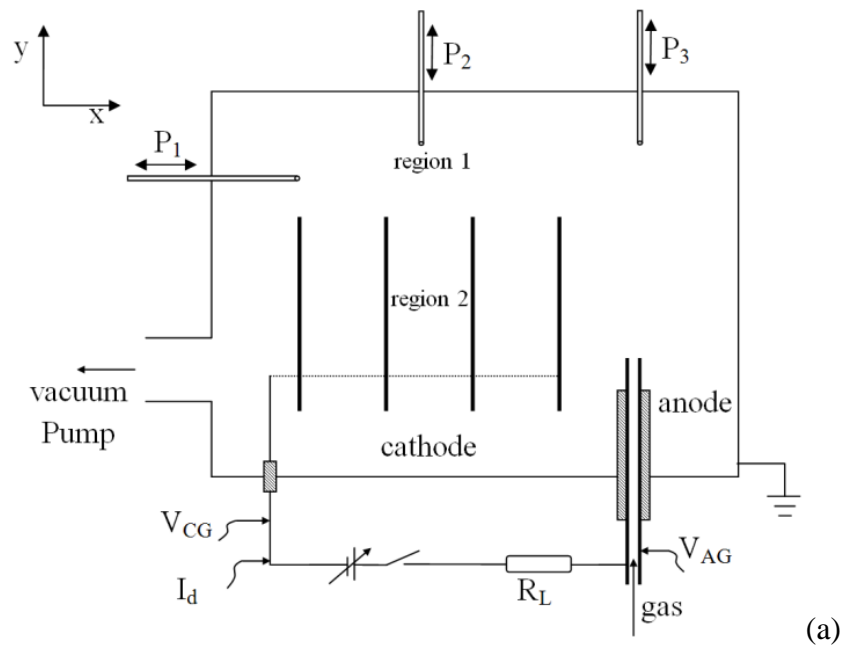
(a)

(b)

Figure 3-3: *(a) A constricted anode - hollow cathode plasma source; P_1, P_2, P_3: Position of the probes (Hairpin probe / Emissive probe/Langmuir probe); V_{CG}: cathode voltage drop with respect to ground, V_{AG}: cathode voltage drop with respect to ground; I_d: discharge current. (b) Photograph of the plasma system showing the position of electrodes*

parallel plate cathodes in the CHAPS provide conditions similar to hollow cylindrical cathodes. The secondary electrons produced by the bombardment of positive ions are trapped between the opposing ion sheaths of the adjacent plates resulting in an efficient plasma production at low pressures.

For creating the plasma, a non-regulated type DC power supply is designed which comprises of a 6 kW, 50 Hz transformer. The output of the secondary is 1.5 kV rated at a maximum peak current of 4 A. The output voltage is increased up to 3 kV using a simple voltage doubler circuit which gives up to 2 A of continuous discharge current. The details of the power supply are described in Appendix 3. The electric potential of the cathode V_{CG} and the anode V_{AG} are measured using the Tektronix high voltage probes (model P6015a) with respect to the grounded chamber. The anode to cathode voltage difference is obtained by subtracting the V_{AG} from V_{CG}. The discharge current I_d is measured as shown in figure 3.3 using a Tektronix current probe (model TCP 202). With the plasma in contact with the grounded chamber allows one to measure the potential difference between the anode and ground with respect to the ground. The potential of the plasma is found to be close to few volts above the ground.

The plasma parameters such as electron temperature and electron temperature are measured using hairpin probe and Langmuir probe and emissive probe.

3.3   Experimental results

In the CHAPS, the working gas is injected through the anode and pumped out from the plasma chamber. Therefore the configuration helps in maintaining a large differential pressure inside the anode. The neutral pressure in the main plasma chamber remains typically 1 Pa – 10 Pa. By applying continuous DC electric potential between the cathode and the anode, we obtained efficient plasma at modest powers (typically 500 W) with density ranging from $1 - 7 \times 10^{10}$ cm^{-3} in different gases such as He, Ar and also molecular gases such as N_2 and O_2. As we increase the potential, we first observe an intense glow engulfing the constricted anode and then the chamber between the electrodes is filled with the plasma. Earlier authors regarded this glow around the anode as a fireball or fire-rod plasma depending on its shape.

3.3.1   Typical picture of the glowing anode

Figure 3.4 shows a typical image of the anodic glow produced in front of the constricted anode. The size of the anode was 30 mm^2 and the size of the cathode was 60000 mm^2. The ratio of the cathode to anode (A_c/A_a)was about 2000. It has been visually observed that the anodic glow is present when $A_c/A_a > 500$. Also the intensity of the anodic glow increase with increase in A_c/A_a. The typical size of the anodic glow is 1.5 cm.
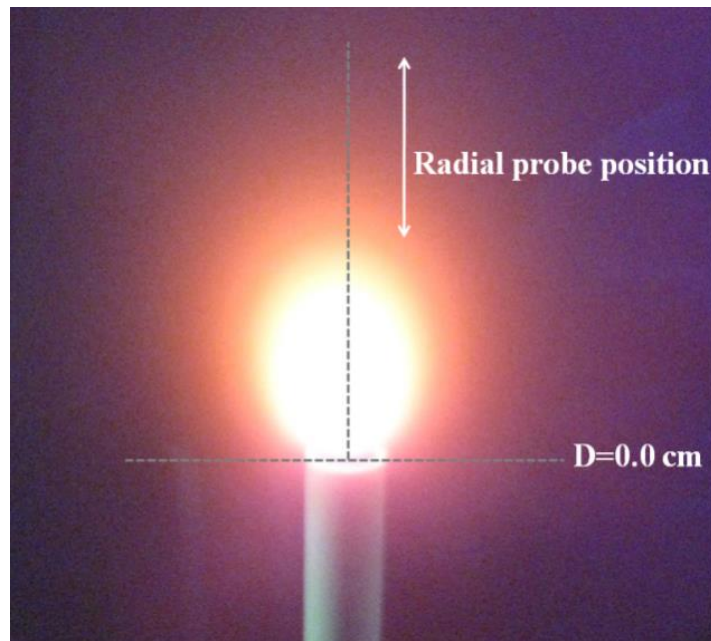
Figure 3-4: *Anode glow in front of the constricted anode produced in a nitrogen discharge operating at 50 W and 4 Pa. Picture also shows the position of the probe in radial direction corresponding to the probe position P3 in figure 3.3(a).*

3.3.2   The role of anode area on the breakdown properties

Figure 3.5 shows the behaviour of the breakdown voltages as a function of effective anode. Four different anode sizes of area 30 mm², 210 mm², 405 mm² and 600 mm² were chosen for the experiment. After the breakdown, for anode area of 30 mm² the anodic glow was well developed; for A_a=210 mm² and 405 mm² , anodic glow was less intense and hazy.
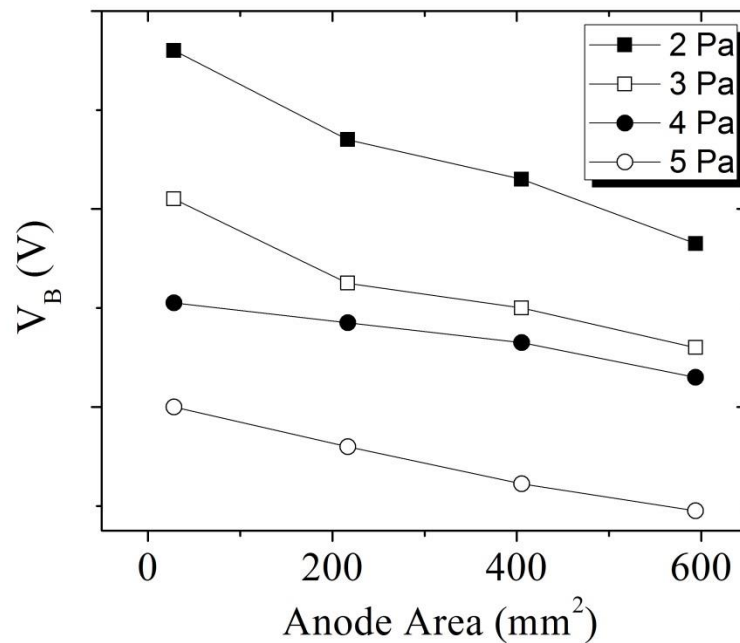
Figure 3-5: *Breakdown voltage characteristics obtained for four different sizes of the anode having surface areas 30 mm², 210 mm², 405 mm² and 600 mm² exposed to the plasma. The working gas nitrogen is introduced through the anode while the flow rate was maintained at 50 sccm and the pressure was varied by adjusting the pumping speed using a manually operated gate valve.*

Figure 3.5 shows the behaviour of the breakdown voltages as a function of effective anode. Four different anode sizes of area 30 mm², 210 mm², 405 mm² and 600 mm² were chosen for the experiment. After the breakdown, for anode area of 30 mm² the anodic glow was well developed; for A_a=210 mm² and 405 mm² , anodic glow was less intense and hazy where as for A_a= 600 mm², the anodic glow was absent. The experiment has been performed for different pressures ranging from 2Pa to 5 Pa of Nitrogen gas.

From figure 3.5 we see that that the breakdown voltage increases on reducing the operating pressure whereas on increasing the effective anode from 30 mm^2 to 600 mm^2 results in 30 % reduction in the breakdown voltage. The increase in breakdown voltage at lower pressure is expected due to the reduction in the electron neutral ionizing collisions. The possible reason behind lowering of the breakdown voltage V_B with increasing anode area is because the energetic electron fluxes at the anode increases with the surface area.

3.3.3   The sustaining voltage and current

Figure 3.6 shows the plot of discharge current versus voltage for N$_2$ gas at an operating pressure of 2Pa. The experiment is performed with two different anodes with areas 30 mm^2 (constricted or small anode) and 500 mm^2 (big anode). It can be seen from the figure that at lower sustaining voltage (up to 700 V) discharge current is equal for both constricted and large area anode. However for sustaining voltages from 700 V to 1250 V, discharge current is higher in case of constricted anode. This result shows that for the fixed power, the constricted anode operates at lower sustaining voltage. This result is particularly important because, as voltage drop across the anode is fixed, lowering the sustaining voltage lowers the voltage drop at the cathode. Therefore lesser amount of sputtering from the cathode takes place on reducing the anode area.
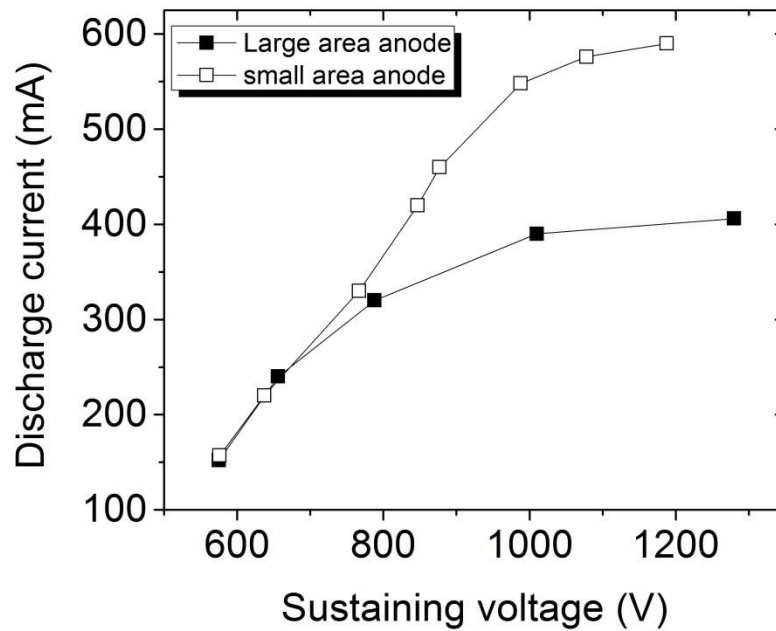
Figure 3-6: *I – V characteristics of a nitrogen discharge operated at a constant 2 Pa pressure shows higher discharge current for a small anode (30 mm^2 area) as compared to the big anode (500 mm^2 area).*

Figure 3.7 and figure 3.8 are the graphs of discharge current and sustaining voltage, plotted against the pressures for values of 2 Pa to 20 Pa for a constricted anode (area = 30 mm^2) and large area anode (area=500 mm^2). The experiment is performed with helium gas at constant power of 400 W. From figure 3.5 it is observed that, in case of constricted anode, discharge current is higher by 20 % as compared with the large area anode. Also the decrease in discharge current with pressure in case of constricted anode is small as compared to the change in the discharge current with the big anode.

Figure 3.8 shows the low sustaining voltage for both constricted and large area anode plasmas for 10 Pa to 20 Pa. However at lower operating pressures, sustaining voltage for large area anode increases rapidly and reaches up to 1200 V. While in case of constricted anode the sustaining voltage rises only up to 400 V.

From figure 3.7 and figure 3.8, it is also evident that gas flow through the anode helps in enhancing the discharge current and reducing the sustaining voltage.
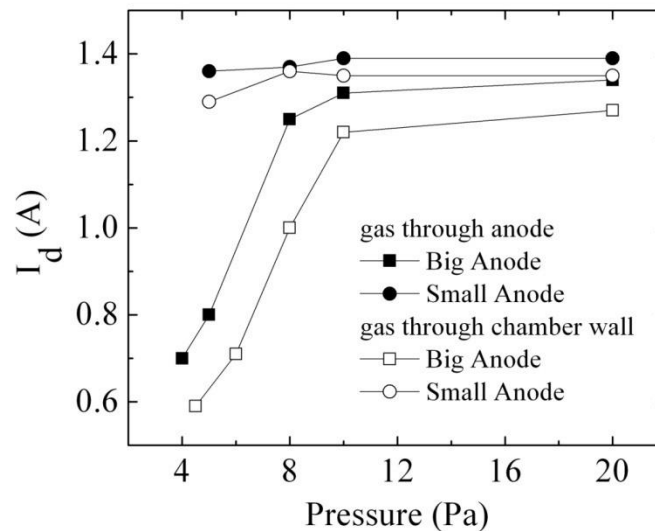
Figure 3-7: *Plot of discharge current verses pressure at a fixed power of 400 W. The working gas is helium, with flow rate 100 sccm. The discharge geometry comprise of 10 annular plates having 2.5 cm separation between the individual plates. The width of each plate is 4 cm. In one case the gas is introduced through the anode while in the other case the gas is directly introduced in to the chamber.*
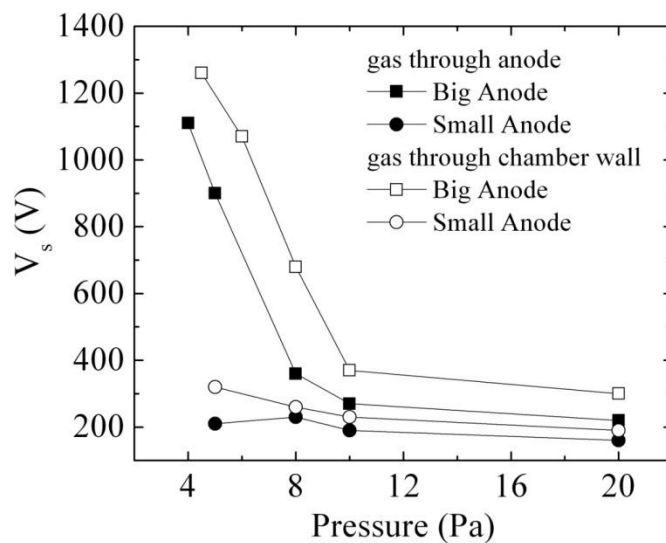
Figure 3-8: *Plot of sustaining voltage as a function of background neutral pressure in the plasma chamber.*

3.3.4 Plasma density dependences on the anode area
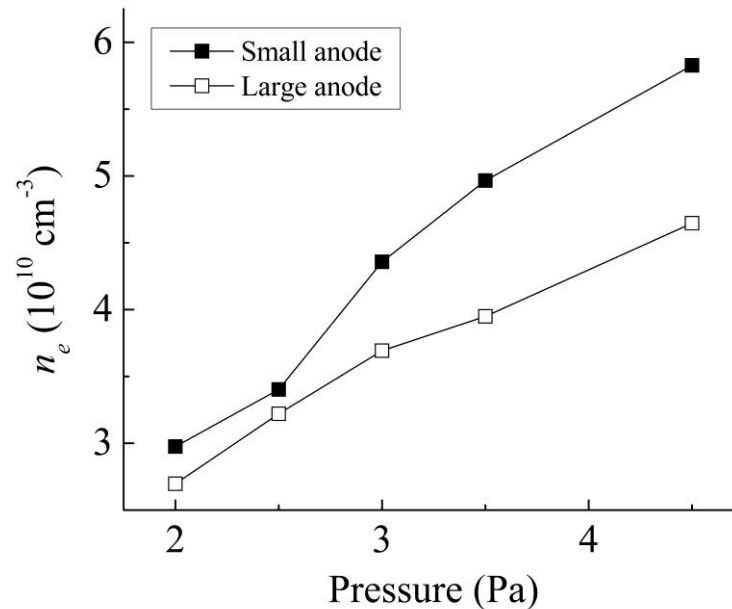
Figure 3-9: *Comparison of electron density outside the cathode plates (region 1 in Figure 3-3) for two anodes having 30 mm² and 500 mm². The operating power was fixed at 400 W.*

Figure 3.9 shows the graph of the bulk electron density which is measured by hairpin probe 4 cm above the semicircular cathode plates (region 1 in figure 3-1) plotted against operating pressure (2Pa to 5 Pa) at the fixed input power 400 W. The data is shown for the small anode (30 mm²) and large anode (500 mm²) and the distance between the cathode plates was d=5 cm. It has been observed that the electron density increases monotonically with increase in the background pressure for both constricted and large area anode and electron density is 20 % higher in case of constricted anode as compared large area anode.

In all above experimental investigations, we studied the effect of anode area on the bulk discharge properties and observed that the area of the anode plays an important role in the determining the bulk plasma properties. The reason for this interesting dependence is definitely the formation of anodic glow in front of the constricted anode. In order to understand this effect it is necessary to study the properties of anodic glow.

3.3.5   Spatial plasma properties in the anodic glow region

This section describes the properties of anodic glow. The glow is formed in an N_2 discharge. The anode area was fixed to the 30 mm^2 with *Ac/Aa* ~ 2000. The distance between the cathode plate wax fixed 5 cm. The radial measurements of plasma parameters are carried out in the anodic region using the probe position P3 as described in figure 3.1 and figure 3.2. The tip of the anode was chosen as zero position.

In figure 3.10, the spatial plasma potential profile and electron temperature profile measured by emissive probe and electron density profile measured by hairpin probe show distinct plasma properties in the anode glow and in the bulk plasma. The results are presented for the discharge operating at fixed input of power of 400 W and at two different pressures of 2 Pa and 5 Pa.

The plasma potential profile illustrates that the bulk plasma potential is about 10 eV which rises to 25 eV inside the anode glow. The transition of plasma potential is rapid and it takes place at D= 1.5 cm which is the boundary of anode glow and bulk plasma. It has been also observed that for 5 Pa pressure the plasma potential inside the anodic glow has a flat profile.
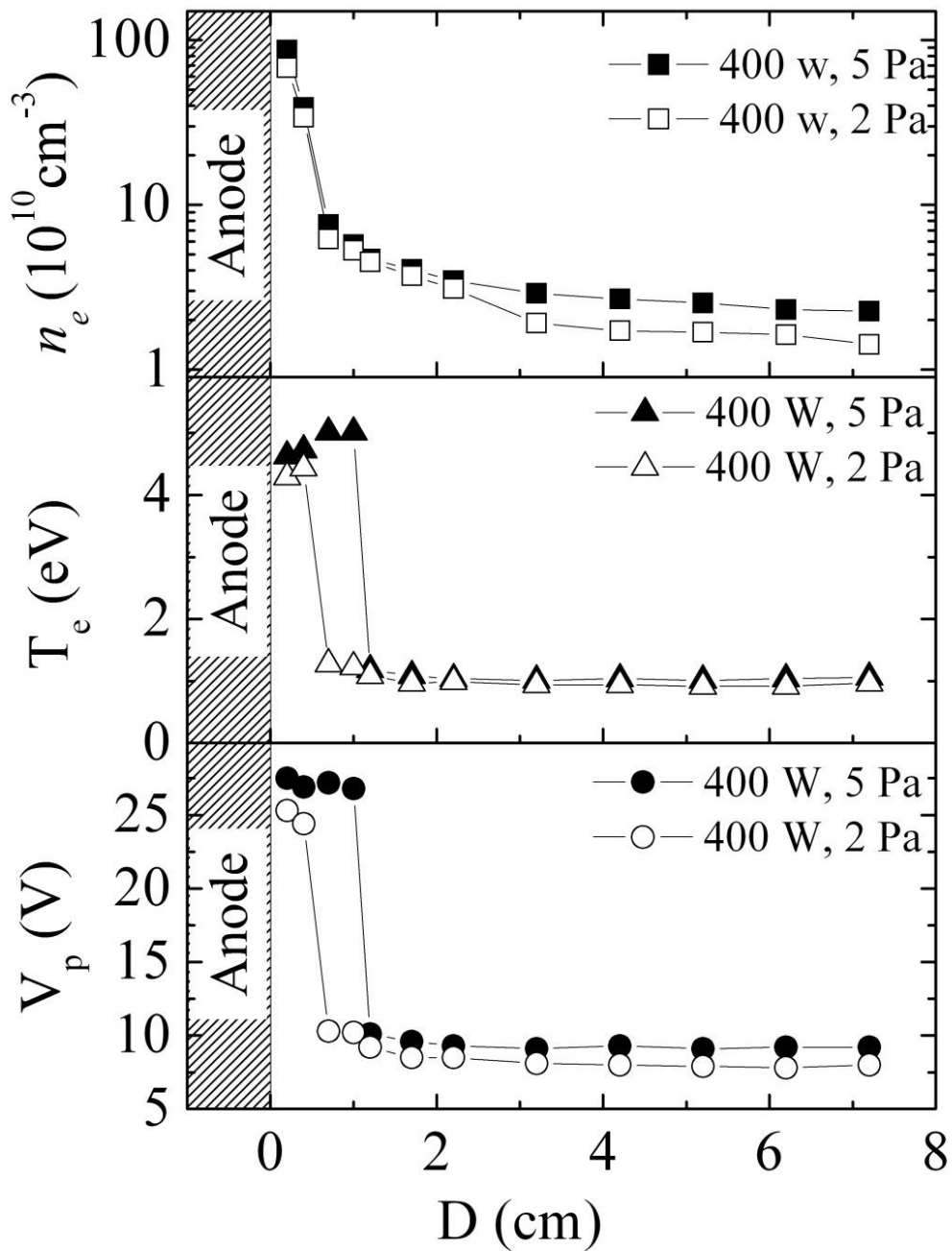
Figure 3-10: *Spatial plasma potential, electron temperature and electron density profile in the anode region along the radial direction for the nitrogen discharge for the nitrogen discharge operating at 2 Pa and 5 Pa pressure and at 400 W input power.*

The electron temperature profile also resembles to that of plasma potential profile wherein it is observed that the value of electron temperature in bulk plasma is ~1 eV which rises to 4-5 eV inside the anode glow.

It shows that the electron density in the anodic glow is two orders of magnitude higher as compared to the bulk electron density. The spatial electron density profile show that the electron density in the bulk plasma is on the order of 10^{10}cm^{-3} whereas increases upto 10^{12} cm^{-3} inside the anodic glow.

3.3.6   The plasma electron density scaling with applied power

So far we have investigated the properties of anodic glow and its influence on the bulk discharge properties. For all those investigations, the peculiarity of particular cathode geometry was not taken into account. The geometry of the cathode consists of equidistant, equipotential, parallel, stainless steel plates. The peculiarity of this cathode geometry is that it allows increasing the A_c/A_a ratio. Also the parallel plate geometry acts as a hollow cathode which helps in increasing the ionization efficiency in the cathode region by the hollow cathode effect. Thus it is essential to study the effect of this particular cathode geometry as it directly affects the plasma properties in the bulk and anode region by (a) increase in the area ratio A_c/A_a, thereby affecting the voltage drop at the anode. (b) Increase in the ionization efficiency by hollow cathode effect gives rise to increase in the discharge current and therefore it increases the overall current towards the constricted anode.

This and the next section describe the experimental investigations related to the cathode geometry. The area of the anode is kept constant at 30 mm^2 and the working gas nitrogen

was introduced through the hollow anode at a constant flow rate of 50 sccm. The cathode assembly consists of 4 semicircular stainless steel plates. The distance between the plates is varied from d= 2 to d= 7 cm.

Figure 3-11 (a) and (b) show graphs of electron density measured 4 cm above the parallel plate cathode (region 1 in figure 3-3) versus power (50 - 400 W) at different pressure values (2 Pa to 5 Pa). Figure (a) corresponds to d= 3 cm and figure (b) corresponds to d= 5 cm.

For d= 3 cm (figure 3.11 (a)), we observe that the electron density monotonically increases for 3 to 5 Pa pressure. However for the operating pressure of 2 Pa, density tends to saturate beyond 150W. These observations can be explained by considering the cathode sheath width. As the sheath width is inversely proportional to the plasma density, more plasma is present between the plates at higher operating pressure of 5 Pa than at 2 Pa. The electric field in this case would be normal to the cathode surface which helps in accelerating the secondary electrons emitted from the cathode towards the opposing sheath. As more secondary electrons are trapped the efficiency of the discharge improves and the electron density tends to increase with the applied power. However saturation is reached as the sheath voltage also increases with the applied power which makes the sheath width again comparable with the separation between the plates.
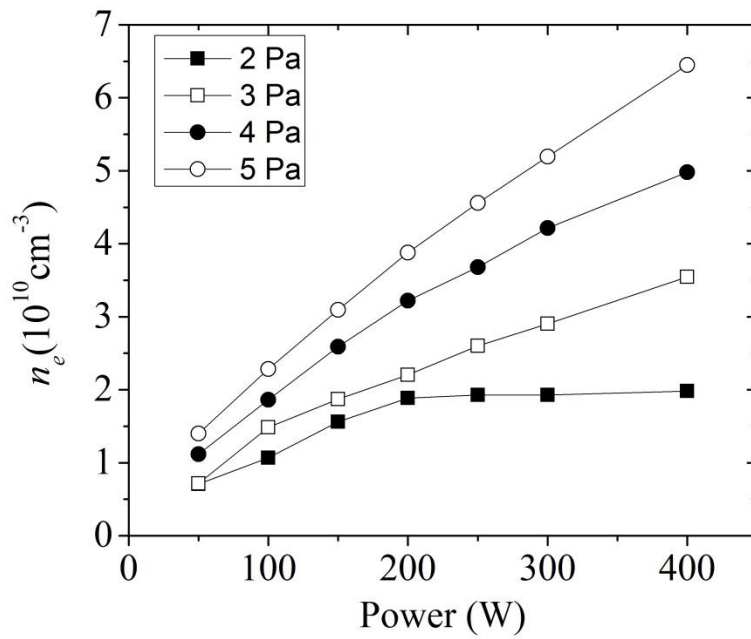
(a)
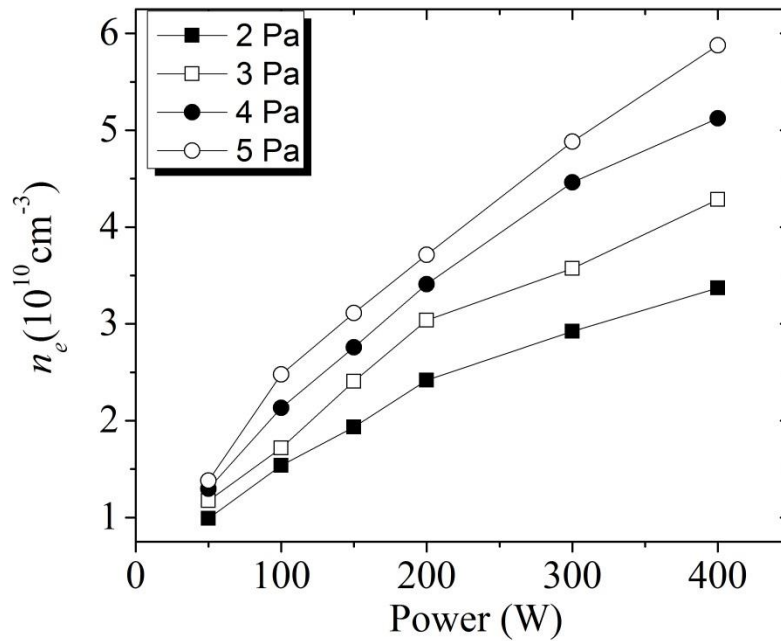
(b)

Figure 3-11: *The graph of electron density measured by hairpin probe versus power above 4 cm from the parallel plate cathode. The distance between the cathodes plates was (a) 3 cm and (b) 5 cm.*

When the distance between the plates increases from d=3 cm to d= 5cm , the electron density increases monotonically for all the pressure values (2-5 Pa) and it is observed that the rate of increase with applied power increases with increase in the background pressure.(figure 3.11 (b)).

The above discussion suggests that the separation between the plates need to be greater than the sheath width to achieve the better efficiency of the discharge.

3.3.7   The effect of cathode spacing on the measured density in the bulk plasma

Figure 3-12 shows the comparison of plasma density in region 1 (see figure 3.3, 4 cm above the semicircular cathode plates) for d= 3cm, 5 cm and 7 cm. The discharge was operated at the background pressure of 2 Pa.
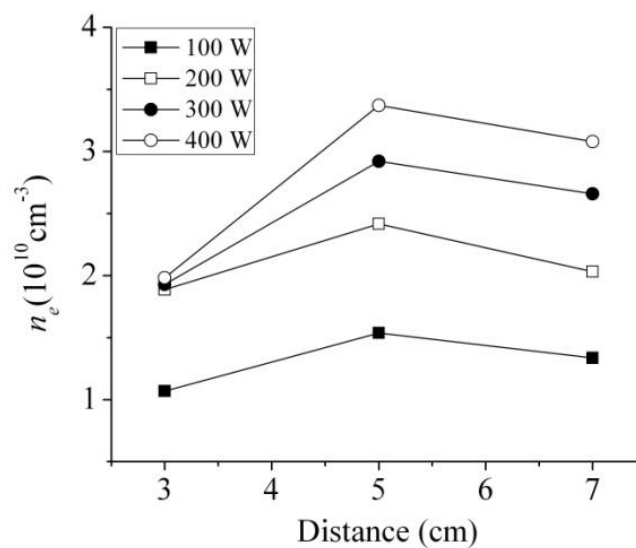
Figure 3-12: *Electron Density variation with the distance between the parallel plates. The operating conditions are the same as Figure 3-11.*

As observed in figure 3-12, the highest electron density is obtained when the plate separation is d=5 cm. For d = 3.0 cm, the sheaths tends to overlap at low densities. The secondary electrons can be barely confined if the total sheath width becomes comparable with the distance between the adjacent plates. Hence this will act adversely on the efficiency of the source. The electron density also falls if the plate separation is increased to 7.0 cm. This is because the losses of secondary electrons can also increase as the plate separation becomes comparable with the radius of the semicircular plates. For the efficient trapping of secondary electrons from the plates, the physical dimension of the cathodes should be of the order of 3 times greater than the separation between the individual plates to obtain effects similar to that of cylindrical hollow cathodes. This observation highlights that in order to operate the discharge at lower pressures the physical dimension and the separation between the plates must be chosen appropriately for that particular operating condition.

3.4   Discussion

3.4.1   Model for the observed density in the anodic glow

The role of the anode in the DC discharge is to repel the excess current towards the anode due to thermal motion of electrons. Thus the potential drop across the anode with respect to plasma in the glow discharge is negative. If the area of the anode is reduced, the effective current reaching at the anode surface reduces. In order to balance the net discharge current

(or current at the cathode), electron repelling potential at the anode transforms to the electron attracting potential. The positive potential drop at the cathode can be estimated by equating the anode and cathode current. The current collected by the anode is given by

$$I_a = e n_a v_a A_a \tag{3.1}$$

where v_a is the velocity of the plasma electrons reaching the anode surface, n_a is the plasma density at the anode and A_a is the area of the anode. Similarly we define n_c as plasma density near the cathode and A_c as area of the cathode. The current at the cathode constitutes of ion current to the cathode and secondary electron current from the cathode to the bulk plasma. The ions of mass M move towards the cathode with Bohm speed $v_b = \left(\dfrac{e T_e}{M} \right)^{1/2}$ and bombard the cathode surface to eject secondary electrons from the cathode. The yield of secondary electrons depends on the coefficient of secondary electrons γ. If V_c is the voltage drop at the cathode, then cathode current is given by

$$I_c = e n_c A_c \left[\left(\frac{k T_e}{M} \right)^{1/2} + \gamma \left(\frac{2 e V_c}{m} \right)^{1/2} \right] \tag{3.2}$$

If we consider $n_a = n_c$ then from Eq. 3.1 and Eq. 3.2, we write

$$en_a v_e A_a = en_c A_c \left[\left(\frac{kT_e}{M} \right)^{1/2} + \gamma \left(\frac{2eV_c}{m} \right)^{1/2} \right]$$

Therefore

$$v_a = \frac{A_c}{A_a} \left[\left(\frac{kT_e}{M} \right)^{1/2} + \gamma \left(\frac{2eV_c}{m_e} \right)^{1/2} \right]$$ (3.3)

And therefore the voltage drop across the anode is given by

$$V_A = \frac{m_e}{2e} \left(\frac{A_C}{A_A} \right)^2 \left[\left(\frac{kT_e}{M} \right)^{1/2} + \gamma \left(\frac{2eV_C}{m_e} \right)^{1/2} \right]^2$$ (3.4)

Eq. 3-4 reveals that voltage drop at the anode is directly proportional to the $(A_c/A_a)^2$ and it also depends on the voltage drop at the cathode. If the area of the anode is made sufficiently small as compared to the cathode then the voltage across the anode grows significantly high as shown in the figure 3-13.
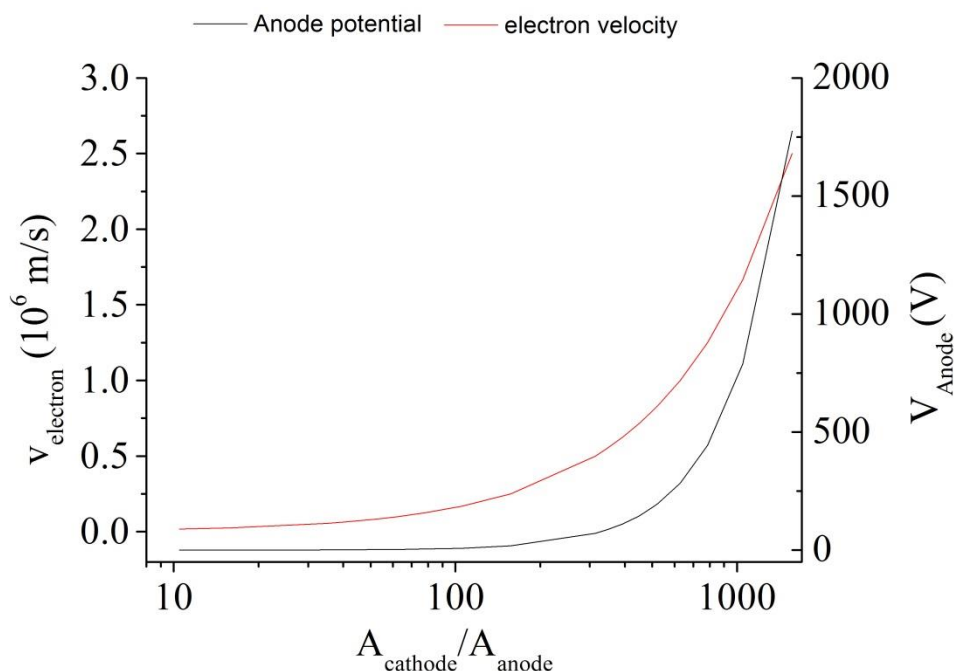
Figure 3-13: *Mean electron velocity and Anode potential are plotted as a function of cathode to Anode area ratio*

It can be seen from the figure 3-13 that the anode voltage drop starts increasing rapidly as the ratio of cathode to anode area exceeds 300. In our case of constricted anode, this ratio is 500-2000 so the potential drop at the anode should have been 100-800 V. However the observed potential drop across anode with respect to plasma is just 15 V. The reason behind this discrepancy is the formation of double layer in the anode region.

From figure 3.13 we can see that as the anode area decreases, the electrons are attracted towards the anode with greater velocity. Energetic electrons undergo ionizing collisions with the neutrals and the electron -ion pair is created in the anode sheath. The newly created electrons rapidly move towards the anode while the positive ions respond slowly by drifting away from the anode and thus double layer evolves. Two distinct spherical layers,

outer positive space charge layer and inner negative space charge layer attached to anode, are produced between the anode and the bulk plasma. The surface of the positive space charge layer acts as a virtual anode with increased surface area. This increase in anode area decreases the potential drop across anode and adjusts itself so as to maintain the positive potential drop which is equivalent to the ionizing potential of the background gas. From figure 3.10 we observe that plasma potential in the bulk is $V_{P,B} = 10$ V and inside the anode glow the potential increases to $V_{P,G} = 25$V and the difference between $V_{P,G}$ and $V_{P,B}$ is 15 V, which is close to the ionization potential of the nitrogen gas (14.53 eV).

As newly born ions move away from the anode, the plasma potential in the anode layer flattens as observed in the plasma potential profile plotted in figure 3.10 for the nitrogen discharge operating at 400 W, 5Pa; and also observed numerically by Conde et.al. [73].

While calculating potential drop at the anode in eq.3.4, we assumed that the plasma density in the near-anode region and plasma density in the cathode region are equal. However due to the ionization process in the anode region this assumption is not true. Because of the intense electric field at the anode, the accelerated electrons dump their energy to produce localized heating of the plasma. The electron neutral collision frequency, $v_{iz,}$ is proportional to p $\exp(-\varepsilon_{iz} /T_e)$; where p is the neutral pressure and ε_{iz} is the ionization potential of the gas. There as electron temperature increases, v_{iz} rises , therefore an intense ionization results in the creation of an anode glow.

In order to find the electron density to the anodic glow, current collected by the anode (I_A) given by (and the current at the cathode (I_c) given by (3.2) are equated i.e.

$$en_a v_a A_a = en_c A_c \left[\left(\frac{kT_e}{M} \right)^{1/2} + \gamma \left(\frac{2eV_c}{m} \right)^{1/2} \right]$$ (3.5)

The above equation is rewritten as the ratio of plasma density at anode and plasma density at cathode.

$$\frac{n_a}{n_c} = \frac{A_c}{A_a} \left[\gamma + \sqrt{\frac{m}{M}} \sqrt{\frac{kT_e/2e}{V_c}} \right] \sqrt{\frac{V_c}{V_a}}$$ (3.6)

The above equation shows that the density near the anode increases as the area of the anode increases. For a typical experimental condition, $(V_c/V_a)^{1/2} \approx 4$, $A_c/A_a \approx 2000$, $\gamma = 0.2$ for stainless steel at 200 eV and for N_2 the ratio $(m/M)^{1/2} \approx 4.5 \times 10^{-2}$, Eq. 3-6 yields $n_a / n_c \approx 100 \sim 1000$. This means that the plasma density in the anode region is two to three orders of magnitude higher as compared to the plasma density in the cathode region.

Figure 3.10 shows the spatial plasma density measurements in the anodic and bulk plasma for nitrogen discharge operating at 2 Pa and 5 Pa and at 400 W of power. The graph shows that the electron density in the bulk plasma is about $3 \times 10^{10} \text{cm}^{-3}$ whereas inside the anode glow electron density is about 10^{12}cm^{-3}. The enhancement in the anodic plasma density as compared to the bulk density is in good agreement with the value obtained in Eq. 3-6. From the above results we can conclude that the plasma density near the anode scales similarly with the cathode to anode area ratio.

3.5   Summary and conclusion

In this chapter we investigated the DC properties of the constricted hollow anode plasma source. The emphasis of the study was to investigate the origin and properties of the anodic glow in the DC discharge.

In our studies, the gross discharge property showed that higher efficiency can be achieved by minimizing the surface area of the anode exposed to the plasma. This enhancement is attributed to the formation of the luminous anodic glow near the constricted anode. Since the constricted anode is the part of the discharge circuit, therefore, its properties plays a crucial role in the sustainment of the plasma at lower pressure. The anode potential self-consistently adjusts itself with the background pressure and the applied power. The rise in the anode potential with reference to the plasma corresponds to the ionization potential of the gas. The strong electron heating due to reduction in anode area enhances the secondary ionization in the anode region which in turn increases the plasma density in the anode region by up to 2 to 3 orders of magnitude.

Chapter 4   Properties of the anodic glow

4.1   Introduction

The bright luminous glow observed around the constricted anode is characterized with sharp gradients in density and temperature. Because of the accelerating potential at the anode the electrons are quickly absorbed while a space charge of positive ions is left behind which are pushed away from the anode. The violation of quasi-neutrality in the local region creates a double layer structure in the anodic glow. The double layer is a region of periodic non-neutral region which is characterized by a sharp gradient in potential structure. As mentioned in chapter 3, the double layers are reportedly observed in various laboratory plasmas [31, 69, 74-76] as well as in space plasmas [68, 77, 78]. Since the phenomenon taking place in the anodic glow is similar to the plasma double layer, a large number of papers deal with the theoretical understanding of the properties of the anodic glows [30, 35, 73, 79-82]. Recent work on the anodic glow show that the ion acoustic and electron plasma waves have been observed to be launched from the anodic double layer [33, 82, 83].

Occurrence of anodic glow or fireball in front of positively biased electrode is always associated with the observation of linear or non-linear oscillations in the electrode current. These current oscillations are attributed to the plasma instabilities in the presence of anodic

glow which arise due to the excitation and ionization phenomenon in the anode sheath region [33, 80, 84-86]. Recent studies on the rise and fall time of the current pulse and the frequency of the current oscillations show the direct correlation to the ionization time in the anodic glow [35, 83]. These studies are particularly important to understand the process of anodic glow formation. Although the subject of much attension, most of these studies on the anodic glows have been carried out in a Double Plasma device where the anode is not part of the discharge forming circuit. Therefore the effect of secondary electrons from the cathode surface on the properties of anodic glow is negligible [33, 36, 79, 82].

Unlike the earlier works on anodic glow at a positive biased probe, in our case the anodic glow is a part of the discharge circuit. Additionally, the parallel plate geometry of cathode has a direct influence on the secondary electron production from the cathode surface. The important result discussed in this chapter regards to the oscillation in the discharge current in the frequency range of 250 to 400 kHz. The oscillation frequency is linked to the phenomena happening at the cathode and therefore depends on the cathode sheath potential, the ion flux and the secondary electron emission from its surface.

4.2   Experimental results

The experimental results presented in this section refer to the experimental set-up described in figure 3.3 which consists of semicircular parallel plates acting as cathode and the stainless steel constricted hollow anode. The working gas nitrogen is introduced through the anode at a flow rate of 50 sccm.

4.2.1 Temporal behaviour of discharge current

Figure 4.1 shows a typical time dependent discharge current. In this figure we observe that, although the discharge was operated by applying a continuous regulated voltage, the discharge current shows oscillations with the frequency of 300 kHz. The peak to peak variation of the discharge current is over 40 % with respect to the time averaged current. The density variation in the bulk plasma was not significant suggesting the phenomenon is localized at the anode. As the pressure was varied from 2 to 10 Pa (figure 4.2) the oscillation frequency was found to be increasing with pressure. On the other hand, the frequency tends to fall linearly when the applied power was raised from 50 to 400 W (figure4.3). This is discussed in section 4.3
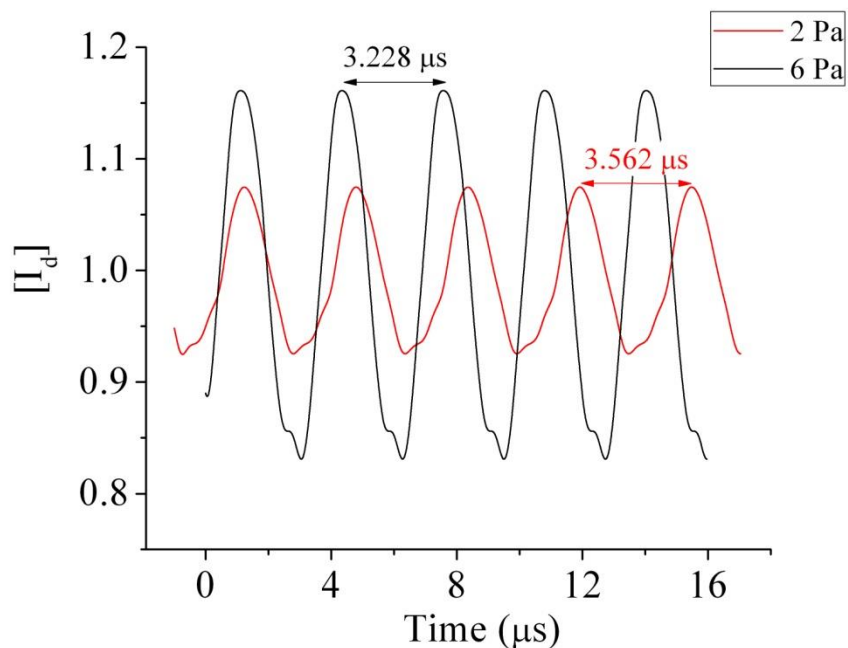

Figure 4.1: *Oscillation in the discharge current. The current on the y−axis is normalised with the mean value of the discharge current. The period of current oscillation for 2 Pa is higher compared with that of 6 Pa.*
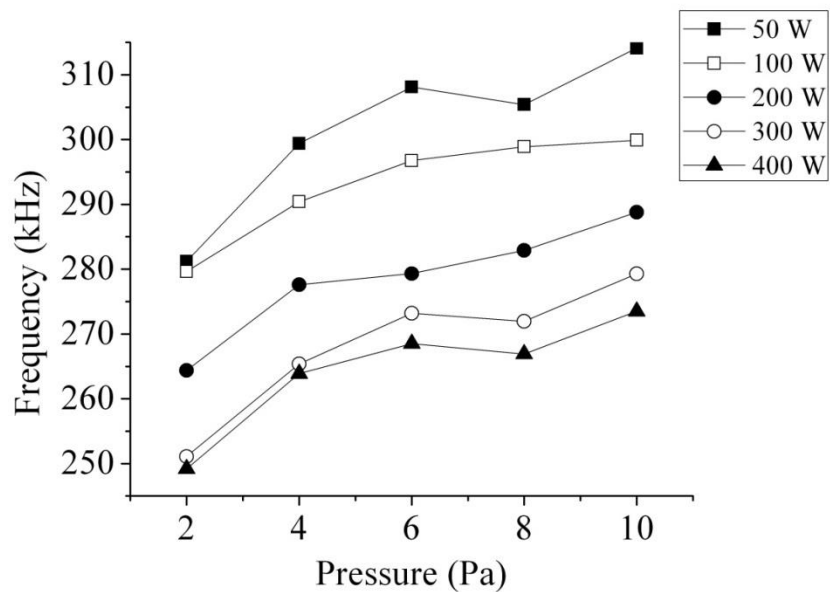
Figure 4.2: *Frequency of discharge current oscillations with the background pressure*
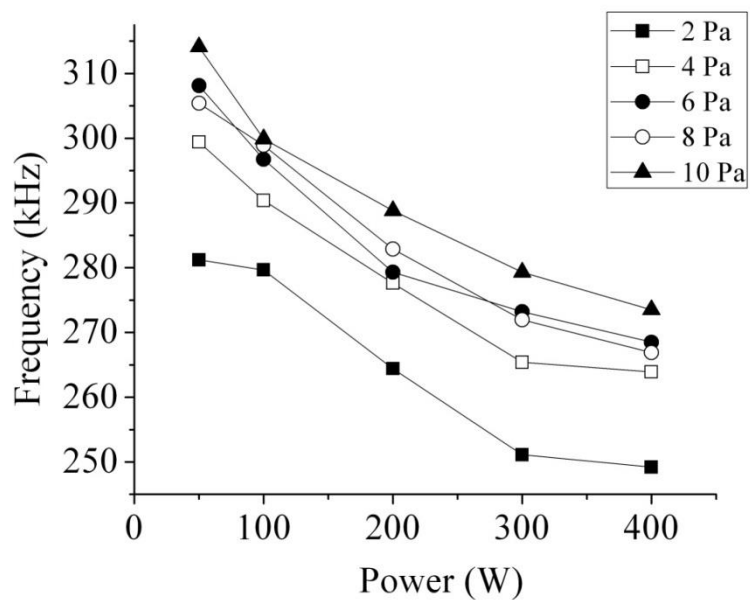
Figure 4.3: *Frequency of discharge current oscillations with the power*

4.2.2 Relative voltage dependencies at cathode and anode with pressure and power

In tandem with the behavior of oscillation frequency, the relative power distribution at the electrodes with pressure and power is also interesting.
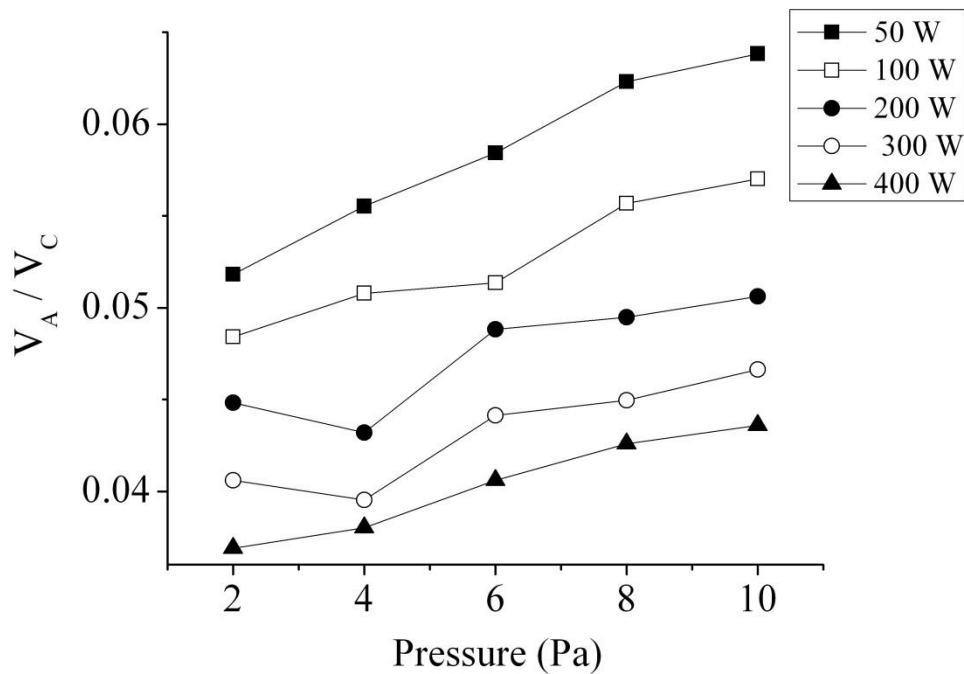
Figure 4.4: *Plot of normalized anode to cathode potential with pressure.*

In figure 4.4 the ratio of voltages on the anode to the cathode (V_a/V_c) is plotted as a function of operating pressure. Both V_a and V_c are measured with respect to ground using a high voltage probe. The ratio V_a/V_c shows an increasing trend suggesting the relative power at the anode must be increasing with increase in the operating pressure. In contrast to above observation, in figure 4.5, we observe that the relative voltage at the anode decreases by upto 30% when the power increases from 50 W to 400 W.
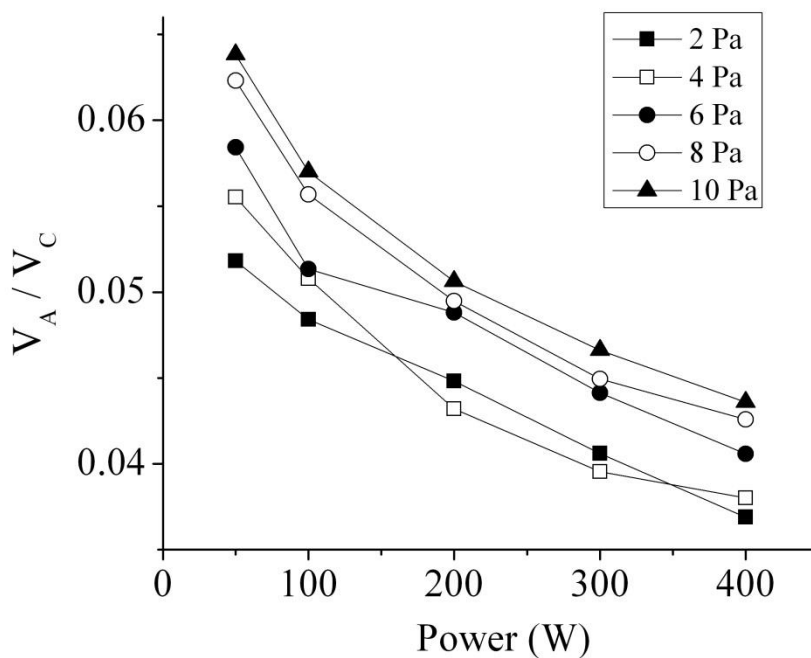
Figure 4.5: *Plot of normalized anode to cathode potential with power*

4.3   Discussion

The discharge current shows the oscillations in the range of 250 to 325 kHz. The oscillation frequency shows some interesting peculiarities such as increase in frequency with operating pressure and contrary decrease with the applied power. By noting the similar tendency in the oscillation frequency and the voltage drop at the anode with the respect to the applied power and pressure, it can be inferred that the oscillation frequency has direct correlation with the relative voltage drop at the anode.

4.3.1 Phenomenological model of anodic sheath expansion

As discussed in chapter 3, the discharge has two distinct ionization mechanisms. The parallel plates act for the confinement of energetic electrons released during ion bombardment at the cathode plates and enhance the ionizing mean free path before the electrons escape outside the cathode region. The small anode enhances the local current density around the anode resulting in locally heating the electrons. As the electron temperature rises near the anode it results in greater electron neutral collision frequency $v_{iz} \propto p \cdot \exp(-\varepsilon_{iz}/T_e)$; where p is the neutral pressure and ε_{iz} is the ionization potential of the gas. Therefore intense ionization sets up in front of the anode a glow or fireball structure develops.

As discussed by Stenzel et al [33], the fireball plasma is physically unstable. After the creation of the electron-ion pair in the anode sheath, the electrons are quickly absorbed while the positive ions response slowly by drifting away from the anode. This creates an excess positive charge in the vicinity of the anode and the sheath transforms into a double layer. The ions created inside the double layer move away from the anode which results in the expansion of the double layer. As the double layer expands, more electrons are collected from the plasma resulting in observed growth in the net discharge current. However as volume of the double layer increases the electric field at the anode drops and reaches a state at which the electron impact ionization reduces significantly. This results in the collapse of the anode glow and the decrease in the anode current. The process repeats itself consistently resulting in the observed oscillation of the discharge current.

According to the above model, it is concluded that the rise and decay of the anode sheath determine the oscillation frequency. The positive ions created inside the anode sheath expand towards the bulk plasma with the sound speed v_s, which is proportional to $T_e^{1/2}$ [83]. Therefore the critical extent of the anode space charge prior to its collapsing can be estimated to be

$$s = \frac{\left(kT_e / M\right)^{1/2}}{f} \tag{4.1}$$

where f is the frequency of oscillation, provided the local electron temperature near the anode is known. Assuming $T_e = 5$ eV, $M = 28$ a.m.u for N_2, and $f = 250$ kHz, we estimate the critical length to be s=16 mm which is typically close to the visual estimate of the dimension of the anode glow. This value is also in good agreement with the experimentally observed values by other researchers [35, 80, 83].

4.3.2 Electron temperature dependencies on oscillation frequency with pressure and power

Figure 4.2 shows that current oscillation frequency increases with the pressure, while in figure 4.3 we observe that frequency decreases with the applied power. The increase in the oscillation frequency suggests rapid expansion of the positive space charge sheath reaching to the critical limit beyond which the anode collapses. This implies that the electron temperature in the anodic sheath must be increasing with the pressure.

From equation 4.1, if the dimension of the anodic glow is known,

$$(T_e)^{1/2} \propto \text{Oscillation frequency}$$

or
$$T_e = f^2 \left(\frac{ms^2}{k} \right)$$
(4.2)

Figure 4.6 shows the graph of electron temperature measured by emissive probe as a function of pressure. The graph also shows the data of normalized electron temperature ($[T_e]$) which is obtained by considering the time period for the expansion of the anode sheath to reach the critical anode sheath thickness before it collapses (Eq. 4.2). $[T_e]$ is calculated from the data plotted in Figure 4.2. The values in Figure 4.6 show 15% rise in electron temperature when the neutral pressure was increased from 2 Pa to 10 Pa.

Figure 4.6: *Graph of normalized electron temperature ([Te]) estimated from the current oscillation frequency and measured electron temperature by emissive probe in the anode double layer versus operating pressure ranging from 2 Pa to 10 Pa for nitrogen discharge at a fixed 100 w input power.*

In figure 4.7, the values of normalized electron temperature ($[T_e]$) are obtained from the data of oscillation frequencies plotted in figure 4.3. Since the oscillation frequency decreases with increases in power, $[T_e]$ also decreases up to 20% when the power is increased from 50 to 400 W. This behaviour of normalised electron temperature $[T_e]$ matches well with the experimentally measured electron temperature values.
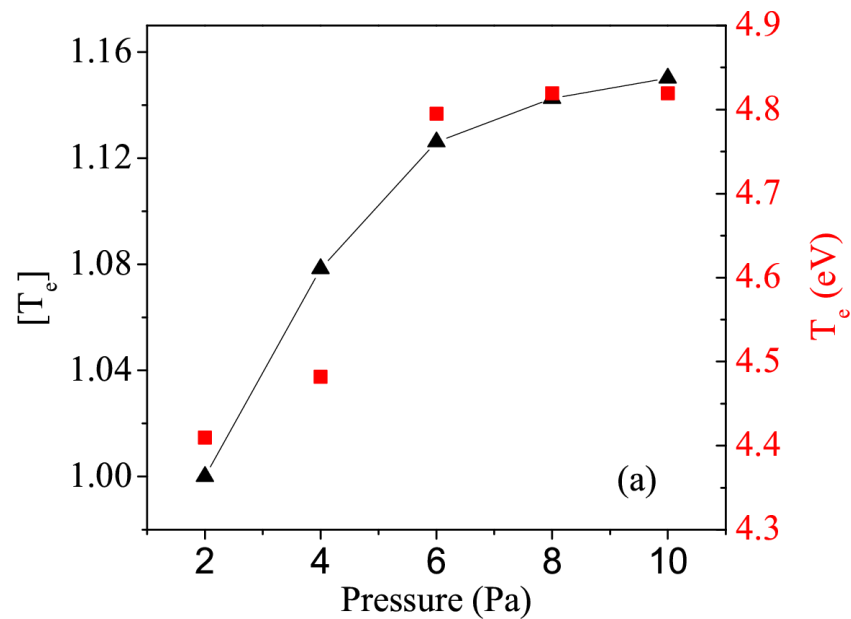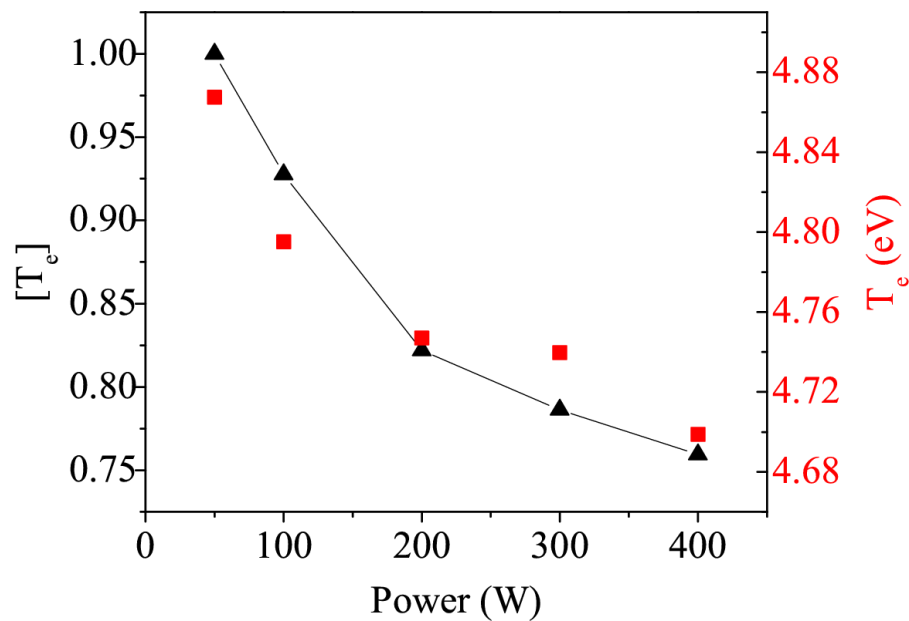
Figure 4.7: *Graph of normalized electron temperature ([Te] estimated from the current oscillation frequency and measured electron temperature by emissive probe in the anode double layer versus input power for nitrogen discharge at operated at 6 Pa*

The rise in local electron temperature with the pressure (figure 4.6) suggests that the electrons must be heated near the anode. This can be possible if more power being deposited at the anode on increasing the background pressure. This point is consistent with figure 4.4 which shows the rise in the anode to cathode potential drop as the pressure was varied from 2 to 10 Pa. The reason behind the increase in the anode voltage is directly related to the increased plasma density with the pressure. As the overall plasma density increases, it results in higher secondary electrons being generated at the cathode due to increase in ion flux. Hence to conserve the total current in the circuit, the current density at the anode must also increase. The increased current density at the anode is followed by increase in the anode potential in order to accelerate the plasma electrons towards the anode. As the power deposition near the anode becomes high the electrons will be locally

heated. As a result the electron temperature will enhance and self-consistently intensify the ionization near the anode as the pressure is increased.

In contrast to the above feature, the local electron temperature near the anode is found to reduce with power. In figure 4.7, a 20% drop in T_e is observed by increasing the power from 50 to 400W. The drop in electron temperature suggests that the anode potential should decrease with power. Indeed this is seen in figure 4.5, as we observe that the relative voltage available at the anode reduces with increasing applied power.

A qualitative explanation for the observed reduction in the V_A/V_C ratio with power can be related to the efficiency of the discharge mechanism. Increasing the external power demands higher electron density to be produced. However, the rate of increase is limited by (i) the number of available neutrals for ionization and (ii) how the energetic electrons are confined between the plates. As observed in figure 3.8 in previous chapter, at a given pressure and for the fixed distance between the cathode plates, the electron density reaches a threshold on increasing the power. Therefore, in order to increase the production of electron–ion pairs, the cathode voltage increases to enhance the secondary emission. At the same time the increase in sheath width results in reducing the plasma volume present between the plates. Hence the efficiency of secondary electron confinement between the plates is directly affected on increasing the power. As the rate of plasma production reduces due to the loss of secondary electrons between the plates, the anode potential self-consistently adjusts to reduce its potential. This results in lowering the local electron

heating near the anode. The discharge current therefore exhibits oscillations at a lower frequency.

Thus we can conclude the above phenomenon to be attributed to the ionization instability which can be controlled by adjusting the cathode plate spacing, applied power and the working gas pressure.

4.4 Summary and Conclusion

When the anode glow is formed in CHAPS, the total discharge current shows oscillations in the frequency range of 250-300 kHz. The frequency of these oscillations is found to be dependent on the applied power and pressure. The current oscillations are attributed to the expansion and the collapse of the anode sheath determined by the characteristic ion sound speed which is directly proportional to $T_e^{1/2}$. It is found that the separation between the plates can influence the observed anode current oscillations. Further, it can also be concluded that the secondary electrons from parallel plate cathode play an important role in the determining the frequency of the current oscillations.

Chapter 5 Investigation of negative ion production in the anodic glow

5.1   Introduction

From the application point of view in fusion devices, negative hydrogen plasmas are important for the production of neutral beams and subsequent heating of the plasma. In the bulk phase, the main process of negative ion formation is by the dissociative attachment of an electron to the molecule [9, 21]. As well established, the metastable and excited molecules have higher dissociative attachment cross section as compared to the ground level molecules [87-91].. However, the required negative ion density at the extractor grid can only be achieved via interaction of ions and metastables with the low work function surfaces. For this caesium is introduced in the discharge that helps in enhancing the density by up to 4 times. However Cs can migrate into the extractor region along with negative ions and can lead to the divergence of the beam, dumping enormous power on to walls of the

acceleration chamber. Therefore it would ideal if a caesium free negative ion source can be developed based on the volume production of negative ions.

Until now, most of the research on the negative ion production is primarily concentrated on the excited molecules present in the plasma volume only. There are some clear evidences that the excited molecules are also present in the sheath and wall region and are important source of negative ions [88, 90, 92]. These findings have encouraged the research on the development of volume process based negative ion source for the fusion application. The anodic glow region provides favourable conditions for the production of negative ions.

The anodic double layer is a source of electron acceleration. The energy gained by electrons due to the double layer potential is released in the form of ionizing and excitation collisions with the background neutrals. Therefore anodic glow acts as a source of excited and metastable molecules. These excited molecules are gas dynamically migrate away from the anodic glow and are available for the effective dissociative attachment process. The anodic glow is also characterised by a spatial gradient in electron temperature. This situation is ideal for understanding the effect of electron temperature on the kinetics of negative ion production and loss in presence of excited molecules.

In the present study, a mixture of argon and oxygen is used as the electronegative gas. The electropositive discharge created by the argon gas is used for comparison. Detail characterization of plasma parameters reveals the presence of high concentration of negative ions in the vicinity of the anodic glow region when a mixture of argon − oxygen was used as compared with the pure electropositive argon gas. The formation of negative ions is described by considering the characteristic spatial dependence of T_e as a function of

distance from the anodic glow. A theoretical estimate of negative ions at each spatial locations show reasonable agreement with experimental data.

5.2   Experimental details

The experiments are performed in the argon and argon – oxygen (50-50%) discharge operating at 2 Pa pressure. Before creating the discharge, vacuum chamber was evacuated to 0.5 mPa pressure and then a pure argon gas and a mixture of argon-oxygen gas is fed through the hollow anode. The equal composition of Ar/O_2 mixture is created by passing the argon gas to evacuated chamber to 1Pa and then simultaneously introducing oxygen so that total system pressure is 2Pa.
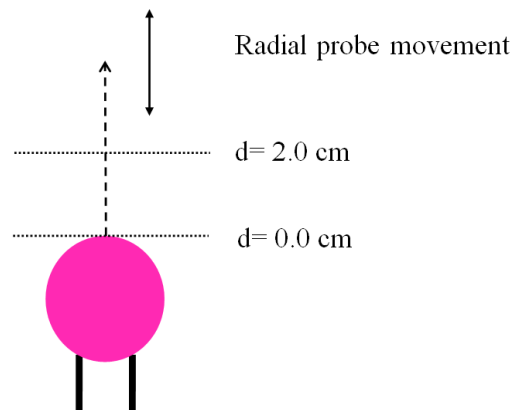

Figure 5.1: *The reference point for the measurement of the plasma properties in the anodic glow.*

Once plasma is created, an anodic glow similar to the glow shown in figure (3.2, chapter 3) is observed. Spatial plasma properties in the anodic glow region are measured by introducing the probe in the vertical direction from port 3 (P3) as shown in figure (3.1 (a),

chapter 3). The reference point for the probe measurements was set with the edge of the anodic glow and considered as d=0.0 cm (figure 5.1).

5.3   Experimental Results

5.3.1   Comparison of argon and argon-oxygen discharge properties

(a)   (b)
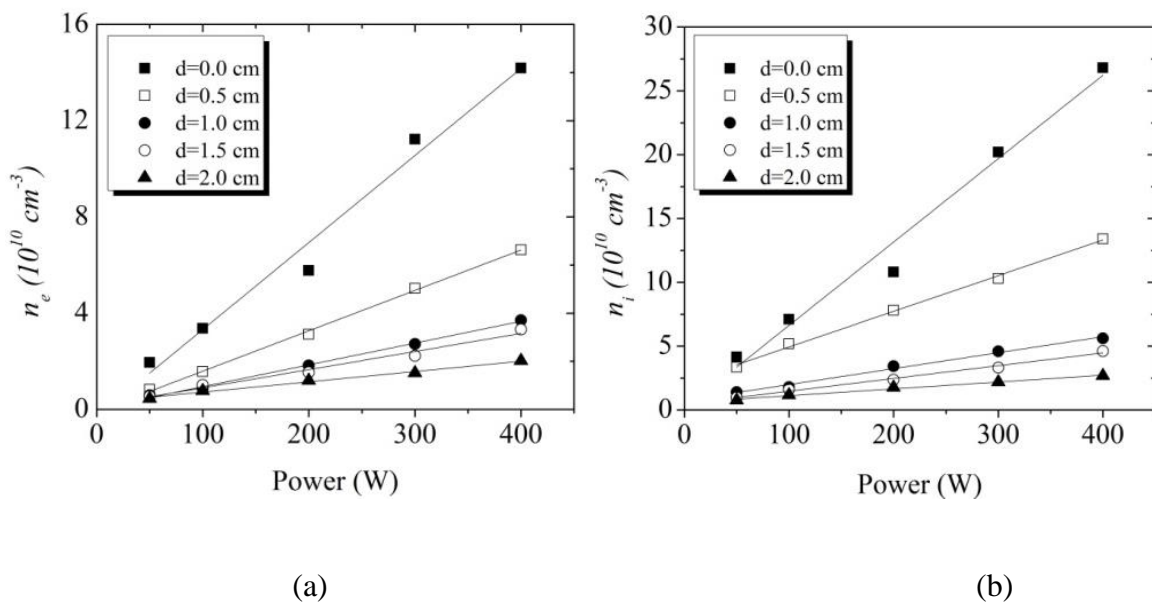
Figure 5.2: *Plot of (a) electron density and (b) positive ion density as function of power measured locally at d= 0.0 cm to d= 2.0 cm using hairpin probe and planar Langmuir probe*

Figure 5.2 (a) and (b) show the graph of electron density and ion density as a function of applied power. Measurements are carried out locally at a distance of d=0.0 cm to d= 2.0 cm from the edge of the anodic glow as shown on figure 5.1.

The electron density and ion density in the anodic region scale linearly with power and the plasma density decreases with increase in the distance from the edge of the anodic glow.

Although both the graphs have similar trend, the electron density is in the range of upto 15 $\times 10^{10}$ cm^{-3} whereas the ion density is almost double and lies between $1-28 \times 10^{10}$ cm^{-3}.

The data in figure 5.2(a) and (b) is replotted as a ratio of ion density to electron density (n_i/n_e) versus the distance which shown in figure 5.3. At d=0.0 cm, the value of n_i/n_e is between 1.7 to 2.2 and it increases upto 2.0 to 4.0 for the input power 50 W to 400 W. The graph also shows the ratio of n_i/n_e for the argon gas discharge. The value of n_i/n_e in case of Ar lies in the range of 0.7 to 1.5, typically close to 1.

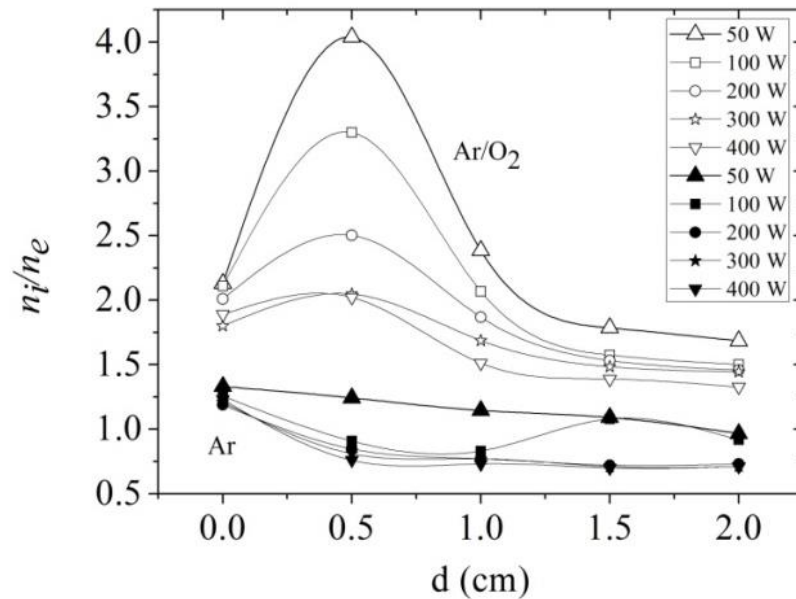**Figure 5.3:** *Comparison of electron and positive ion density platted as a graph of n_i/n_e versus distance from the edge of the anodic glow.*

In a quazineutral plasma, positive ion density and electron density are equal i.e. $n_i=n_e$. Therefore, the ratio $n_i/n_e \sim 1$, as observed in case of the argon. However, in case of Ar/O$_2$discharge, the deviation of n_i/n_e from unity suggest the existence of oxygen negative

ions which gives rise to the new quazi-neutral equilibrium between the positive and negative species in the plasma, $n_i=n_e+n_-$.

The validity of the presence of negative ions can be tested by measuring the space potential in front of the anodic glow. Figure 5.4 (a) and (b) shows the spatial plasma potential profile for argon and Ar/O$_2$ discharge. In the graph, we see that for both Ar and Ar/O$_2$ gases, from d=0.0 cm to 1.0 cm, the plasma potential rapidly drops from ~ 25V to ~10 V. After this fall, from d=1.0 cm to 2.0 cm, an almost flat plasma potential profile is observed. Since addition of O$_2$ into the discharge do not show any peculiarity, the possibility of the existence of the positive space charge in from the anodic glow for the case Ar/O$_2$ discharge as against pure argon case can be ignored.

In order to confirm the existence of negative ions in front of the anodic glow, we calculated the electric field in front of the anodic glow. This electric field is calculated by two ways. In first case, we directly measure the difference between the plasma potential and use,

$$E = -\frac{dV}{dx} \tag{5.1}$$

and corresponding distance between two data points plotted in figure 5.4.

(a)   (b)
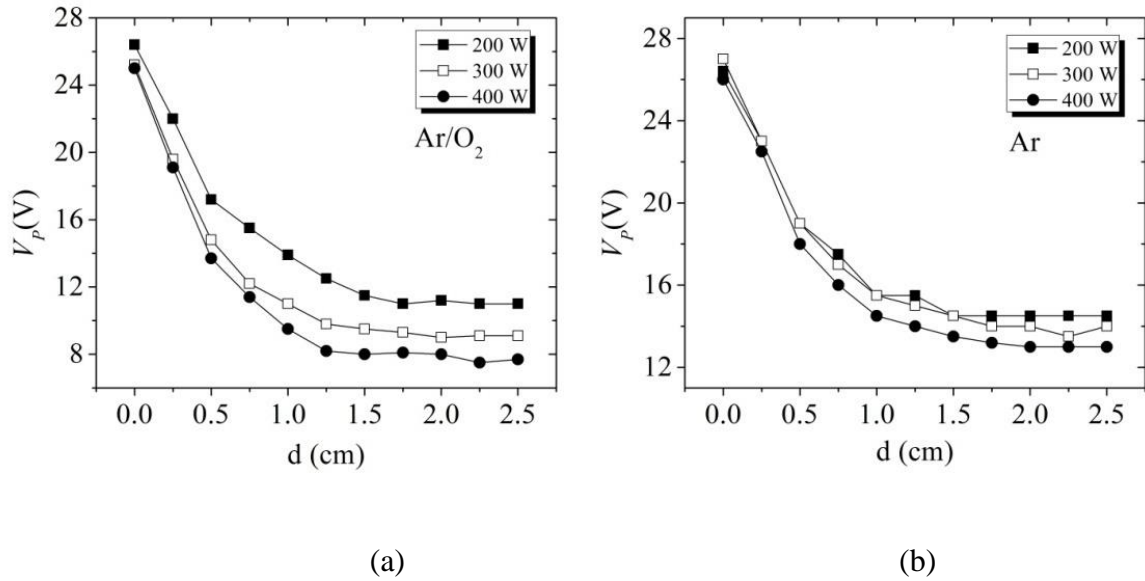
Figure 5.4: *Plasma potential versus the radial distance from the edge of the anodic glow for (a) Pure argon discharge and (b) Ar/O₂ discharge*

In the second case, electric field is estimated by assuming ambipolar diffusion of positive ions from the anodic glow towards the bulk of the discharge to balance the flux of negative charges and positive charges.

For electropositive gas fulfilling quazi-neutrality $n_i=n_e$, the ambipolar electric field is given by

$$E = \frac{D_i - D_e}{\mu_i + \mu_e} \frac{\nabla n}{n}$$

Here, it is assumed that $\Gamma_e = \Gamma_i = \Gamma$ and $\Gamma = -D\nabla n \pm \mu n E$. However, if we consider the quazineutrality in the presence of negative ions in front of the anodic glow, then the flux of positive ions will be balanced by the flux of electrons and negative ions.

$$\Gamma_i = \Gamma_e + \Gamma_-$$

The ambipolar electric field developed in presence of negative ions is then written as

$$E = \frac{D_i \nabla n_i - D_e \nabla n_e - D_- \nabla n_-}{\mu_i n_i + \mu_e n_e + \mu_- n_-} \tag{5.2}$$

Here the value of n_- is taken as the $n_- = n_+ - n_e$.

From eq. 1.3, the value of diffusion coefficient for each species is given as

$$D_i = \left[\frac{\pi \lambda^2 k T_i}{8M}\right]^{1/2}, \quad D_e = \left[\frac{\pi \lambda^2 k T_e}{8m}\right]^{1/2} \text{ and } D_- = \left[\frac{\pi \lambda^2 k T_-}{8M_-}\right]^{1/2}$$

Also from eq. 1.4, the mobility for each species is

$$\mu_i = \cdot \left[\frac{\pi \lambda^2}{8k T_i M}\right]^{1/2}, \quad \mu_e = \cdot \left[\frac{\pi \lambda^2}{8k T_e m}\right]^{1/2} \text{ and } \mu_- = \cdot \left[\frac{\pi \lambda^2}{8k T_- M_-}\right]^{1/2}$$

We clearly see that the diffusion coefficient and mobility depends on the temperature of the species. For calculating the ambipolar electric field (E) at each spatial location, we assumed $T_i = 0.025$ eV room temperature), and $T_- = 10$ $T_i = 0.25$ eV [58]. Also the value of electron temperature at each corresponding point is obtained by emissive probe (figure 5.7).

Table 5.1 shows the values of ambipolar electric field obtained using above equations and assumptions.

Table 5.1: *The values of ambipolar electric field in front of the anodic glow in argon-oxygen discharge*

	Ambipolar electric field (V/m)	
Distance (d) (cm)	300 W	400 W
0.25	1978	1925
0.75	832	817
1.25	307	220
1.75	373	412

Figure 5.5 shows the graph of electric field calculated from eq. 5.1 and the data shown in table 5.1 using eq. 5.2. The values are plotted as a function of distance. It is seen from the figure that, for d = 0.0 to 2.0 cm, the values electric field calculated from eq. 5.1 matches well with the measured values of electric field (eq. 5.2).
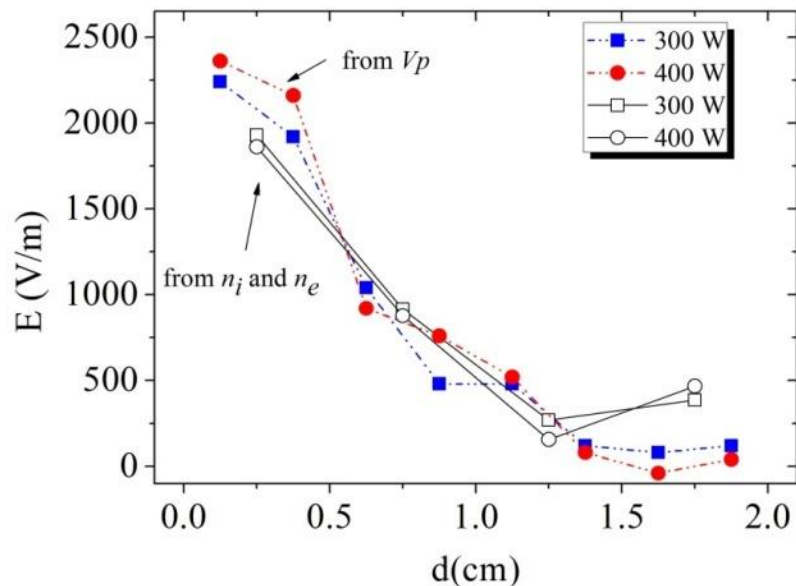
Figure 5.5: *Graph of electric field versus distance as calculated by (a) considering the ambipolar diffusion in presence of negative ions and (b) from the direct measurement of spatial plasma potential.*

Therefore it can be concluded that the difference in the positive ion density and electron density is due to the presence of negative ions (O^- and/or O_2^-). The maximum value of n_i/n_e as high as 2-4 suggest that the conditions are favourable for the creation of negative O_2 ions at specific distance, in this case d = 5.0 mm, outside the anode.

5.4   Discussion

5.4.1   Negative ion formation in the Ar/O$_2$ discharge

In the argon-oxygen plasma the dominating negative ion species is O⁻[9, 76, 93, 94] which is produced by the dissociative attachment process. Following are some important reactions

involving the dissociative attachment process in which an electron gets attached to either ground state (O_2) or excited (O_2^*) or metastable (O_2^M) oxygen molecules and then the molecule splits into a negative ion and a neutral.

$$e + O_2 \rightarrow O + O^- \qquad K_{da1} = 8.8 \times 10^{-17} \times \exp(-4.4/T_e) \qquad\qquad \text{R1}$$

$$e + O_2^* \rightarrow O + O^- \qquad K_{da2} = 4.19 \times 10^{-15} \times T_e^{-1.376} \times \exp(-5.19/T_e) \qquad \text{R2}$$

$$e + O_2^M \rightarrow O + O^- \qquad K_{da3} = -1.69 \times 10^{-18} + 6.27 \times 10^{-16}/T_e \qquad\qquad \text{R3}$$

$$- 1.30 \times 10^{-16}/T_e^2 + 9.60 \times 10^{-18}/T_e^3$$
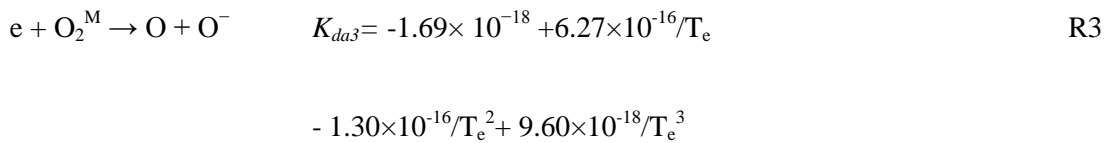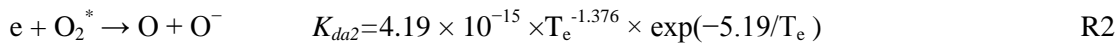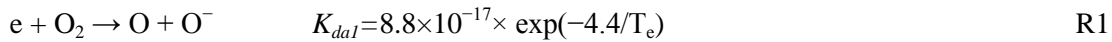
Here K_{da} represents the reaction rate constant for the given dissociative attachment process with a unit $m^3 s^{-1}$. The value of K_{da} directly depends on the electron temperature of the system under consideration.

The major oxygen negative ion losses are due to

(A) the interaction of negative ions with the oxygen and argon species (mutual neutralization)

$$O^- + O_2^+ \rightarrow O + O_2 \qquad K_{rec1} = 1.5 \times 10^{-13} \times (300/T_g)^{0.5}$$
$$\text{R4}$$

$$O^- + O^+ \rightarrow 2O \qquad K_{rec2} = 2.7 \times 10^{-13} \times (300/T_g)^{0.5}$$
$$\text{R5}$$

$$O^- + Ar^+ \rightarrow O + Ar \qquad K_{rec3}=1.4 \times 10^{-13} \times (300/T_g)^{0.5} \qquad \text{R6}$$
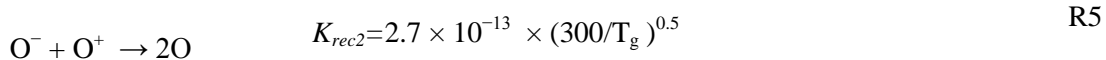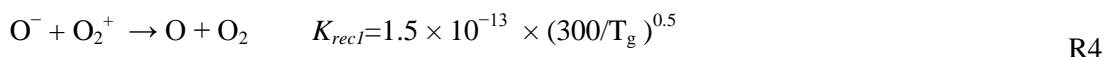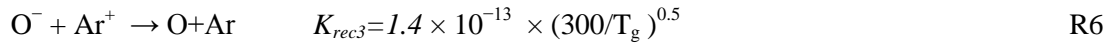
(B) the interaction of electron with the negative ion (electron detachment)

$$O^- + e \rightarrow O + 2e \qquad K_{det}=2 \times 10^{-13} \exp(-5.5/T_e) \qquad \text{R7}$$
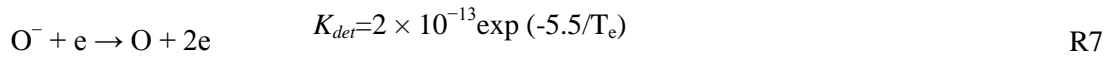
The rate constant for the mutual neutralization depends only on the gas temperature. Also the order and magnitude of K_{rec1} and K_{rec2} and K_{rec3} is similar, therefore we assume, $K_{rec1}=K_{rec2}=K_{rec3}=K_{rec} \sim 1.5 \times 10^{-13} \times (300/T)^{0.5}$.

Considering K_{da} values for reactions 1 to 3 involving dissociative attachment of O_2, O_2^* and O_2^M;along with a constant value of K_{rec} for reaction 4 to 6, the ratio of rate of production and loss of negative ions (K_{da}/K_{rec}) is plotted for electron temperature ranging from 1 eV to 7eV (figure 5.6).
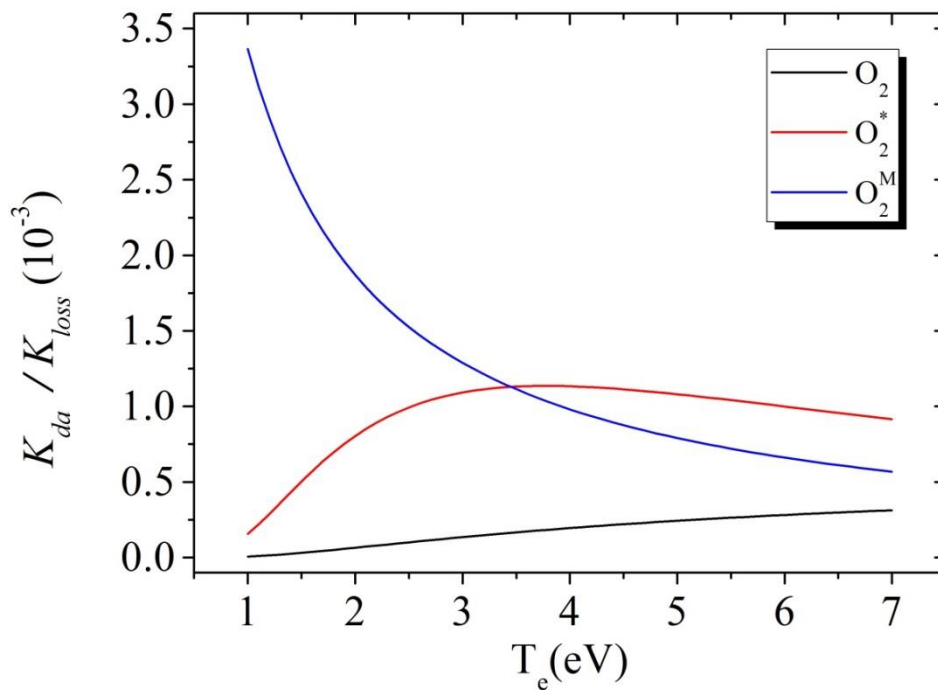
Figure5.6: K_{da}/K_{det} *versus* T_e

The graph shows that for the DA of ground state O_2, the value of K_{da}/K_{rec} increases with increase in electron temperature. For the DA of O_2^M, the ratio has maximum value for $T_e = 1$ eV which reduces exponentially as the electron temperature increases. For DA of O_2^* the value of ratio K_{da}/K_{rec} increases for $T_e= 1$ to 3 eV and after a peak value at $T_e=3$ eV, ratio shows a declining trend for $T_e > 3$ eV. From the graph, it can be also be inferred that for $T_e < 3$eV, DA of O_2^M is the dominating process; whereas for $T_e > 3$eV, DA of O_2^* is a preffered negative ion production mechanism. For $T_e \sim 3$eV, we observe a cumulative effect involving DA of both O_2^M and O_2^*. Therefore we can expect to observe maximum negative ion fraction at $T_e \sim 3$eV.

Figure 5.7 shows the graph of spatial electron temperature measured in front of the anodic glow for d=0.0 cm to 2.0 cm.
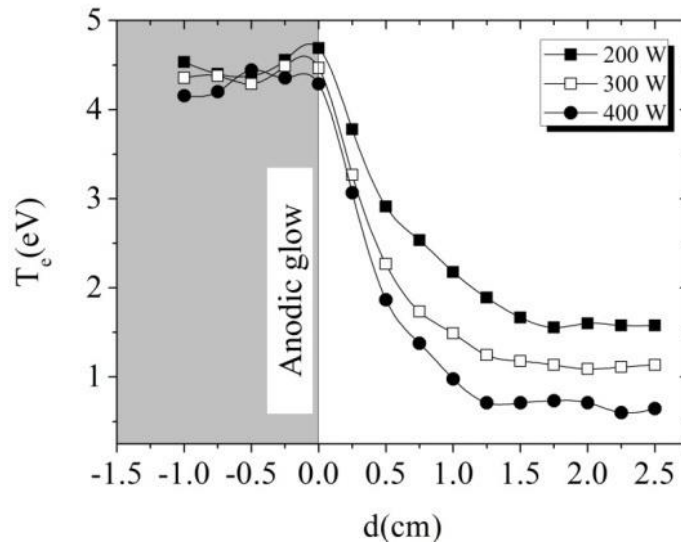
Figure 5.7: *Spatial electron temperature estimated by emissive probe in the anode region*

The electron temperature inside the anodic glow and at the edge of the anodic glow (d=0.0 cm) is equal to 4-5 eV which monotonically decreases as d increases. At d=0.25 cm to d=0.5 cm, $T_e \sim$ 2-3 eV. Therefore we observe the maximum fraction of negative ions (n_i/n_e ~ 2 to 4 in figure 5.3) at d= 0.5 cm.

The rate of negative ions production by reactions 1 to 3, is given by

$$\left[\frac{dn_-}{dt}\right]_{prod} = (K_{da})[n(O_2)]n_e \qquad (5.3)$$

Where $n(O_2)$ is the density of neutral oxygen molecules in a discharge which is determined from the partial pressure of oxygen in a vacuum chamber. Here we do not have quantitative estimate of individual densities of ground [n(O_2_ground)], excited[n(O_2^*)] and metastable[O_2^M] oxygen molecules. However, total oxyen density

$$n(O_2) = n(O_2^{ground}) + n(O_2^*) + n(O_2^M)$$

From reaction 4 to 6, the negative ion loss rate by ion-ion recombination is given by

$$\left[\frac{dn-}{dt}\right]_{loss} = K_{rec1}n\_n(O_2^+) + K_{rec2}n\_n(O^+) + K_{rec3}n\_n(Ar^+)$$

Since $K_{rec1} = K_{rec2} = K_{rec3} = K_{rec}$, from equation (3) and (4), for the equilibrium negative ion density, we can write

$$1 = \frac{dn\_/dt|_{prod}}{dn\_/dt|_{loss}} = \frac{K_{da}}{K_{rec}} \frac{n(O_2)n_e}{\{n(O_2^+) + n(O^+) + n(Ar^+)\}} \tag{5.4}$$

For the argon-oxygen gas mixture, the sum of density of O_2^+, O^+ and Ar^+ is the total positive ion density n_i. Therefore, equation 5.4 is written as

$$n_- = \frac{K_{da}}{K_{rec}} \frac{n(O_2)n_e}{n_i} \tag{5.5}$$

If the O⁻ loss by electron detachment process (reaction 7) is taken into account, then from equation 5.4, the equilibrium negative ion density becomes

$$n_- = \frac{K_{da}}{K_{\text{det}}} n(O_2) \qquad (5.6)$$

Whereas if both the mutual recombination and electron detachment processes are considered then

$$n_- = \frac{K_{da} n(O_2) n_e}{K_{rec} n_i + k_{\text{det}} n_e} \qquad (5.7)$$

Figure 5.8 shows the graph of n_- measured by the two probe technique for d=0.0 cm to d=2.0 cm. It is observed that the n_- is maximum at d=0.0 cm and decreases as the distance the anodic glow increases. Graph also shows the calculated values of n- from either of equation (5.5), (5.6) or (5.7). These calculations are performed by considering different production and loss mechanisms to match the experimental values of n_-. The corresponding values of K_{da}, K_{rec} and K_{det} required for these equation are obtained by considering the experimental values of electron temperature at specific location from the edge of the anodic glow.
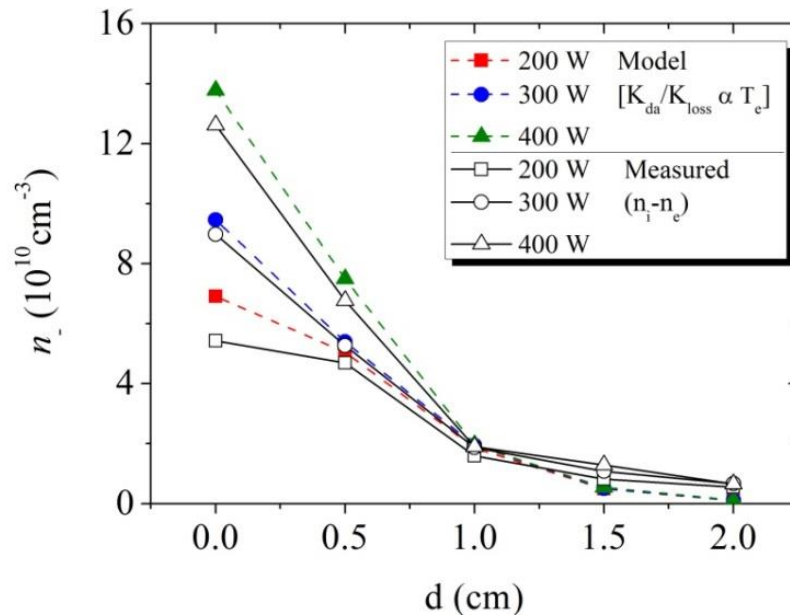
Figure5.8: *The negative ion density estimated by (a) a kinetic model (colored dotted lines) and (b) two probe method (black continuous line)*

The set of production and loss mechanisms are considered to match the experimental data with the model. They are summarized in Table 5.2.

At d=0.0 cm and d=0.5 cm, the electron temperature is 2-5 eV. The value of K_{da} which is used to match the experimental data corresponds to the DA of excited molecules ($O_2^{*}(a^1\Delta_g)$). Further, it is assumed that only excited molecules are present in the discharge which contribute to the formation of negative ions. The main destruction process in this region is considered to be by the mutual recombination process. For d=1.0 cm to d=2.0 cm, the electron temperature is lower ($T_e \sim$ 1-2 eV). In this case the value of K_{da} corresponds to the DA of metastable molecules ($O_2^{M}(A^3\Sigma_+^{u}C^3\Delta_u\ c^1\Sigma_-^{u})$)) Therefore it is assumed that in this region only metastable molecules are present. The negative ion are assumed to be lost by

the electron detachment process. Since we have considered 100 % contribution of either excited or metastable molecules for the DA process at each corresponding location in front of the anodic glow; therefore we can see that the estimated values of n_- are notably higher as compared to the experimental values.

The above assumptions lead us to the fact that, although not 100% but the significant number of excited and metastable oxygen molecules are present in the discharge. The presence of excited and metastable oxygen molecules in the anodic glow region can be attributed to the higher electron temperature inside the anodic glow. The excited oxygen molecules are created due to the electron impact collisions with the ground state molecules. The excited species thus created have a few seconds of lifetime. Therefore these molecules can be gas-dynamically transported out of the anodic glow for longer distances.

Table 5.2: *negative ion production and loss mechanisms in the anodic glow region*

Distance (cm)	Production reaction	Loss Reaction
0.0	DA: O_2^*	Recombination
0.5	DA: O_2^*	Recombination
1.0	DA: O_2^M	Detachment
1.5	DA: O_2^M	Detachment
2.0	DA: O_2^M	Detachment

Figure 5.9 shows the plot of negative ion density as a function of operating powers between 50 W up to 400 W. The graph shows monotonic increase in the negative ion density (n_-) with applied power. This rise in the negative ion density with power can be explained by considering the DA of excited / metastable molecules. As power increases, both excited molecules and number of electrons available for dissociative attachment process increases and therefore we observe a rise in n_- increases with power as shown in figure 5.9.
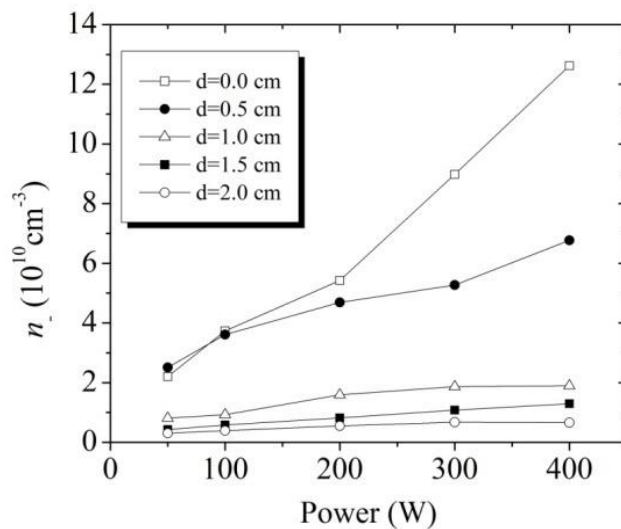
Figure 5.9: *Graph of negative ion density versus power for d = 0.0 cm to d= 1.0 cm*
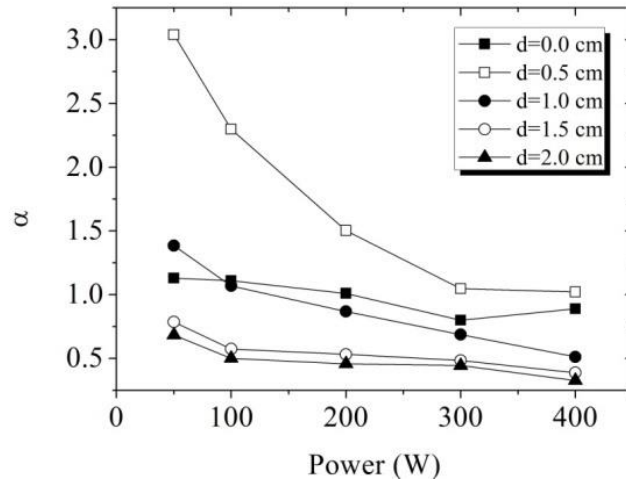
for Ar/O$_2$ discharge

Figure 5.10: *The ratio α=n_ / n_e plotted against input power*

The electronegativity of the plasma is defined as $\alpha = n_-/n_e$. Since $n_- = n_i - n_e$,

$$\alpha = \frac{n_-}{n_e} = \frac{n_+}{n_e} - 1$$

Figure 5.10 shows the power dependence of α in the Ar/O_2 discharge. As power increases α reduces for d = 0.0 cm and d=2.0 cm.

The destruction of negative ion occurs due to the collisions with the positive ions (Ar^+, O_2^+, O^+) and electrons where electron detaches from the negative ion. As power increases, the density of the positive ions and electrons increases which leads to increased negative ion losses. Therefore the rate of rise in the electron density with power is higher than the rate of increases in negative ion density which results in the decrease of α with power as observed in figure 5.10.

5.5   Summary and Conclusion

The properties of electronegative Ar/O_2 gas mixture in the anodic glow region are compared with the electropositive argon gas discharge. Comparison of positive ion density and electron density in case of Ar/O_2 discharge shows a significant deviation in the n_i/n_e from unity. This suggests the presence of high concentration of negative ions near the glow. The presence of negative ions is confirmed by comparing the electric field profiles. The electric field calculations show that the ambipolar diffusion of charged particles is prominent to maintain the charge neutrality in the downstream region the anodic glow.

Negative ion density in the anode region is measured by two probe technique comprising a planar Langmuir probe and the hairpin probe. The measured n_- data is compared with the data obtained from the kinetic model based on the production and loss rates of negative ions. It is shown by matching the experimental data with the model, the dominant negative ion production mechanism is the dissociative attachment process involving the excited and metastable molecules.

The anodic glow region acts a source of excited molecules. These excited molecules migrate to the low electron temperature regions in front of the glow. This situation is useful for the effective production of negative ions by the dissociative attachment process. Thus anodic glow provides favourable conditions for the localized production of negative ions.

Chapter 6   Summary and Outlook

Negative ion plasmas have wide range of applications in plasma processing [9], thrusters for rockets [95], plasma switches, [96] and for the production of neutral beams for plasma heating in fusion devices [20, 97]. Negative ions are also researched for fundamental study such as understanding of pair ion plasma [98]. Clearly study of negative ion production has a far reaching advantages.

As is well understood, the negative ions are formed via three body recombination process in the bulk phase, commonly known as the volume production, but more efficiently by interaction with materials having low workfunction. In the ITER-NBI negative ion source caesium is introduced in the primary discharge in order to achieve the desired density of 10^{18} m^{-3}. If a caesium free negative ion source can be developed; it may help in avoiding unwanted secondary effects resulting from the migration of caesium ions in the accelerator region, and source of secondary electrons that result in arcing between the grids and disrupting the beam.

In order to improve the volume production, it is preferable to reduce the loss rates while increasing the production. This can be achieved by local production of negative ions from the region of interest. Since the negative ions are produced by a two-step process, which is sensitive to electron energy distribution, it is important to design such a source in which the electron temperature can be efficiently controlled.

The negative glow around the constricted anode provides some salient properties that are suitable for the negative ion production. As investigated in Chapter 5, the spatial electron temperature dependence in the anodic glow allows the neutrals injected through the anode a favourable condition to be excited. Some of them can get excited in to meta-stables which play a primary role in the production of negative ions. Another important property of the anodic glow is the spatial dependence of electron temperature that falls away from the glow. In order to retain enough negative ions, it is essential to cool the plasma electrons. In other forms of discharges, this has been achieved by pulsing of the discharge [26],[57]. The electron temperature can also be lowered by increasing the neutral pressure, however in this case, negative ions are lost at greater rate due to increased ion – neutrals collisions.

The anodic glow can provide all the favourable conditions (1) by local production of negative ions in front of the extraction region, thereby minimizing the losses caused by ion-ion and ion neutral interactions, (2) active species generated locally which enhance the chemistry for the volume production of negative ions, (3) a low electron temperature region which minimize the destruction of negative ions that are produced.

A part of the thesis and the main motivation is to understand the kinetics that results in the observed oxygen negative ions in front of the anode. We have used a simple electric probing method for quantifying the negative ions as compared to advanced photo-detachment techniques. The measure electric field obtained are in reasonably good agreement with basic ambipolar diffusion laws, when compared with electropositive argon plasma.

The spatial dependence of negative ions measured using the two probe techniques match very well with the equilibrium model of negative ions formation based on local electron temperature dependences that is experimentally measured by floating emissive probe.

The investigation also leads to a number of important directions/basis for future investigations.

1. Instabilities in the anodic double layer
2. Role of hydrogen plasma
3. Large area negative ions source

Overall the thesis presents an untouched area where we have demonstrated promising applications of the anodic glow for the production of negative ions. Besides the thesis relates the kinetics behind the volume production of negative ions, the plasma diagnostics that are useful for the charactering the negative ion plasmas. The anodic plasma provides the favourable condition as the spatial dependence of electron temperature is important for the production and minimizing losses.

6.1 Evaluation of CHAPS as negative ion source

The negative ion source for Neutral Beam heating system of ITER (and future fusion devices such as DEMO) is required to deliver 40 A of D⁻/H⁻ negative ion current though 0.2 m^2 extraction grid. This demands high density ($\sim 5 \times 10^{18}/m^3$) plasma in front of the extraction grid at low operating pressure of 0.3 Pa pressure.

The properties of the anodic glow plasma demonstrate typical favorable condition for the local production of negative ions in front of the extraction region, thereby minimizing the losses caused by ion-ion and ion neutral interactions.

There are two major issues which need to be addressed in order to realise CHAPS as future negative ion source.

(a) Plasma uniformity in front of the extraction grid

(b) Low pressure (~0.1 Pa) operation of the source

If the plasma in front of the extraction grid is non-uniform, the extracted beam profile may get deviated leading to the power loading on the chamber walls. As mentioned in Appendix 1, the plasma uniformity in CHAPS can be achieved by optimising the distance between the cathode plates. However the low pressure operation of the discharge produced by parallel plate cathode is well above 0.3 Pa as required by the ITER. In this discharge geometry, at low pressure, cathode sheaths become comparable to the distance between the plates. Therefore, the discharge efficiency is reduced and the minimum operating pressure of the discharge is limited only up to 1.0 Pa.

In Appendix 2, a modified design of CHAPS and its basic properties have been discussed. The modified version consists of a device comprised of an enclosed cylindrical hollow cathode having surface area exceeding several orders in magnitude than the anode. The anode is a small tube placed outside the hollow cathode. The hollow cathode and the anode region are separated by a floating stainless steel electrode having a 6.0 mm hole. The gas is injected from the back of the hollow cathode while pumped through hole which creates a differential pressure as high as 10 Pa inside the hollow cathode as compared to the $0.1 - 1$ Pa outside the floating electrode where the anode is situated. By adjusting the gas flow rate a suitable electron neutral ionizing mean free path can be achieved for breakdown. The discharge is sustained with dc power supply at modest operating powers up to 400 W to obtain downstream plasma of density $10^{16} - 10^{17} m^{-3}$. The neutral pressure near the anode is lower however bright plasma can be sustained near the anode as the electric field is concentrated over a small volume. The differential pressure helps to push the plasma outside the hollow cathode region as a jet of plasma sustained at a low pressure. However this modified design is a point source and therefore plasma uniformity over the grid area is difficult to achieve.

Also in the typical density of negative ions in both the sources is in the range of 10^{16}-10^{17} m^{-3} which is about one to two orders of magnitude lower than the plasma density required for ITER NBI source.

In order to achieve these specific requirements, a modified design of CHAPS as shown in figure 6.1 is recommended.
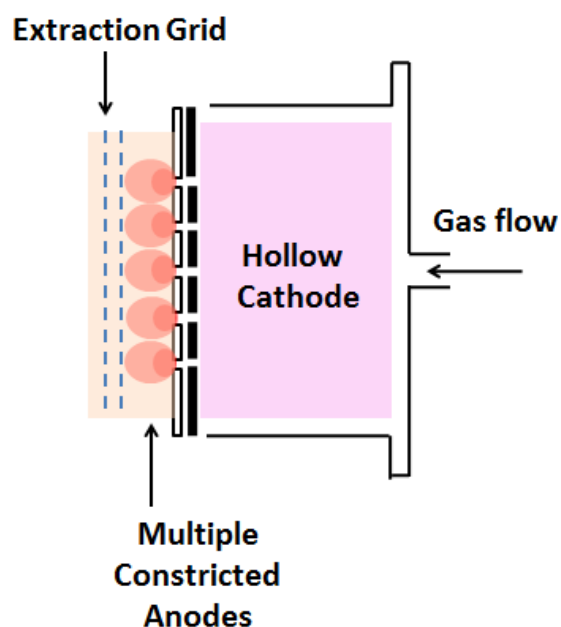
Figure 6.1: *Recommended design of CHAPS to meet the ITER requirements.*

It is also recommended to operate the CHAPS in pulsed DC mode. Following are some of the advantages of operating CHAPS with pulsed DC bias

1. It is possible to improve plasma density by providing higher input power if the discharge is operating in the pulsed DC mode

2. Negative ion density enhances in the off time of the pulse bias due to drop in the electron temperature. Therefore pulsed operation is useful to increase the time averaged negative ion density.

Appendix A Plasma Uniformity in CHAPS

Plasma uniformity is the key requirement to achieve unique material properties over the large substrate area. Negative ion sources used for neutral beam injection system of fusion devices also require uniform electronegative plasma in front of the extraction grid to generate a homogenous negative ion beam. Here we present the properties of CHAPS in cathode region for production of negative ions which can be scalable to arbitrary area.

Experimental details

Figure-1 shows the schematic of the experimental set-up. The base pressure of 10^{-4} Pa in the vacuum chamber is achieved prior to introducing the operating gas, pure Ar or Ar + O_2 in the ratio of 50-50% through the anode. The working pressure inside plasma chamber is in the range 1 Pa–10 Pa maintained using a constant gas flow through commercial mass flow controller.
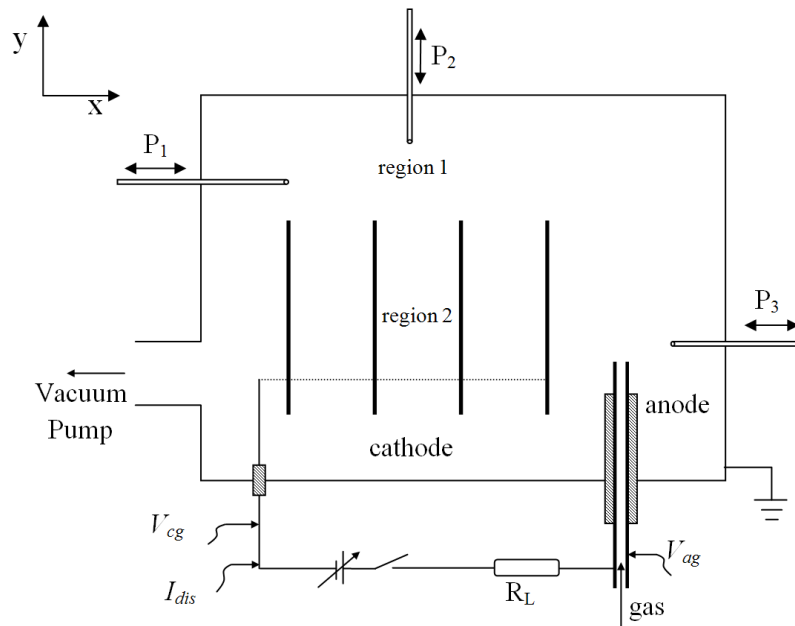
Figure 1: *Schematic of constricted hollow anode plasma source; P1, P2, P3 are the positions of the probes (hairpin probe/emissive probe/Langmuir probe). The discharge is created by applying a DC bias between the cathode and anode.*

As shown in figure 1 the plasma properties along the x-axis are measured using Langmuir probe, hairpin probe and the emissive probes inserted in the plasma chamber at P1. The radial plasma properties in region 1 and region 2 are measured by introducing the probes at P2.

Experimental Results and discussion

The measurement of plasma parameters, n_e, T_e and n_+ are carried out at two specific locations, namely region-1 (outside the parallel plates) and region-2 (between the plates). The negative ions are inferred by comparing the ratio of ion density to electron density.
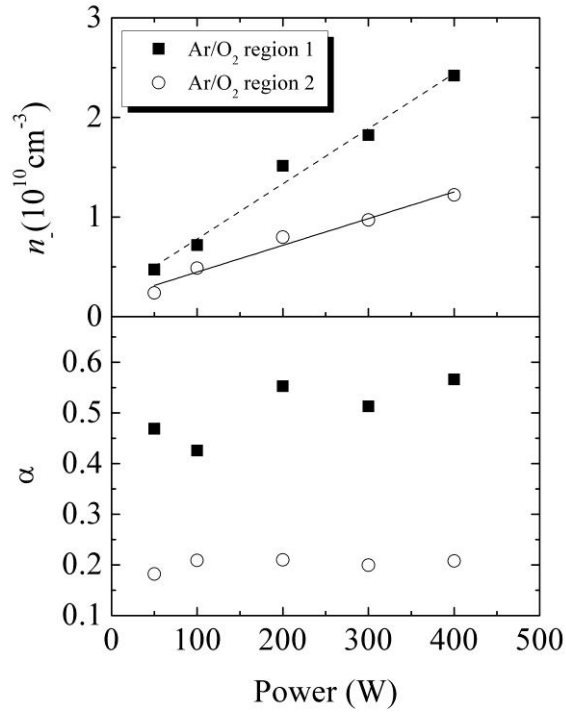
Figure 2: *Plot of (a) negative ion density, n- and (b) electronegativity, α measured in region 1 and 2 using dual probe technique as a function of applied power. The operating pressure of the Ar/O₂ discharge is 3 Pa.*

Figure 2 (a) shows the oxygen negative ion density n_- which linearly increases with the applied power. Typically the density in both regions 1 and 2 is on the order of 10^{10} cm$^-$^{3}with slightly higher density found in region 1 as compared to region-2.

The value of electro-negativity α is calculated from

$$\alpha = \frac{n_-}{n_e} = \frac{n_+}{n_e} - 1$$

which is found 0.4 to 0.6 in region-1 while α in region 2 is close to 0.2 and remains constant with power.

The difference in electronegativities in the two regions is attributed to the characteristic electron temperatures which are found to be significantly different as plotted in figure-5.
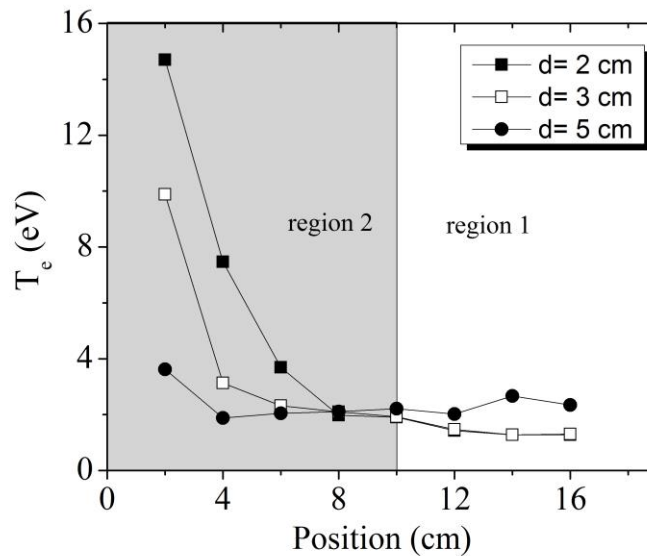
Figure 3: *Graph of spatial electron temperature profile along the y axis (figure 1) in cathode region for nitrogen discharge. Data is plotted for different cathode plate separations (d= 2 cm, 3 cm , 5 cm).*

The electron temperature between the parallel plates is characterized by temperatures of the order of 4 -15 eV as compared to < 2 eV outside the parallel plates. Higher electron temperatures between the parallel plates suggest the presence of fast secondary electrons released from the cathode during ion bombardment which are trapped between the sheaths of the opposing electrodes as similar to hollow cylindrical cathodes. Outside these plates

we observe diffused plasma with the electron temperature dropping by over a factor of two than between the plates. Therefore CHAPS provides distinct electron temperature regions of typically 10 eV between the plates and a low electron temperature of the order of 2 eV as measured outside the plates.

In region 2, the destruction rate of negative ions is more because of higher electron temperature between the cathode plates. On the other hand the presence of energetic electrons in the discharge is also important for the creation of excited O_2 molecule in order to perform the dissociative attachment reaction.

Uniform negative ion density

The spatial profile of oxygen negative ion density in front of the cathode plates (region 1) is obtained by measuring plasma densities by planar Langmuir probe and hairpin probe.

Experiments are carried out with different cathode plate separations to achieve a uniform negative ion density. For Ar/O_2 discharge operated at 3 Pa, the better plasma uniformity is obtained when distance between each cathode plate was 5 cm. Figure 6 shows the plot of n_- against the probe position.
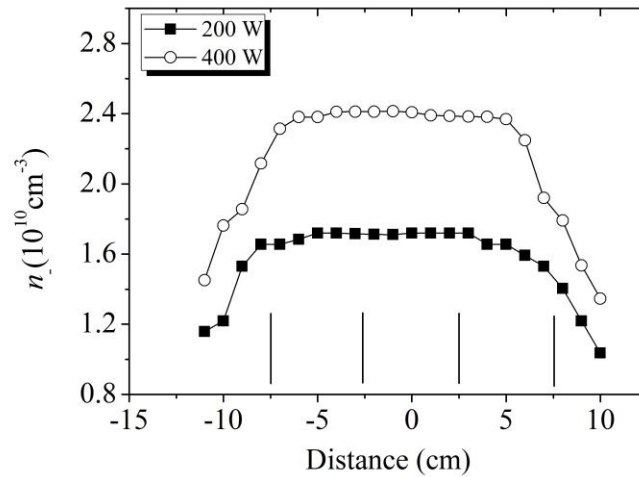
Figure 4: *Graph of negative ion density along x-axis in front of the parallel plate cathode. Measurements are taken above 4.3 cm from the edge of the cathode plates (probe position P1 in figure 1). Graph also shows the position of the cathode plates.*

For 200 W and 400 W power, a flat negative ion density profile is observed over a span of 10 cm in front of the cathode plates, which is limited only by the number of plates. However the negative ion density drops on the either side of the end plates.

Summary

The investigations on Ar/O$_2$ discharge in a DC constricted hollow anode plasma source are presented. A dual probe technique comprising a planar Langmuir probe and the hairpin probe is used for measuring the negative ion concentration and the electronegativity in the cathode region of CHAPS

The spatial electron density profile measurements show high concentration of negative ions above the parallel plate. This is attributed to the distinct electron temperature regions

created by the parallel plate cathode geometry which enhance the negative ion production by dissociative attachment.

A uniform negative ion density in front of the cathode plates is simply achieved by optimizing the distance between the cathode plates.

Appendix B   Constricted Plasma Source

In this section properties of a Constricted Plasma Source are presented. The source is based on a design first explained by Anders in 1995. The source consists of differentially pumped hollow cathode in conjunction with a small anode isolated by a constricted insulated electrode with a small orifice. The device helps in producing a plasma jet exiting from the high pressure (10 Pa) region inside the hollow cathode through the constricted electrode into the downstream anode plasma which stays at a low pressure of 0.1 to 0.5 Pa.

Experimental set-up and working principle

The plasma source consists of an enclosed cylindrical hollow cathode in conjunction with a small anode mounted on the exit aperture of the cathode. The electrode assembly is mounted inside the electrically grounded vacuum chamber such that both cathode and anode are floating with respect to chamber. A base vacuum of 10^{-6} mbar is created inside the vacuum chamber and pure argon or argon – oxygen gas mixture (50 % Ar, 50% O_2) is passed through the hollow cathode –constricted anode assembly. The pressure outside the cathode was maintained in the range of 0.1 Pa – 1 Pa. The DC discharge is created with a DC power supply at modest operating powers up to 400 W to obtain downstream plasma jet of density $10^{16} – 10^{17}$ m^{-3}. The anode voltage drop is observed to be minimum when the

sharp anode glow is created just near the anode (figure 1(a)). At this point the typical anode voltage drop is 40-50 V which depends on the pressure, flow rate and the type of gas. Although the neutral pressure near the anode is lower, bright plasma can be sustained near the anode as the electric field is concentrated over a small volume. The differential pressure helps to push the plasma outside the hollow cathode region as a jet of plasma sustained at a low pressure.

The spatial properties of the plasma near the anode are measured using hairpin resonance probe for measuring electron density and an ion flux probe for positive ions density. The plasma potential and electron temperature is estimated using a floating emissive probe. These point measurements are carried out relative to the edge of the anode glow, $d = 0.0$ cm as shown in figure 2

Figure 1: *A view of a Constricted plasma source - A small hollow anode is mounted on the a hollow cathode aperture; (b) a hazy anode double glow (high anode voltage drop), (c) fully developed anode glow (minimum anode voltage drop)*
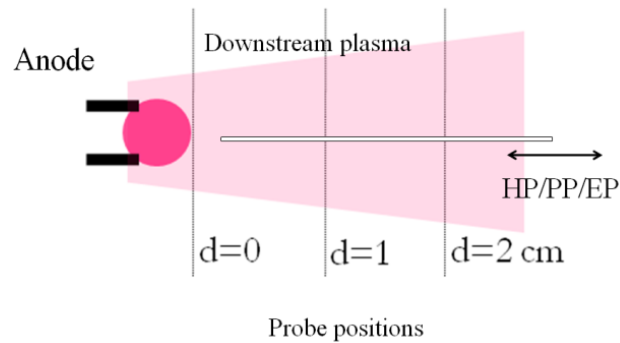
Figure 2: *Spatial plasma parameters measurement from the edge of anode glow. HP: Hair pin probe, PP: Planar Langmuir probe, EP: Emissive probe*

Experimental results and discussion

Discharge properties with Argon gas

Figure 3 shows the graph of electron density measured at d=0 cm, to d= 2.0 cm away from the edge of the anode glow at different operating powers (200 W, 300 W, 400 W). Plasma density is on the order of 10^{16} m^{-3} and increases with power. The plasma density decreases as the distance from the anode glow increases. The drop in electron density is a result of ambipolar diffusion of positive ions in the expanding beam plasma. The electron density also drops as a result of very low ionization.

Figure 3: Graph of electron density versus axial distance along the plasma jet at 200 W –

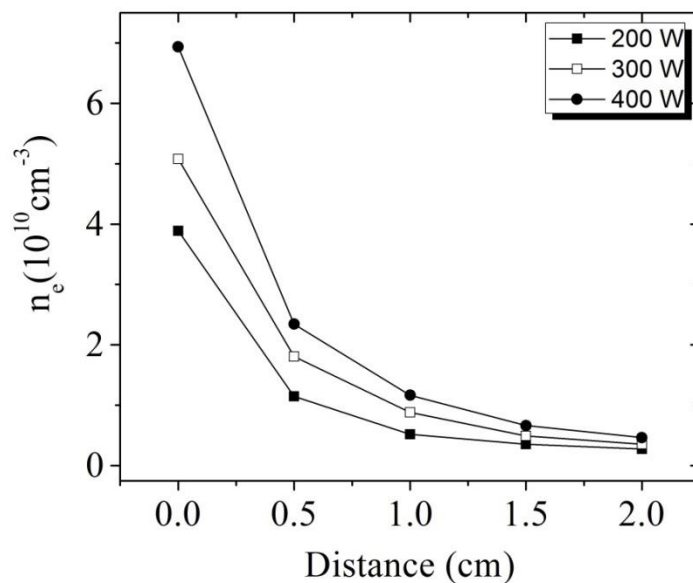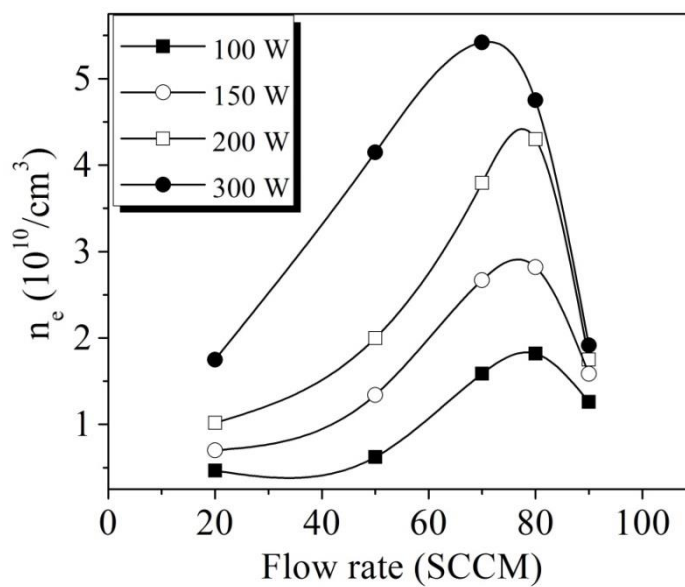400 W power for argon-oxygen gas at 0.65 Pa

Figure 4: Plot of electron density as a function of gas flow rate for 100 W-300 W power

Plasma density depends on the gas flow rate. At a given pressure and power, the plasma density increases with the gas flow rate and after reaching maximum at certain critical value, plasma density is found to decrease with increase in the flow rate as shown in figure 4 where the electron density data is plotted for $20 - 100$ sccm flow rate and for power 100 W to 300 W at constant 1×10^{-2} mbar pressure in the anode region. This nonmonotonic behavior of electron density with gas flow rate at constant power can be attributed to the differential pressure inside the hollow cathode. At the constant pressure outside the hollow cathode, increases in gas flow rate increases number of neutrals inside the hollow cathode which leads to increase in the number density at the given power. However, at higher flow rates, electron temperature decreases due to increase in pressure inside the cathode cavity which leads to reduction in the electron $-$ neutral ionizing collisions and thus overall plasma density decreases.

Estimation of negative ion density and electronegativity

The density of negative ions can be estimated by taking the difference between the positive ion density measured by the ion flux probe and the electron density measured by the hairpin resonance probe i.e. $n_- = n_+ - n_e$. Figure shows the plot of negative ion density as a function of operating powers between 150 W up to 400 W at constant background neutral pressure of 0.65 Pa near the anode.
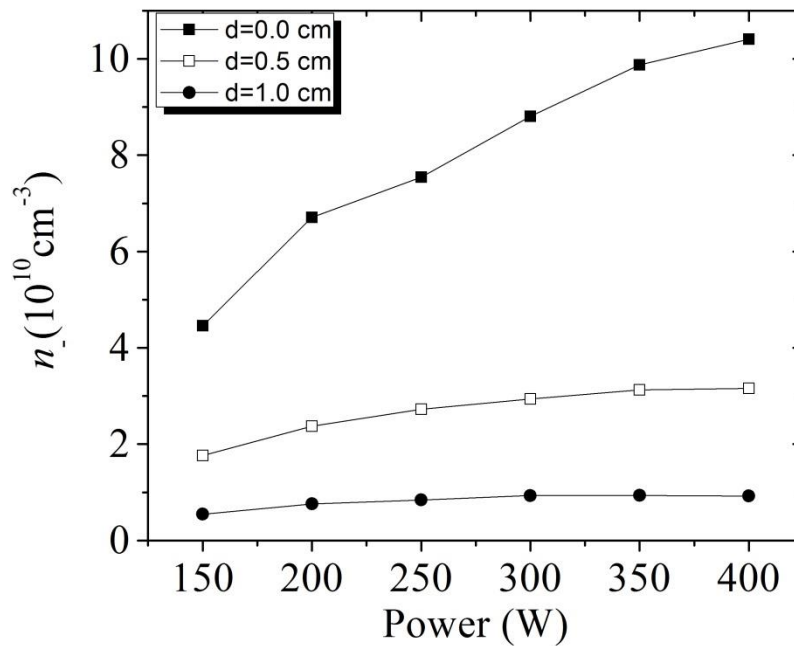
Figure 5: Graph of negative ion density versus power for d = 0.0 cm to d= 1.0 cm for Ar/O$_2$ discharge operation at 0.65 Pa pressure near the anode region

The graph shows monotonic increase in the negative ion density (n_-) with applied power. n_- is maximum at d=0.0 cm and it decreases as distance from anode glow increases. This rise in the negative ion density with power can be explained by considering the formation process of O^- in the Ar/O$_2$ discharge. At low pressure, the dissociative attachment of electrons to the excited oxygen molecule is dominant process
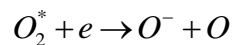
$$O_2^* + e \rightarrow O^- + O$$

As power increases, both excited molecules and number of electrons available for dissociative attachment process increases and therefore $n\_$ increases with power as shown in Figure.
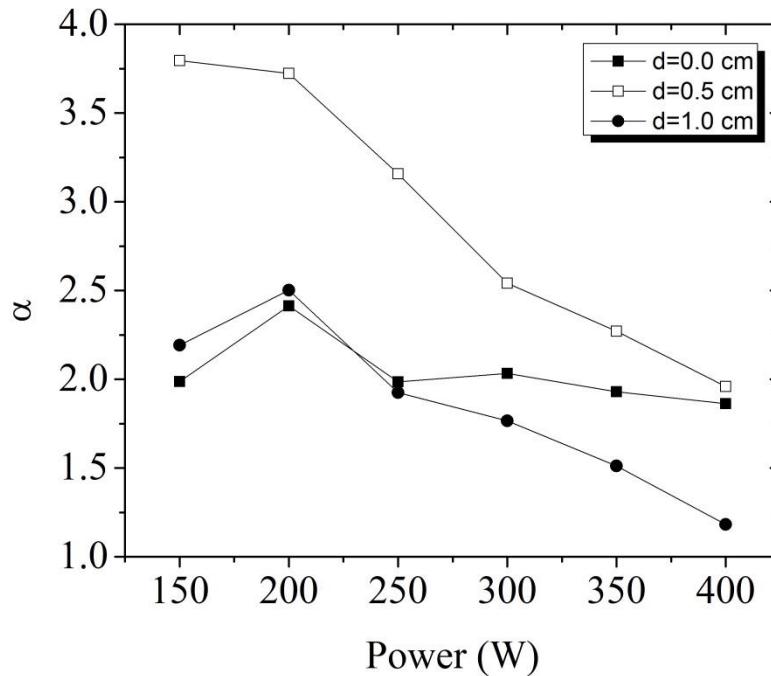
Figure 7: The ratio $\alpha = n\_ / n_e$ plotted against input power

Figure 7 shows the power dependence of α in the Ar/O_2 discharge at 0.6 Pa. As power increases α reduces for d = 0.5 cm and d=1.0 cm however at d= 0.0 cm the decreases in α is minimum as compared to d= 0.5 and cm and d= 1.0 cm.

The destruction of negative ion occurs due to the collisions with the Ar+ and electrons which increases with the input power (e.g. $O^- + e \rightarrow O + 2e$, $O^- + Ar^+ \rightarrow O + Ar$). Therefore the

rate of rise in the electron density with power is higher than the rate of increases in negative ion density which results in the decrease of α with power as observed in figure 7.

Summary and Conclusion

The Constricted Plasma Source is characterized by intense plasma on the order of 10^{11} cm^{-3} in front of the constricted anode and high density ($\sim 10^{10}$cm^{-3}) downstream plasma at the operating pressure as low as 0.3 Pa and at the moderate input power of upto 500 W. Plasma density in front of the anode depends on the gas flow rate. Plasma density scales linearly with operating power and pressure. A high concentration of negative ions ($\sim 10^{10}$ cm^{-3}) in the downstream plasma region is measured at low working gas pressure (0.6 Pa). Electronegativity (α) of the Ar/O$_2$ discharge has been calculated from the ratio of negative ion density to the electron density. The high value of α (1 to 5) indicates that plasma is highly electronegative. α is maximum at 5 mm distance away from the anode which suggest the localized production of negative at that point. If the source is mounted in front of the extraction grid, the negative ions produced in the downstream plasma can be efficiently accelerated with minimum loss of negative ions by collisions with background neutrals and charged species. The low pressure operation of the discharge and localized production of high concentration of negative ions in the bulk of the plasma are the key properties which make the constricted plasma promising for the ITER NBI system.

Appendix C DC power Supply

DC power supply: A Voltage doubler

A DC power supply used in our experiments consists of a voltage double circuit which converts the input AC to DC. The advantage of using a voltage double circuit over a usual full wave rectifier circuit is that the magnitude of the DC output is twice that of input peak voltage which is helpful to get the breakdown at lower pressures.
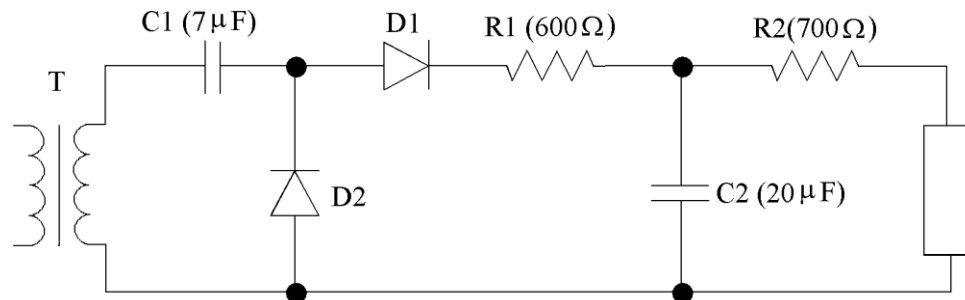

Figure 1: Voltage doubler circuit

Circuit operation

The schematic of the voltage double circuit is shown in figure 2-5. During the first negative half-cycle, D1 is forward biased and C1 charges to a voltage equal to the peak voltage

(V_{peak}) of the transformer. During the following positive half cycle, D1 is reverse biased and therefore conducts no current. The voltage on C1 adds to the transformer output voltage, so a voltage of $+2V_{peak}$ appears at the anode of D2. Since C2 is not charged, D2 becomes forward biased and thus the voltage at the C1 is passed to C2 until $V_{C1}=V_{C2}$.

On the next negative half-cycle, C1 charges again to V_{peak}, through D1. In the second positive half-cycle, C2 is still charged to $V_{C1\_first\ cycle}$, while the voltage at the anode of D2 is rises to $+2Vpeak$. So Again, C1 transfers part of its charge to C2, but this time $V_{C2\_second\ cycle} > V_{C2\_first\ cycle}$. This process continues, with C1 being fully recharged to v_p on each negative half cycle, and then charging C2 to a voltage close to $+2V_{peak}$.

In the above circuit, R1 and R2 are power resistor used as current limiters.

In our experiments, the line input (230V, 32A) is converted to the maximum of AC 1.5 kV, 4A through the step-down transformer. A voltage double circuit converts this AC to the maximum DC output of 4.5 kV, 2A which is measured across the capacitor (C2). The output power of the circuit is controlled by a variable transformer which controls the power supplied to the step-down transformer. The output power is fed to the electrodes through a load resistor (R2). This DC voltage doubler power supply can be used with both the floating electrodes.

References

1.   Forbes. *End of fossil fuel - Forbes.com*. 2009   31-March-2012]; Available from: http://www.forbes.com/2009/07/24/peak-oil-production-business-energy-nelder.html.

2.   ITER-Organization. *ITER - the way to new energy*. 2012   31-March-2012]; Available from: http://www.iter.org/proj/iterhistory.

3.   EFDA. *European fusion devenlopment agreement*. 2012   31-March-2012]; Available from: http://www.efda.org.

4.   Dani, I., et al., *Atmospheric-Pressure Plasmas for Solar Cell Manufacturing.* Contributions to Plasma Physics, 2009. **49**(9): p. 662-670.

5.   Uhrlandt, D., et al., *Low-pressure mercury-free plasma light sources: experimental and theoretical perspectives.* Journal of Physics D: Applied Physics, 2005. **38**(17): p. 3318.

6.   Perrin, J., et al., *The physics of plasma-enhanced chemical vapour deposition for large-area coating: industrial application to flat panel displays and solar cells.* Plasma Physics and Controlled Fusion, 2000. **42**(12B): p. B353.

7.   Chen, F.F., *Industrial applications of low-temperature plasma physics.* Physics of Plasmas, 1995. **2**: p. 2164-2175.

8.   Lieberman, M.A., *The Langmuir isotherm and the standard model of ion-assisted etching.* Plasma Sources Science Technology, 2009. **18**: p. 4002.

9.   Lieberman, M.A. and A.J. Lichtenberg, *Principles of Plasma Discharges and Materials Processing, 2nd Edition*. Principles of Plasma Discharges and Materials Processing, 2nd Edition, by Michael A. Lieberman, Alan J. Lichtenberg, pp. 800. ISBN 0-471-72001-1. Wiley-VCH , April 2005., ed. M.A. Lieberman2005.

10.   Bhoj, A.N. and M.J. Kushner, *Repetitively pulsed atmospheric pressure discharge treatment of rough polymer surfaces: II. Treatment of micro-beads in He/NH3/H2O and He/O2/H2O mixtures.* Plasma Sources Science Technology, 2008. **17**: p. 5025.

11.   Gubala, V., et al., *Functionalization of cycloolefin polymer surfaces by plasma-enhanced chemical vapour deposition: comprehensive characterization and analysis of the contact surface and the bulk of aminosiloxane coatings.* The Analyst, 2010. **135**: p. 1375.

12. Kong, M.G., et al., *Plasma medicine: an introductory review.* New Journal of Physics, 2009. **11**: p. 5012.

13. Langmuir, I., *The Interaction of Electron and Positive Ion Space Charges in Cathode Sheaths.* Physical Review, 1929. **33**: p. 954-989.

14. Crookes, W., *On a Fourth State of Matter.* Royal Society of London Proceedings Series I, 1879. **30**: p. 469-472.

15. Shkarofsky, I.P., *The Particle Kinetics of Plasmas.* American Journal of Physics, 1967. **35**: p. 551-552.

16. Chen, F.F. and S.E. von Goeler, *Introduction to Plasma Physics and Controlled Fusion Volume 1: Plasma Physics, Second Edition.* Physics Today, 1985. **38**: p. 87.

17. Rose, G. and H.U. Widdel, *Results of Concentration and Mobility Measurements for Positively and Negatively Charged Particles Taken Between 85 and 22 km in Sounding Rocket Experiments.* Radio Sci., 1972. **7**(1): p. 81-87.

18. Lebedev, V.S., L.P. Presnyakov, and I.I. Sobel'man, *Photodissociative absorption by H 2 + in the solar photosphere.* Astronomy Reports, 2000. **44**(5): p. 338-347.

19. Bacal, M. and G.W. Hamilton, *H/-/ and D/-/ production in plasmas.* Phys Rev Lett, 1979. **42**: p. 1538-1540.

20. Fantz, U., et al., *Negative ion RF sources for ITER NBI: status of the development and recent achievements.* Plasma Physics and Controlled Fusion, 2007. **49**: p. 563.

21. Brown, I.G., *The Physics and Technology of Ion Sources, Second, Revised and Extended Edition.* The Physics and Technology of Ion Sources, Second, Revised and Extended Edition, by Ian G. Brown (Editor), pp. 396. ISBN 3-527-40410-4. Wiley-VCH , September 2003., ed. I.G. Brown2003.

22. Bacal, M., P. Berlemont, and D.A. Skinner, *Volume production of hydrogen negative ions*, in *Society of Photo-Optical Instrumentation Engineers (SPIE) Conference Series*, H.E. Brandt, Editor 1989. p. 528-535.

23. Dimov, G.I., *Tandem surface-plasma source: A new concept for a dc negative ion source.* Review of Scientific Instruments, 2002. **73**: p. 970-972.

24. Morse, E.C., *A tandem, microwave-driven cusp negative ion source*, in *California Univ., Berkeley Report*1991.

25. Hopkins, M.B., M. Bacal, and W.G. Graham, *Enhanced volume production of negative ions in the post discharge of a multicusp hydrogen discharge.* Journal of Applied Physics, 1991. **70**: p. 2009-2014.

26. Hopkins, M.B. and K.N. Mellon, *Enhanced production of negative ions in low-pressure hydrogen and deuterium discharges.* Phys Rev Lett, 1991. **67**: p. 449-452.

27. Franklin, R.N., *The plasma-wall boundary region in negative-ion-dominated plasmas at low pressures.* Plasma Sources Science Technology, 2000. **9**: p. 191-198.

28. Franklin, R.N., *Electronegative plasmas - why are they so different?* Plasma Sources Science Technology, 2002. **11**: p. 31-A37.

29. Franklin, R.N. and J. Snell, *Modelling discharges in electronegative gases.* Journal of Physics D Applied Physics, 1999. **32**: p. 2190-2203.

30. Baalrud, S.D., B. Longmier, and N. Hershkowitz, *Equilibrium states of anodic double layers.* Plasma Sources Science Technology, 2009. **18**: p. 5002.

31.   Charles, C., *TOPICAL REVIEW: A review of recent laboratory double layer experiments.* Plasma Sources Science Technology, 2007. **16**: p. 1.

32.   Stenzel, R., C. Ionita, and R. Schrittwieser, *Plasma Fireballs.* Ieee Transactions on Plasma Science, 2008. **36**: p. 1000-1001.

33.   Stenzel, R.L., C. Ionita, and R. Schrittwieser, *Dynamics of fireballs.* Plasma Sources Science Technology, 2008. **17**: p. 5006.

34.   Emeleus, K.G., *Anode glows in glow discharges: outstanding problems.* International Journal of Electronics, 1982. **52**(5): p. 407-417.

35.   Gurlui, S., et al., *Experimental and Theoretical Investigations of Anode Double Layer.* Japanese Journal of Applied Physics, 2005. **44**: p. 3253.

36.   Schrittwieser, R.W. *Double Layers and Other Nonlinear Potential Structures in Plasmas*. in *Double Layers and Other Nonlinear Potential Structures in Plasma*. 1993.

37.   Anders, A. and G.Y. Yushkov, *Low-energy linear oxygen plasma source.* Review of Scientific Instruments, 2007. **78**: p. 3304.

38.   Miljevic, V.I., *Characteristics of the Hollow Anode Ion-Electron Source.* IEEE Transactions on Nuclear Science, 1985. **32**: p. 1757.

39.   Miljevic, V., *Cylindrical hollow anode ion source.* Review of Scientific Instruments, 2002. **73**: p. 751-753.

40.   Miljevic, V., *Hollow anode ion-electron source.* Review of Scientific Instruments, 1984. **55**: p. 931-933.

41.   Anders, A. and S. Anders, *The working principle of the hollow-anode plasma source.* Plasma Sources Science Technology, 1995. **4**: p. 571-575.

42.   Anders, A. and M. Kühn, *Characterization of a low-energy constricted-plasma source.* Review of Scientific Instruments, 1998. **69**: p. 1340-1343.

43.   Arslanbekov, R.R., A.A. Kudryavtsev, and R.C. Tobin, *On the hollow-cathode effect: conventional and modified geometry.* Plasma Sources Science Technology, 1998. **7**: p. 310-322.

44.   Kolobov, V.I. and L.D. Tsendin, *Analytic model of the hollow cathode effect.* Plasma Sources Science Technology, 1995. **4**: p. 551-560.

45.   Donkó, Z., *Hybrid model of a rectangular hollow cathode discharge.* Physical Review E, 1998. **57**: p. 7126-7137.

46.   Rasser, B., J.N.M. Van Wunnik, and J. Los, *Theoretical models of the negative ionization of hydrogen on clean tungsten, cesiated tungsten and cesium surfaces at low energies.* Surface Science, 1982. **118**(3): p. 697-710.

47.   I. Langmuir, H.M.M.-S., *Studies of Electric Discharges in Gases at Low Pressures.* Gen. Elec. Rev., 1924. **27**: p. 449

48.   Karkari, S.K., A. Vetushka, and J.W. Bradley, *Measurement of the plasma potential adjacent to the substrate in a midfrequency bipolar pulsed magnetron.* Journal of Vacuum Science Technology, 2003. **21**: p. L28-L32.

49.   Kemp, R.F. and J.M. Sellen, Jr., *Plasma Potential Measurements by Electron Emissive Probes.* Review of Scientific Instruments, 1966. **37**: p. 455-461.

50. Stenzel, R.L., *Microwave resonator probe for localized density measurements in weakly magnetized plasmas.* Review of Scientific Instruments, 1976. **47**: p. 603-607.

51. Karkari, S.K., et al., *A floating hairpin resonance probe technique for measuring time-resolved electron density in pulse discharge.* Measurement Science and Technology, 2007. **18**: p. 2649-2656.

52. Piejak, R.B., et al., *The hairpin resonator: A plasma density measuring technique revisited.* Journal of Applied Physics, 2004. **95**: p. 3785-3791.

53. Boyd, R.L.F. and J.B. Thompson, *The Operation of Langmuir Probes in Electro-Negative Plasmas.* Royal Society of London Proceedings Series A, 1959. **252**: p. 102-119.

54. Braithwaite, N.S.J. and J.E. Allen, *Boundaries and probes in electronegative plasmas.* Journal of Physics D Applied Physics, 1988. **21**: p. 1733-1737.

55. Karkari, S.K., et al., *A technique for obtaining time- and energy-resolved mass spectroscopic measurements on pulsed plasmas.* Measurement Science and Technology, 2002. **13**: p. 1431-1436.

56. Bacal, M., *Photodetachment diagnostic techniques for measuring negative ion densities and temperatures in plasmas.* Review of Scientific Instruments, 2000. **71**: p. 3981-4006.

57. Dodd, R., et al., *Negative ion density measurements in a reactive dc magnetron using the eclipse photodetachment method.* Plasma Sources Science Technology, 2010. **19**: p. 5021.

58. Sirse, N., et al., *The temporal evolution in plasma potential during laser photo-detachment used to diagnose electronegative plasma.* Plasma Sources Science Technology, 2011. **20**: p. 5003.

59. Quandt, E., H.F. Döbele, and W.G. Graham, *Measurements of negative ion densities by absorption spectroscopy.* Applied Physics Letters, 1998. **72**: p. 2394.

60. Conway, J., et al., *Using the resonance hairpin probe and pulsed photodetachment technique as a diagnostic for negative ions in oxygen plasma.* Plasma Sources Science and Technology, 2010. **19**(6): p. 065002.

61. Bradley, J.W., et al., *Resonance hairpin and Langmuir probe-assisted laser photodetachment measurements of the negative ion density in a pulsed dc magnetron discharge.* Journal of Vacuum Science & Technology A: Vacuum, Surfaces, and Films, 2011. **29**(3): p. 031305-7.

62. Quandt, E., I. Kraemer, and H.F. Döbele, *Measurements of negative-ion densities by cavity ringdown spectroscopy.* EPL (Europhysics Letters), 1999. **45**(1): p. 32.

63. Amemiya, H., *Plasmas with negative ions-probe measurements and charge equilibrium.* Journal of Physics D: Applied Physics, 1990. **23**(8): p. 999.

64. Chabert, P., et al., *Electrostatic probe measurement of the negative ion fraction in an SF 6 helicon discharge.* Plasma Sources Science and Technology, 1999. **8**(4): p. 561.

65. Nikitin, A.G., F.E. Balghiti, and M. Bacal, *Comparison of negative ion density measurements by probes and by photodetachment.* Plasma Sources Science and Technology, 1996. **5**(1): p. 37.

66.   Curley, G.A., et al., *Negative ions in single and dual frequency capacitively coupled fluorocarbon plasmas.* Plasma Sources Science and Technology, 2007. **16**(1): p. S87.

67.   Straňák, V., et al., *Study of Electronegative Ar/O2 Discharge by Means of Langmuir Probe.* Contributions to Plasma Physics, 2008. **48**(5-7): p. 503-508.

68.   Newman, D.L., et al., *Formation of Double Layers and Electron Holes in a Current-Driven Space Plasma.* Physical Review Letters, 2001. **87**: p. 255001.

69.   Charles, C. and R.W. Boswell, *The magnetic-field-induced transition from an expanding plasma to a double layer containing expanding plasma.* Applied Physics Letters, 2007. **91**: p. 1505.

70.   Johnson, J.C., N.D. Angelo, and R.L. Merlino, *A double layer induced ionisation instability.* Journal of Physics D: Applied Physics, 1990. **23**(6): p. 682.

71.   Merlino, R.L. and J.J. Loomis, *Double layers in a plasma with negative ions.* Physics of Fluids B: Plasma Physics, 1990. **2**(12): p. 2865-2867.

72.   Nema, S.K., et al., *Plasma polymerization using a constricted anode plasma source.* Surface and Coatings Technology, 2004. **179**(2–3): p. 193-200.

73.   Conde, L., C. Ferro Fontán, and J. Lambás, *The transition from an ionizing electron collecting plasma sheath into an anodic double layer as a bifurcation.* Physics of Plasmas, 2006. **13**: p. 3504.

74.   Meige, A., et al., *Propagating double layers in electronegative plasmas.* Physics of Plasmas, 2007. **14**: p. 3508.

75.   Plihon, N. and P. Chabert, *Ion acoustic waves and double-layers in electronegative expanding plasmas.* Physics of Plasmas, 2011. **18**: p. 2102.

76.   Plihon, N., P. Chabert, and C.S. Corr, *Experimental investigation of double layers in expanding plasmas.* Physics of Plasmas, 2007. **14**: p. 3506.

77.   Singh, N. and R.W. Schunk, *Current-driven double layers and the auroral plasma.* Geophysical Research Letters, 1982. **9**: p. 1345-1348.

78.   Lakhina, G.S., S.V. Singh, and A.P. Kakad, *Ion- and electron-acoustic solitons and double layers in multi-component space plasmas.* Advances in Space Research, 2011. **47**: p. 1558-1567.

79.   Sanduloviciu, M. and E. Lozneanu, *On the generation mechanism and the instability properties of anode double layers.* Plasma Physics and Controlled Fusion, 1986. **28**: p. 585-595.

80.   Song, B., N. D'Angelo, and R.L. Merlino, *On anode spots, double layers and plasma contactors.* Journal of Physics D Applied Physics, 1991. **24**: p. 1789-1795.

81.   Song, B., N. D'Angelo, and R.L. Merlino, *Stability of a spherical double layer produced through ionization.* Journal of Physics D Applied Physics, 1992. **25**: p. 938-941.

82.   Pohoață, V., et al., *Properties and control of anode double layer oscillations and related phenomena.* Physical Review E, 2003. **68**: p. 16405.

83.   Dimitriu, D.G., et al., *Common physical mechanism for concentric and non-concentric multiple double layers in plasma.* Plasma Physics and Controlled Fusion, 2007. **49**: p. 237-248.

84. Stenzel, R., et al., *High-Frequency Instabilities in Sheaths and Fireballs.* IEEE Transactions on Plasma Science, 2011. **39**: p. 2448-2449.

85. Stenzel, R.L., et al., *Electron-rich sheath dynamics. I. Transient currents and sheath-plasma instabilities.* Physics of Plasmas, 2011. **18**: p. 2112.

86. Stenzel, R.L., et al., *Electron-rich sheath dynamics. II. Sheath ionization and relaxation instabilities.* Physics of Plasmas, 2011. **18**: p. 2113.

87. Gudmundsson, J.T. and E.G. Thorsteinsson, *Oxygen discharges diluted with argon: dissociation processes.* Plasma Sources Science Technology, 2007. **16**: p. 399-412.

88. Stoffels, E., W.W. Stoffels, and G.M.W. Kroesen, *Plasma chemistry and surface processes of negative ions.* Plasma Sources Science Technology, 2001. **10**: p. 311-317.

89. Bacal, M., *Volume production of hydrogen negative ions.* Nuclear Instruments and Methods in Physics Research B, 1989. **37**: p. 28-32.

90. Bacal, M., *Physics basis and future trends for negative ion sources (invited).* Review of Scientific Instruments, 2008. **79**.

91. Bacal, M., *Physics aspects of negative ion sources.* Nuclear Fusion, 2006. **46**: p. 250.

92. Stoffels, E., et al., *Near-surface generation of negative ions in low-pressure discharges.* Journal of Vacuum Science Technology, 2001. **19**: p. 2109-2115.

93. Dodd, R., S. You, and J.W. Bradley, *O- density measurements in the pulsed-DC reactive magnetron sputtering of titanium.* Thin Solid Films, 2010. **519**: p. 1705-1711.

94. Corr, C.S., P.G. Steen, and W.G. Graham, *Instabilities in an inductively coupled oxygen plasma.* Plasma Sources Science Technology, 2003. **12**: p. 265-272.

95. Aanesland, A., A. Meige, and P. Chabert, *Electric propulsion using ion-ion plasmas.* Journal of Physics: Conference Series, 2009. **162**(1): p. 012009.

96. Rose, D.V., et al., *Towards a fully kinetic 3D electromagnetic particle-in-cell model of streamer formation and dynamics in high-pressure electronegative gases.* Physics of Plasmas, 2011. **18**(9): p. 093501-10.

97. Krylov, A., et al., *Caesium and tungsten behaviour in the filamented arc driven Kamaboko-III negative ion source.* Nuclear Fusion, 2006. **46**(6): p. S324.

98. Oohara, W., Y. Kuwabara, and R. Hatakeyama, *Collective mode properties in a paired fullerene-ion plasma.* Physical Review E, 2007. **75**(5): p. 056403.